SANDIA REPORT
SAND2025-05194
Printed April 2025

Sandia National Laboratories

Processes in Salt Repositories for Radioactive Waste Disposal

Kristopher L. Kuhlman & Melissa M. Mills

Prepared by
Sandia National Laboratories
Albuquerque, New Mexico 87185
Livermore, California 94550

Issued by Sandia National Laboratories, operated for the United States Department of Energy by National Technology & Engineering Solutions of Sandia, LLC.

Available to DOE and DOE contractors from

U.S. Department of Energy
Office of Scientific and Technical Information
P.O. Box 62
Oak Ridge, TN 37831

Telephone: (865) 576-8401
Facsimile: (865) 576-5728
E-Mail: reports@osti.gov
Online ordering: http://www.osti.gov/scitech

Available to the public from

U.S. Department of Commerce
National Technical Information Service
5301 Shawnee Road
Alexandria, VA 22312

Telephone: (800) 553-6847
Facsimile: (703) 605-6900
E-Mail: orders@ntis.gov
Online order: https://classic.ntis.gov/help/order-methods

ABSTRACT

This document summarizes the key processes (thermal, hydrological, mechanical, and chemical; THMC) impacting the features of a deep geological repository for radioactive waste in salt. Some processes are natural and on-going whether the repository is there or not, and other processes are driven by the perturbation associated with the repository. The features considered here include both engineered and natural components of the repository system. The engineered barrier system (EBS) in a salt repository is quite different from those implemented for a repository in clay or crystalline rocks, because it is comprised mostly of granular salt and salt-compatible cements, rather than bentonite.

When compared to other rocks (i.e., silicates), salt has unique properties that make it an excellent potential host rock. Openings and fractures in salt creep closed readily. Salt has high thermal conductivity, which can reduce peak temperatures. Additionally, far away from the excavations the porosity of salt is unconnected, which leads to essentially zero advective or diffusive transport. The small amount of hypersaline brine occurring in salt minimizes microbial activity, reduces colloid-assisted transport, and eliminates in-package criticality (i.e., chloride is a neutron poison).

At the end of the report, we present a brief outline for a potential salt repository, including considerations avoided in previous repository disposal concepts. We propose considering higher-temperature processes in future disposal concepts, rather than trying to minimize the thermal perturbation of the repository. Since hot salt is drier, a dry repository would limit corrosion, gas generation, and solute transport. Openings and fractures creep shut faster in hot salt. Therefore, higher temperatures could be seen as beneficial, rather than something to minimize, through increased spacing between waste packages (increasing repository costs).

This page intentionally left blank.

ACKNOWLEDGMENT

This report summarizes knowledge gained over the last ten years of salt disposal research. Several of the concepts were matured through key international collaborations. The authors thank the group of researchers working in this field for many interesting interactions through workshops, conferences, and project meetings.

The authors especially acknowledge the group of researchers working on the topic as part of the Brine Availability Test in Salt (BATS) at Sandia, Los Alamos, and Lawrence Berkeley National Laboratories and at the WIPP site in Carlsbad, New Mexico. The authors also gratefully acknowledge the participants of DECOVALEX-2023 Task E, who worked to understand and predict brine migration in heated salt since 2020 and the participants of DECOVALEX-2027 BATS II task, who have continued to work on the problem since 2024. Finally, the authors thank the GRS-led team on the KOMPASS collaboration and the BGE TEC/Sandia team involved with the RANGERS project, which advanced the understanding and simulation of granular salt reconsolidation and engineered barrier systems for salt repositories, respectively.

The authors have received funding from the US Department of Energy Office of Nuclear Energy Spent Fuel and Waste Science and Technology Campaign over the last decade to plan, carry out, and draw understanding from laboratory and field experiments. These experiments were intended to improve the technical basis for disposal of spent nuclear fuel and high-level radioactive waste in salt. In March 2025, US Department of Energy Office of Nuclear Energy (NE-8) redirected the disposal research program. As part of the program pivot, they will no longer fund domestic or international salt-related disposal research. This report therefore seeks to document the state of understanding in the program at the time of this change. The authors thank Rick Jayne for providing a careful technical review of the entire report.

This page intentionally left blank.

CONTENTS

This page intentionally left blank.

LIST OF FIGURES

LIST OF TABLES

This page intentionally left blank.

ACRONYMS & DEFINITIONS

BGE TEC	BGE TECHNOLOGY, a subsidiary of Bundesgesellschaft für Endlagerung (BGE), the Federal Company for Radioactive Waste Disposal in Germany
BGR	Bundesanstalt für Geowissenschaften und Rohstoffe, the Federal Institute for Geosciences and Natural Resources in Germany
COVRA	Centrale Organisatie Voor Radioactief Afval, the Central Organization for Radioactive Waste in the Netherlands
DECOVALEX	Development of Coupled models and their Validation against Experiments
DOE-EM	DOE Office of Environmental Management
DOE-NE	DOE Office of Nuclear Energy
EBS	engineered barrier system
EDZ/EdZ	excavation damaged/disturbed zone
FEHM	Finite Element Heat and Mass transfer (LANL $TH^2MC_{PPT/DIS}$ simulator, with infinitesimal mechanical deformation)
FEPs	features, events, and processes
FLAC	Fast Lagrangian Analysis of Continua (Itasca TH^1M simulator, with finite deformation and salt creep constitutive laws)
GRS	Gesellschaft für Anlagen- und Reaktorsicherheit GmbH, a nuclear safety company in Germany
LANL	Los Alamos National Laboratory
LBNL	Lawrence Berkeley National Laboratory
OpenGeoSys	Open-source finite element multi-physics simulator
PA	performance assessment
PFLOTRAN	Parallel reactive FLOw and TRANport (SNL/PNNL TH^2MC simulator, with ability to simulate $C_{PPT/DIS}$, C_{TRACER}, and C_{FULL} [low ionic strengths only], with infinitesimal mechanical deformation)
RWM	Radioactive Waste Management, disposal authority in the United Kingdom
SNL	Sandia National Laboratories
THMC	thermal-hydrological-mechanical-chemical processes
TOUGH	Transport Of Unsaturated Groundwater and Heat (LBNL $TH^2C_{PPT/DIS}$)
TOUGH-FLAC	Coupled model using TOUGH and FLAC (LBNL $TH^2MC_{PPT/DIS}$)
TOUGH-REACT	TOUGH with full chemistry reactions (LBNL TH^2C_{FULL})
WIPP	Waste Isolation Pilot Plant (DOE-EM site)
WP	waste package

This page intentionally left blank.

1. INTRODUCTION

This report presents relevant features and processes in a deep geological repository for disposal of heat-generating radioactive waste in salt, from the point of view of coupled process models and performance assessment (PA) models, finishing with aspects of an updated salt disposal concept. This report is an update of the 2019 report "Processes in Salt Repositories" [130], updated with research and development funded over the last 5 years by the US Department of Energy (DOE) Office of Nuclear Energy (DOE-NE) Spent Fuel and Waste Science and Technology Program under the Salt Disposal Research and Development work package. This recent work includes the Brine Availability Test in Salt (BATS) heater test at the Waste Isolation Pilot Plant (WIPP) [141, 139, 140], the 2020-2023 Phase of Development of Coupled Models and their Validation against Experiments (DECOVALEX) Task E [131, 133], and the international projects KOMPASS (on granular salt reconsolidation [50, 79]) and RANGERS (on engineered barrier systems – EBS [239, 240]).

Geologic salt is widely considered a potential host medium for radioactive waste disposal, since 1955 when the US Atomic Energy Commission convened a National Academies of Sciences expert panel to recommend best practices for radioactive waste disposal from US nuclear weapon production and the growing US nuclear power industry [101]. Multiple viable deposits of bedded and domal salt exist in the US [120, 196] and around the world [81]. US heat-generating radioactive waste is mostly spent fuel assemblies from power reactors and solidified high-level waste from defense activities comprised of liquid reprocessing waste that either has or eventually will be turned into vitrified glass logs [244]. Permanent geologic disposal of solid radioactive wastes may involve placing waste packages or canisters into horizontal boreholes starting from, or laid directly on the floor of, rooms mined into stable geologic salt deposits. The disposal rooms will be completed with granular salt backfill and salt-compatible cement seals (e.g., Sorel cements). Differing from common designs for crystalline and argillite host rock repositories for heat-generating waste, salt repositories do not rely on imported bentonite for backfilling, sealing, and closing drifts. Salt repositories can use native granular salt for backfilling and long-term sealing.

The WIPP is an operating, licensed deep geologic repository for transuranic defense waste in bedded salt in southeastern New Mexico, operated by the DOE Office of Environmental Management (DOE-EM). This report discusses conditions relevant to a hypothetical future repository for spent fuel and high-level (i.e., heat-generating) radioactive waste relevant to DOE-NE, but data and knowledge gained from WIPP and other non-disposal salt facilities (e.g., salt caverns or salt mines) are also valuable towards this goal.

Salt is considered a viable candidate medium for deep geological disposal of radioactive waste [95] because:

- salt has high thermal conductivity for a geologic material ($\approx$ 5 to 6 $\mathrm{W/(m \cdot K)}$);
- salt far from excavations has ultra-low porosity ($\leq 0.1\%$) that is largely unconnected, resulting in vanishingly small permeability ($\ll 10^{-20}\ \mathrm{m^2}$) and effective diffusion coefficient ($\rightarrow 0\ \mathrm{m^2/s}$);

- salt has no regional groundwater flowing through it (as demonstrated by its geological stability over millions of years, despite its high solubility);
- hyper-saline brines are biologically simple [183] and have reduced colloid mobility [157, 14];
- high chloride concentrations in brines eliminate risk of in-package criticality [97, 42];
- salt can be mined easily and cheaply with a continuous miner (i.e., no drill-and-blast needed) and unprocessed mined salt (i.e., run-of-mine material) is an excellent backfill; and
- fractures and damage around excavations, as well as open pores in granular salt backfill, will eventually close and heal to the same favorable properties as undisturbed salt.

The last ten years have seen significant international work on salt disposal research, much of it presented at the annual meetings of the US/German Workshop on Salt Repository Research, Design & Operation [165, 32, 92], which has been a key forum to discuss many of the projects and studies mentioned in this report.

It is of central importance to understand and predict the availability of brine in salt surrounding radioactive waste [136, 143, 129, 135]. The availability of brine to excavations in salt is a function of the initial distribution of the different types of water in salt, and the distribution of damage around the excavation that provides the connected porosity and permeability allowing vapor and liquid brine to move. The amount and movement of brine is important in a salt repository because brine is required for:

- waste package (i.e., metal) corrosion;
- waste form (i.e., oxides or glasses) corrosion and radionuclide mobilization;
- liquid-phase transport of radionuclides away from the repository (gas phase transport is often neglected); and
- most gas generation processes, which can pressurize brine and drive releases.

The BATS field test was a heater-test experiment (2018–2025) located in horizontal boreholes at WIPP, funded by DOE-NE. The field tests were designed with previous experiments on heated salt in mind [144, 136, 128, 143, 142]. BATS included a shakedown phase [85], a BATS 1 phase where heated and unheated arrays of horizontal boreholes were drilled and monitored during multiple heating and tracer experiments [140], and a BATS 2 phase where a new heated array was drilled and monitored during repeated heater tests [139, 141]. The tests were designed and analyzed by Sandia, Los Alamos, and Lawrence Berkeley National Laboratories and were implemented through the WIPP Test Coordination Office (funded by DOE-EM). Temperatures, acoustic emissions, electrical resistivity tomography, fiber optic distributed sensing (temperature and strain), and gas stream composition (both isotopic and species) were monitored during heating, cooling, and tracer addition. These data are described in the above listed reports and several conference and journal papers [69, 280, 40], and were used in tasks for DECOVALEX-2023 and DECOVALEX-2027.

In DECOVALEX-2023 Task E (2020–2023) and DECOVALEX-2027 task BATS II (2024–2027), modeling teams from the US (Sandia, Los Alamos and Lawrence Berkeley National Laboratories), Germany (Bundesanstalt für Geowissenschaften und Rohstoffe – BGR and Gesellschaft für Anlagen- und Reaktorsicherheit – GRS), The Netherlands (Centrale Organisatie Voor Radioactief Afval – COVRA), and

The United Kingdom (Radioactive Waste Management – RWM and Quintessa Limited) participated in a range of comparisons between observations and numerical models [133, 131].

KOMPASS-I and KOMPASS-II were the first two parts (started in 2018) of an on-going multi-lateral collaboration (now called MEASURES, starting in 2025), led by GRS, on the topic of granular salt reconsolidation [50, 79]. The project includes laboratory granular salt reconsolidation experiments seeking to standardize and systematically consider the effects that testing conditions have on the salt reconsolidation process. The laboratory components are balanced by both micro-structural investigations into crystal-scale deformation mechanisms and macroscale (cm- to m-scale) numerical modeling of lab reconsolidation tests.

RANGERS was a bi-lateral collaborative project between Sandia National Laboratories and BGE TEC (2020–2024) that demonstrated methodologies and modeling for performance assessment (PA) and integrity evaluation of the EBS in a salt repository system [239, 240].

The next chapters discuss the features of a repository, the types and distribution of brine in salt, and the processes to be included in either process and PA models for a heat generating waste repository in salt. Typically a process would first be included in a process model to understand it and test its impacts on model predictions, then later could be included in PA models if deemed critical. Since PA models may serve multiple uses during their lifetimes (i.e., optimization, re-design, consideration of new waste streams), the number of simplifying conservatisms should be kept to a minimum. What is conservative for one purpose may not be conservative for a new purpose.

This page intentionally left blank.

2. SALT REPOSITORY FEATURES AND PROCESSES

The general nature of thermal, hydrological, mechanical, and chemical (THMC) processes in salt has been known since the late 1950s [101, 235, 214], but the details regarding implementation and constitutive laws have only been well-understood and confirmed since large-scale heated brine migration field and laboratory tests in the 1980s at Asse in Germany, WIPP in New Mexico, and Avery Island in Louisiana [237, 86]. Numerical modeling the web of subsurface coupled processes (Figure 2-1) is an active area of research in repository science [267, 266, 268, 289, 269], reservoir geomechanics [297], carbon sequestration [65], and hydrogen storage [1], among other earth science fields, leading to the development of generic modeling tools for numerical simulation of coupled processes.

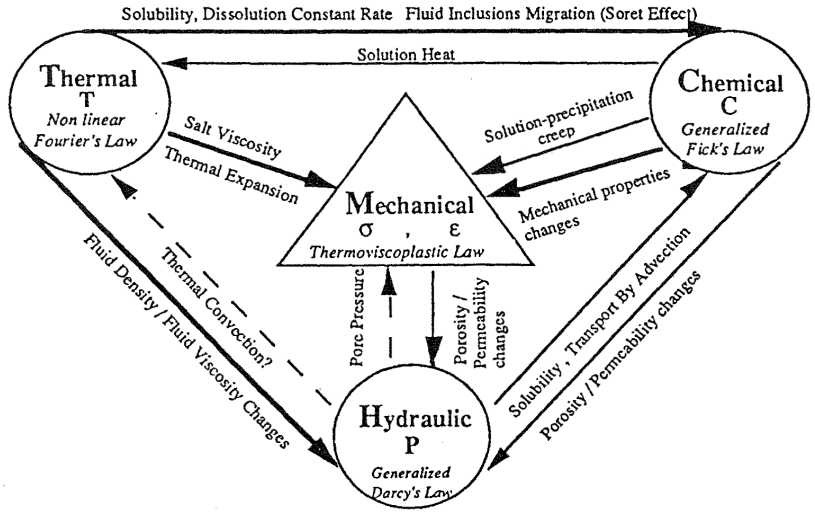

Figure 2-1. Illustration of THMC couplings in salt [47].

At proposed mined repository depths ($\leq$ 1 km depth) and thermal loads ($<$ 10 W to a few kW per canister [244]) THMC processes in salt become close to *equally* important and tightly coupled with one another, often including non-linear temperature, stress, or moisture dependencies to constitutive behaviors. Except under special experimental designs or restrictive circumstances, we usually cannot predict in isolation a single process from a THMC experiment in salt. The thermal-mechanical (TM) problem in salt is characterized by the strong dependence of mechanical properties on temperature; faster creep at elevated temperature. The thermal-hydrological-mechanical (THM) problem in salt (Figure 2-1) is characterized by strong dependence of salt's hydraulic properties on mechanical deformation, thermomigration of fluid inclusions, pressure solution of brine films on salt crystals and grains [250, 108], the effect of pore pressure on stress, and the differential thermal expansion of salt and brine. Chemical effects further complicate the THMC representation, with additional coupling due to the rapid precipitation and dissolution of salt in the pore space, the different mechanical behavior of salt when including even a small

amount of moisture (i.e., the Joffe effect [271, 272]), and including possible creation of heat pipes around heat sources in granular salt.

In this report we neglect biological effects, since they would be slight for a salt repository, where the activity of water is usually < 0.75, making it difficult to maintain all but halophile life [183].

2.1. FEPs and Models

In a post-closure safety case for a deep geologic repository, the aim is not to predict the future, or even identify everything the future could hold, but rather to provide confidence all credible futures will be safe [134]. The safety case is the integration of arguments and evidence that describe, quantify, and substantiate safety, and the level of confidence in safety for a deep geological repository [111]. PA is a key component of the safety case, but natural analogues also provide an important line of independent evidence to support claims regarding the long-term geological stability and viability of salt [182].

Exhaustive databases of features, events, and processes (FEPs) relevant to deep geological repositories have already been assembled and are maintained by the Nuclear Energy Agency [184]. Features are the logical components of a repository system (Figure 2-2). Events and processes are things that can happen to features, either discretely (events) or continuously (processes). Features are connected by processes and events to other features and likewise events and processes are connected through the features they act upon; this can be visualized as a "FEP matrix" [77]. This report is primarily about processes (rather than events), and how they apply to features of the repository disposal system.

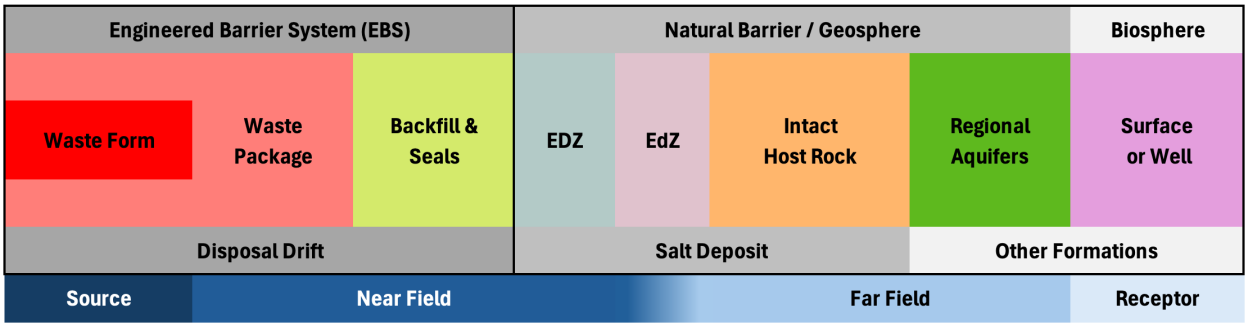

Figure 2-2. High-level features and conceptual regions of a salt repository system from source (left) to receptor (right) [77]. EDZ and EdZ are introduced in detail in Section 4.

Starting from a comprehensive international list, FEPs are either included or excluded based on the host rock, disposal site, disposal concept, and waste form. All FEPs that are included in (i.e., "screened into") a safety case must be represented somehow in the PA, either as part of the base scenario (i.e., the nominal case) or as a variant scenario, where a feature providing a key safety function fails early or otherwise behaves in an off-nominal way [134].

In the context of a repository safety case, a "process model" is any numerical, conceptual, or mathematical model that simulates the impact of one or more processes occurring in the features that comprise engineered or natural components of a repository system. In the near-field of a salt repository, these processes include [143]:

- brine, gas, and heat flow;
- advective and diffusive transport of solutes including radionuclides;
- gas generation (which may increase gas pressure, driving fluid advection);
- chemical reaction like waste package corrosion, waste form dissolution, sorption and reaction of solutes with solid phases, and mineral precipitation and dissolution;
- mechanical deformation of non-salt backfills, cementitious materials, and waste packages; and
- elasto-visco-plastic deformation of the intact and granular salt surrounding the excavation.

Process models may be developed for stand-alone simulations aimed at testing understanding, justifying parameterizations, or screening out processes. Process models may also be further matured and developed for incorporation into PA models, the goal of which is to assess the consequence associated with transport radionuclides from the repository to the biosphere or to the accessible environment (Figure 2-2).

Process models can be used to simulate processes occurring on features across a wide range of time and space scales, but are often validated against data collected under field and lab conditions where things are changing fastest (similar to early time after waste emplacement) and have the steepest gradients (in and immediately around the disposal drift – Figure 2-2). Challenges of scale arise when integrating process models into PA simulations due the coupling between far-field transport processes occurring over long time (thousands to millions of years) and distance (kilometers) scales and near-field processes occurring over short time (up to hundreds of years) and distance (up to meters) scales. Sometimes processes at the lab scale are different from those at the repository scale requiring careful extrapolation (e.g., granular salt reconsolidation, § 4.2.1.1–non-Darcy flow, § 4.4.4–metal corrosion, or § 4.3.3–creep at low deviatoric stresses). Because PA simulations often include Monte Carlo uncertainty analysis, the need for computational efficiency creates an additional challenge, which may be addressed by using coarser numerical model meshes, simplified physics, or even look-up-tables, compared to a stand-alone "full resolution" process models.

Stand-alone process models that predict in-drift evolution of the system during pre-closure and early post-closure times may also be used to predict initial conditions for simplified PA models. Process models may also be used to "screen out" some physical processes from PA models as inconsequential with respect to the consequences of radionuclide release and transport to the biosphere.

2.2. Repository System Disturbances

Processes are continuously occurring in the natural and repository systems, while events are discrete in time. Even continuous processes are primarily driven by perturbations associated with the engineered features of the repository system (i.e., the system was largely quiet before repository construction). Repository design, simulation, and optimization requires understanding, accommodating, and minimizing disturbances to the extent possible. For a salt repository, perturbations include:

- thermal disturbance, peaking during the first $\approx 1,000$ years due to waste decay heat;
- hydrological disturbance during pre-closure due to depressurizing the excavation and removing water from the host rock via mine ventilation (less extensive in salt);

- gas pressure disturbance due to gas generation in later post-closure (less in a dry system);
- mechanical disturbance from mined openings in pre-closure and early post-closure (salt heals naturally);
- microbial disturbances brought into the repository during operational period (much less in salt);
- reduction potential (i.e., redox state) associated with the operational period (system will rapidly become anoxic after closure);
- radioactivity effects (α, β, γ) from radioactive waste (largely confined within waste packages);
- chemical, hydrological, and mechanical disturbances due to incidental man-made infrastructure in repository (e.g., ground control, tunnel lining, cables); and
- chemical, hydrological, and mechanical disturbances associated with drift and shaft seals, backfill, and other intentional engineered barrier components (partially made from salt in a salt repository).

These perturbations illustrates the long-term process disturbances associated with the features a salt repository are somewhat smaller than a similar deep geological repository in other rock types. The thermal perturbation could be interpreted to be positive, rather than a liability. Hotter salt repositories (with larger or more closely spaced waste packages) may present more benefits to long-term containment than a cooler repository with a larger footprint. A cooler repository with a larger footprint would likely be more expensive to create and seal than a hotter repository with a smaller footprint.

The repository is designed and built to ensure post-closure safety, but its design will also be subject to the constraints of pre-closure worker safety and costs associated with construction.

2.3. Engineered Barrier System in Salt Repositories

The engineered barrier system (EBS) includes the human-made or at least human-altered features of the repository (Figure 2-2). The EBS, unlike the natural barrier (i.e., geosphere) and biosphere features, can be designed and optimized to improve the performance, cost, or robustness of the overall repository system. Salt-based repositories are designed with different EBS components than most other repository designs in crystalline or argillite rocks, which use bentonite clay to seal and backfill around waste packages. Salt repositories typically use granular salt for backfill, often called "run-of-mine" salt or "crushed salt" produced from standard mining of drifts (not specifically *crushed* after mining, but sometimes very large particles are removed). This incorporates the simple use of material sourced from the excavation process, rather than importing large amounts of material from elsewhere, while simultaneously needing to dispose of the material mined out to make the excavations. The direct use of mined salt for backfill is already a large optimization and cost-savings measure over repository designs that rely on other imported materials, such as bentonite.

A consequence of the large differences between the EBS in a salt repository from the EBS in a crystalline or argillite repository, is that salt-repository specific backfills and cements are specialized and are an ongoing subject of research in the salt repository community. Bentonite has seen more use, experience, and research in the oil and gas and construction industries, than more specialized salt EBS components.

The international KOMPASS projects (KOMPASS-I, KOMPASS-II, and MEASURES) have been investigating aspects of the reconsolidation of granular salt, including the execution of laboratory tests, used to calibrate numerical models to predict granular salt reconsolidation in a repository [50, 79]. The RANGERS project developed and simulated THMC behavior of the EBS for salt a salt repository [239, 240, 238]. The international RANGERS project produced a State-of-the-Art report [238], summarizing the current state practices used in different countries and discussing key findings from several recent relevant projects on the topic of EBS.

Plain run-of-mine granular salt, without additions, is conceptually very simple to implement and will achieve low permeability upon reconsolidation [96]. The factors affecting the precise time it takes to achieve full reconsolidation include: water content, stress state, grain size, and temperature. Laboratory tests can reconsolidate granular salt with moisture at elevated temperatures in days to weeks. The reconsolidation process, under conditions expected in a repository, can vary from tens to hundreds of years, depending on the conditions.

Investigations have been made into different additives to include in granular salt (e.g., bentonite or attapulgite), to reduce the initial high permeability of the granular material in drift seals at emplacement (Figure 2-3), to buffer the brine chemistry (e.g., MgO at WIPP [62]), or to increase the long-term sorption properties of the backfill [33]. However, too many additives in granular salt backfill may end up hindering the reconsolidation process, increase the late-time permeability after reconsolidation, or reduce its thermal conductivity (thermal conductivity of clay is lower than salt). Any potential benefits of additives should be balanced against their additional financial costs, operational complexity, and possible reduced performance after reconsolidation.

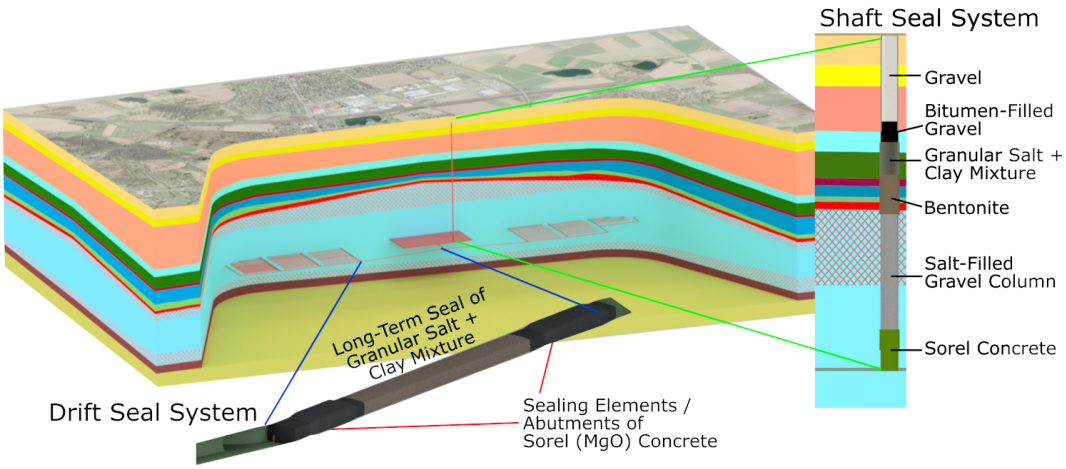

Figure 2-3. EBS components (drift and shaft seals) from RANGERS [239].

Because granular salt backfill is ≈ 30 to 40% porosity at emplacement, cementitious seals or abutments can be emplaced on one or either end of the granular salt backfill in drifts to provide low-permeability seal properties immediately at emplacement [239]. The cementitious seals and abutments only need to provide sealing function until the granular salt has reconsolidated to low enough porosity and permeability to take over the sealing function, expected to happen over a few hundred years.

Cementitious seals in a salt repository are necessarily different from those in non-saline systems [124]. Repository designs in other disposal media (e.g., argillite or crystalline rocks) tend to minimize cement

usage, because it can locally create hyper-alkaline brines that can degrade some minerals in the host rock or bentonite backfill and adversely impact actinide solubility and mobility [288]. In salt repositories these geochemical issues are less of a concern because there is less water, and the granular salt backfill and host rock are less susceptible to change at high pH. Additionally, low-pH cements using fly ash or other alternatives are also possible. The chloride associated with halite and hypersaline brine will degrade ordinary Portland cement [31], so the cements either need to be made with brine instead of fresh water (i.e., salt concrete [277, 278, 198, 197]) or they are a salt-specific alternative formulation like Sorel cement (made from MgO, as opposed to CaO [78, 114]). Utilizing granular salt as aggregate in brine-based cements allows for additional compatibility to the host rock, potential beneficial creep behaviors, and reduced material costs. The interaction between more rigid and brittle cements and more compliant and creeping granular backfill and salt host rock must also be considered in the design [125].

The EBS contains both horizontal seals in the drifts within the repository footprint and shaft seals between the repository elevation and the surface (Figure 2-3). Drift seals can be located between disposal panels or between the disposal system and the infrastructure area. Drift seals can be emplaced in a staged manner during the completion of the repository. The shaft seals are installed when the repository is finally closed [94]. Figure 2-3 shows drift seals and shaft seals in a hypothetical RANGERS repository design, with the components of the shaft seals tailored for the geologic units encountered. The RANGERS example was for a hypothetical pillow (i.e., gently deformed bedded salt) or bedded salt geology. There are two key differences between the drift seals and shaft seals: 1) shaft seals are vertical or are steep ramps, so their seals are easier to emplace (i.e., gravity assists in emplacement), and 2) shaft seals are multi-barrier systems that include both granular salt that will reconsolidate and redundant water-stop components (e.g., asphalt, cements, and bentonite) to prevent water from overlying units reaching the repository [94, 110]. Drift seals are either purely cementitious or granular salt, or a combination of the two. Drift seals do not usually include water-stop components.

Because of the large excavation damaged zone (EDZ) associated with excavations in salt compared to stronger rocks like crystalline granites or gneisses (see § 4.3, Mechanical Processes), an effort is often made to either mine out part of the EDZ before installation of drift seals or plug fractures in the EDZ with grout, to reduce the amount of fracture porosity and permeability in the salt adjacent to the seal. Since the EDZ is an accumulation of damage through time, and the difference in stress state from trimming (i.e., mining away a small amount near the wall) is slight compared to the stress differential associated with the initial mining, this approach is often successful at removing potential flow pathways (i.e., the EDZ does not grow significantly upon trimming). The ADDIGAS project demonstrated the ability of trimming to remove or at least reduce the extent of the EDZ at the Asse underground research lab in Germany [119]. Demonstrations conducted at WIPP illustrated the feasibility of grouting open fractures in anhydrite marker beds in the floor of the excavation [2].

Another additional repository EBS component, not specific to salt repositories, is the addition of a high-porosity infrastructure area at the bottom of the shaft filled with non-salt backfill. The addition of an area filled with silica-based gravel, that will not creep closed, reduces potential gas pressurization effects (i.e., provide an air-filled buffer volume). This may slow down the late-time re-saturation of the repository, in the case brine were able to migrate through multiple water-stops and reach the bottom of the shaft seal from overlying aquifers.

3. BRINE IN SALT

Understanding salt behavior is critical in a salt repository because it makes up both the host rock (i.e., natural barrier) as well as the backfill and seals (i.e., engineered barrier). Salt has a unique THMC behavior compared to most silicate rocks (silicates do not significantly creep and do not have temperature-dependent brine components under repository conditions) and even compared to metals (which do creep, but do not experience significant pressure solution, a pore-scale chemical-mechanical coupling). Brine contributes in multiple ways to salt's unique character, so this report begins with a discussion on brine types in salt and their migration [188, 204]. Table 3-1 summarizes the relationship between the primary water forms in geologic rock salt (both bedded and domal): intergranular brine, intragranular fluid inclusions, water of hydration, and water in non-salt components [56].

Water Form	**Bedded Salt Fraction**	**Stability at Unloading**	**Stability at Heating**	**Bedded vs. Domal**
Hydrous minerals	$\leq$ 5% mass frac.	Stable	Mobile at $T > 200\,^{\circ}$C (Fig 3-4, curve B)	$\approx$same
Clay mineral water	1 to 2% mass frac.	Stable	Mobile at $\approx$ 100 $^{\circ}$C (Fig 3-4, curve C)	<clay
Intragranular inclusions within crystals	$\leq$ 1% vol. frac.	Stable	Mobile under ∇T, decrepitation at $T > 250\,^{\circ}$C	much less ≈ 0.1
Intergranular inclusions between crystals	0.1 to 0.2% vol. frac.	Mobile if grain boundary is part of fracture network	Mobile under ∇T, decrepitation at $T > 250\,^{\circ}$C	$\approx$same
Clay pore water	$\leq$ 5% clay $\times$ clay porosity (30%)	Mobile (driven by gas exsolution)	Additional release if not gone already due to unloading	<clay

Table 3-1. Summary of water types in geologic salt, from most stable to least stable.

Roedder [219] and the NBS Monograph on rock salt properties [80] both summarize geologic salt water content values in the literature. Measuring brine content in salt rocks is more difficult than other rock types, requiring special methods and sample preparation [220].

3.1. Brine Types

Figure 3-1 shows a medial cross-section from an X-ray computed tomography scan of WIPP salt core from BATS, illustrating the main types of water discussed here. Water in the clay pores is the largest and most mobile reservoir of water in bedded salt deposits (e.g., the Permian Salado Formation at WIPP). Clay pore water is usually mobile upon unloading the rock, because the brine starts at lithostatic pressure

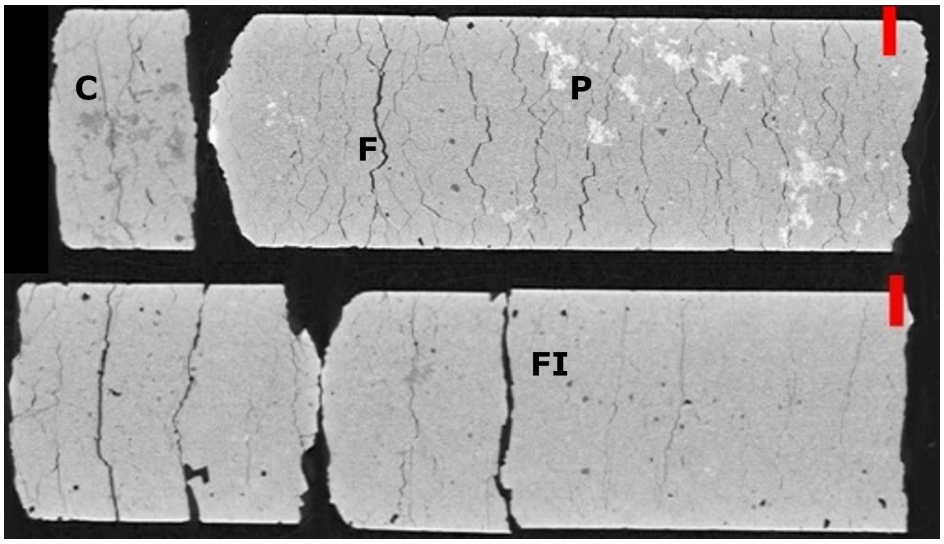

Figure 3-1. X-ray CT images from salt core. C is clay (darker gray), P is polyhalite (lighter gray), F is fracture (from EDZ and core handling), FI is fluid inclusion; red scale bars are 20 mm [16].

and the clay is considered undercompacted before the rock is depressurized through access from a nearby excavation [59, 60, 58, 57]. This brine is the main contribution to "popcorn" (i.e., efflorescence – Figure 3-2a), which follows bubbling dampness observed on the drift ribs (i.e., walls) immediately after mining, and is preferentially found in areas of higher clay content. Bubbling is likely due to gas exsolving from high-pressure brine upon depressurization [284]. Popcorn continues to grow slowly as far out as 1.5 to 2 years after mining. Popcorn formation has been observed to renew after trimming (i.e., slightly enlarging) areas [59, 58], indicating the source of the brine is very near the excavation surface.

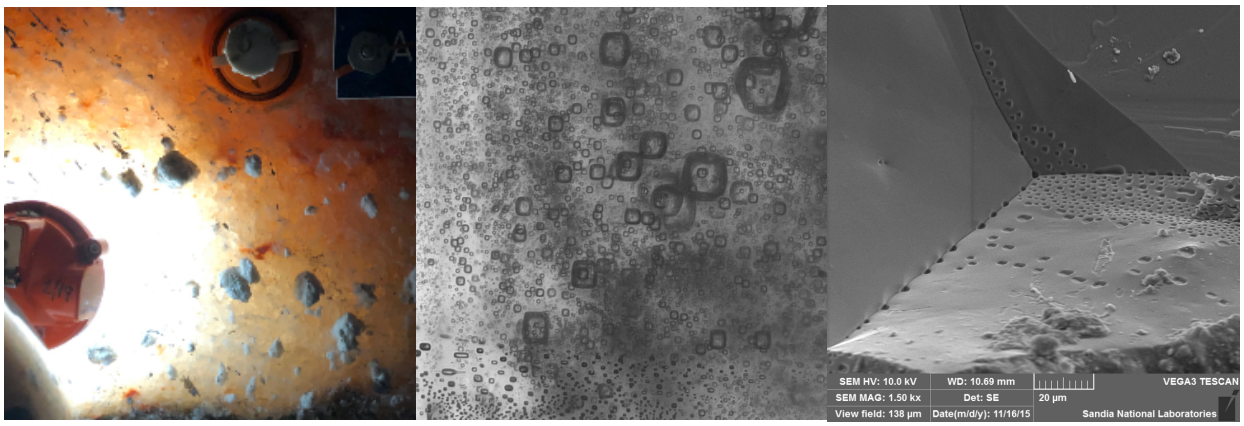

(a) headlamp and efflorescence (i.e., popcorn) visible on surface of drift.

(b) halite with primary fluid inclusions (field of view ≈ 600μm, image by BGR).

(c) isolated intergranular fluid inclusions along healed grain boundaries.

Figure 3-2. Images of WIPP brine.

Fluid inclusions are the next most abundant form of water in bedded salt [220, 219], but they are not available to flow under a pressure gradient, they are released to connected intergranular porosity usually during heating or accumulation of fracture damage (e.g., they are released when the sample is powdered,

as is done for thermogravimetric analysis in Figure 3-4). Fluid inclusions are either primary or secondary. Primary fluid inclusions are from the initial evaporation process, are usually found in chevron patterns, are intragranular, and are distributed approximately fractally (small inclusions are common, large inclusions are rare – Figure 3-2b). Secondary fluid inclusions form during the salt recrystalization process, and are often along grain boundaries (i.e., intergranular – Figure 3-2c). Domal salt is often recrystallized to the point that it has no remaining primary fluid inclusions. Essentially, primary fluid inclusions are almost all intragranular, but not all intragranular fluid inclusions are primary.

Although intergranular brine is the smallest component of water in bedded geologic salt [254], the intergranular brine likely occupies the main pathway from the far field to the excavation (assuming damage preferentially occurs between crystals, rather than through crystals). The gas-filled intergranular porosity can be closed by hydrostatic loading and brine-filled intergranular porosity can become disconnected through hydrostatic loading, while the intragranular porosity is largely fixed without thermal or chemical changes (Figure 3-3). Microscopic observations [90] of damage in salt cores from a 20-year old WIPP excavation found that the intergranular porosity and observed fracture aperture increase up to the excavation face ($\approx$ 2.5% porosity and $>$ 300 μm aperture), above the observed small values ($<$ 0.5% porosity and $<$ 100 μm aperture) in cores obtained from the far field ($>$ 5 m away from drift). Many mentions of fluid inclusion volumes in the literature lump together inter- and intra-granular fluid inclusions. Geologists interested in extracting information about ancient evaporative environments are exclusively interested in primary fluid inclusions [262, 263]. Figure 3-4 does not include fluid inclusions, because the 0.1 g samples were powdered and dried at 70 °C before the high-temperature thermogravimetric analysis.

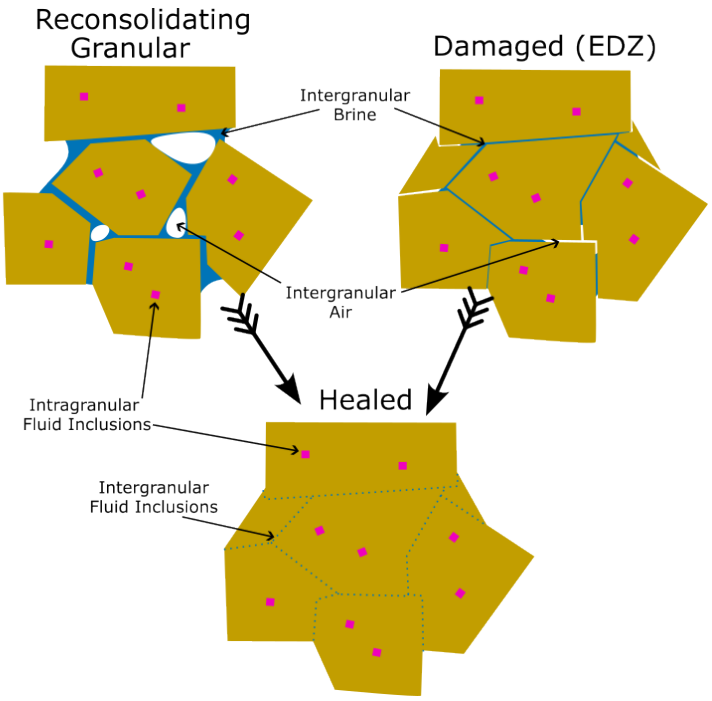

Figure 3-3. Intergranular and intragranular brine for reconsolidating salt at $\gg$ 5% porosity (top left), damaged salt in the EDZ at $\approx$ 1.5 to 2.5% porosity (top right), and healed salt with disconnected intergranular fluid inclusions $\leq$ 0.1% porosity (bottom). Derived from [192].

Recent analysis of stable water isotopes in Salado Formation primary fluid inclusions and brine collected in BATS boreholes has provided evidence supporting the claim that only a small amount of brine col-

lected in boreholes from primary fluid inclusions ($\ll$ 20%) [69]. The isotopic signature of brines collected from different horizontal boreholes during heating or cooling is different from the isotopic signature of fluid inclusions measured in the lab under controlled conditions. The isotopic makeup of water in clay porosity, or the water in hydrous minerals has not been directly measured yet, but it is assumed their composition must account for some of the observed difference.

Hydrous minerals represent a potentially large amount of water, but this water is usually quite stable, being released only at elevated temperatures. The main hydrous minerals in WIPP salt are polyhalite ($K_2Ca_2Mg(SO_4)_4 \cdot 2H_2O$), gypsum ($CaSO_4 \cdot 2H_2O$), bassanite ($2CaSO_4 \cdot H_2O$), and inter-layer waters in clays (at WIPP, corrensite is common – an ordered mixed-layer chlorite/smectite [61]). Polyhalite is the most common hydrous mineral in WIPP salt, with a dehydration temperature of approximately 280 °C [179] (see "Polyhalite-bearing rock salt" curve in Figure 3-4), above the temperature expected in most salt repositories (i.e., this is at or above the expected temperature of decrepitation for most bedded salts). Water released from clays upon heating is another source of water, at lower temperatures than polyhalite [122]. Figure 3-4 shows one curve for "clay-bearing rock salt" with significant water loss at 100 °C. As thermogravimetric analysis samples are powdered before testing, these clay samples would have released any mechanically confined fluid in clay (i.e., pore water) or fluid inclusion brine before testing; the water content in the clay-bearing sample should only be intercalcated water in clays (i.e., water associated with layers in the clay structure).

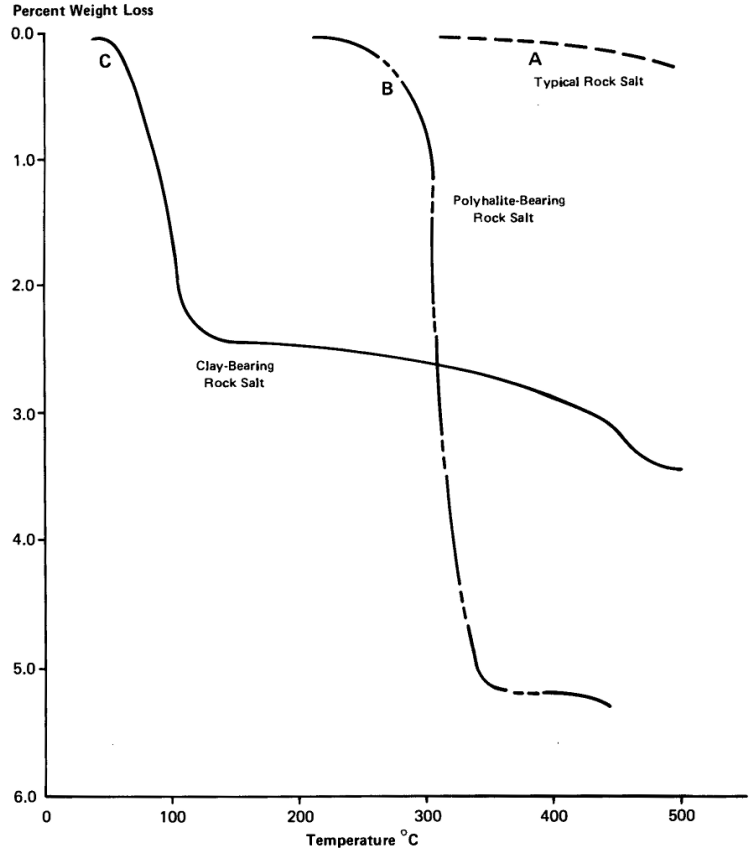

Figure 3-4. Characteristic thermogravimetric analyses from powdered Salado Formation bedded salt samples (no fluid inclusions or mechanically held clay water) [206].

Domal salt is typically drier than bedded salt (rightmost column in Table 3-1) with approximately 1/10 as many fluid inclusions as bedded salt, because it has usually been buried deeper and has buoyantly moved upwards (i.e., halokenesis, diagenesis, or metamorphism [65, 117]). Halokenesis is a process [80] which:

1. recrystallizes the salt–*eliminating* most primary intragranular fluid inclusions;
2. sometimes also changes stabilizes hydrated mineral phases (i.e., higher dehydration temperature, like bassanite to polyhalite); and
3. homogenizes or breaks up layering that existed in the source bedded salt (e.g., boudinage).

The connectivity of planes of intergranular fluid inclusions may also be impacted by the equilibrium dihedral angle [151, 104]. Under certain conditions (i.e., chemical equilibrium between the brine and solid phases), the connectivity of the intergranular porosity in salt is a function of pressure and temperature [217, 216]. When the dihedral angle (i.e., fluid inclusions at junctions where three salt crystals come together) is above the critical value (60°), geometric and thermodynamic arguments indicate intergranular porosity will not be connected, as shown in Figure 3-2c. Unconnected porosity makes both the permeability and the effective diffusion coefficient go to zero before the porosity goes to zero. The dihedral angle can drop below the critical value (i.e., permeability and effective diffusion coefficient will tend to increase for the same porosity) at pressures and temperatures found at depths below typical radioactive waste repositories (e.g., depths greater than 2 km at 100° C). It has been shown conclusively via experiments [166, 156] that permeability of actual geologic salt does not measurably increase due only to the pressure and temperature configuration leading to a dihedral angle $< 60°$. The Lewis and Holness lab experiments used to justify the importance of dihedral angle [151] were made in a idealized and significantly fluid-excess system of pure NaCl and deionized water. A lack of sufficient intergranular brine, or a non-ideal brine chemistry (i.e., other species like K^+, Mg^{++} and $SO_4^=$) can impact surface tension that contribute to dihedral angles, further reducing connected porosity [216].

3.2. Brine Migration Mechanisms

Laboratory permeability testing in the 1950s and 1960s illustrated porous media flow under a large laboratory-imposed pressure gradient through salt cores from the Grand Saline salt dome mine [214, 82]. Despite this early understanding that salt has a non-zero permeability when it is damaged, most early research into brine migration focused on thermomigration of fluid inclusions down a temperature gradient, through salt crystals. The historic surge in fluid inclusion research was fueled by field and laboratory observations made during Project Salt Vault in the late 1960s [27, 26] and significant interest in thermomigration of fluid inclusions dominated through the mid 1980s [199, 237]. Data collected during project Salt Vault was fitted by Jenks [115] using a simple exponential model, which saw wide application. Rübel et al. [223] surmised the Jenks model [115] was fitted to anomalous data, making most subsequent applications of this model inappropriate.

Fluid inclusions migrate through halite crystals due to an imposed temperature gradient [286, 287, 27, 37], driven by solubility and possibly also due to stress effects [298]. Single-phase liquid fluid inclusions move up a temperature gradient (towards the heat source), while bi-phase fluid inclusions (gas and brine) move down a temperature gradient (away from a heat source). The rate of fluid inclusion migration is slow (e.g., 1 to 5 cm/yr at 1.5 °C/cm [219]) and size dependent (0.1 mm inclusions moving 30% slower than 1 mm

inclusions [219]). There is also a threshold gradient under which fluid inclusions do not move, given their stability over geologic time in the presence of a constant geothermal gradient. Most fluid inclusions only migrate a few mm to cm before they encounter an open fracture (i.e., most heat sources are near excavations). Fluid inclusions may leave tracks in the salt, indicating where they migrated, which contribute to the intergranular porosity and permeability [147, 38, 37]. Fluid inclusions will rupture (i.e., decrepitation) if the vapor pressure of the brine exceeds the strength of the surrounding crystal. Unconfined samples of WIPP salt decrepitate at $\approx$ 250 °C, while salt from other bedded formations can get as high as 380 °C before decrepitating. Domal salt typically does not decrepitate, even up to 400 °C [26]. Confined salt can experience higher temperatures without decrepitation, compared to unconfined salt. Sizes of individual fluid inclusions and the overall densities of fluid inclusions in a sample will influence the decrepitation temperature.

The network of microfractures and open grain boundaries make up a discrete fracture network or an equivalent porous medium. This network is what gives damaged salt its connected porosity, permeability, and effective diffusion coefficient. Brine-saturated clay produces brine as a source term to the intergranular fracture network upon being de-stressed (driven by brine pressure and gas exsolution [284]). Fluid inclusions could also be treated as an intergranular fracture network brine source term, where brine is released to the fracture network, once inclusions have migrated under a temperature gradient to a grain boundary [220]. Decrepetation of fluid inclusions and dehydration of hydrous minerals could also be included as an intergranular porosity source term triggered at a specific temperature, but adding vapor that readily dissolves salt to become brine [122].

The significance of brine flow due to pressure gradients through connected intergranular porosity in damaged or dilated salt has been shown in numerous field and laboratory studies [9, 133]. A thermoporoelastic conceptual model for intergranular brine flow in salt has been successfully applied to unheated and heated brine transport in bedded salt [160, 161, 9]. Hadley [87] developed an alternative conceptual model for vapor flow associated with an evaporation front. These models assumed liquid or vapor movement in connected intergranular porosity and left out intragranular fluid inclusions to simplify mathematical and numerical models. Olander et al. [191] developed a conceptual model including both intergranular vapor flow and intragranular fluid inclusion movement. Ratigan [208] developed a numerical model including intragranular fluid inclusions and intergranular brine flow, but it did not include thermal expansion effects on the intergranular porosity. Current numerical models for brine flow in granular salt assume a porous or fractured continuum (e.g., FEHM, TOUGH2, PFLOTRAN) with water and vapor moving under pressure gradients and solutes diffusing under concentration gradients. Most numerical models do not incorporate fluid inclusion thermomigration along with intergranular brine and vapor migration. Rutqvist et al. [225] illustrated an implementation of fluid inclusion migration with intergranular brine and vapor flow using a dual-porosity conceptual model using TOUGH2.

These detailed conceptual models regarding the distributions and types of brine sources and their various migration mechanisms in salt have not all been fully implemented and tested in most process models, but parts of them have been implemented in different places. The larger question of if, how, and in what way to implement these in PA models has not yet been fully addressed. PA models usually treat brine migration in a simplistic and idealized manner. PA models have not yet fully implemented the range of intergranular brine source terms described here, triggered at different stresses, temperatures, and temperature gradients.

4. SALT REPOSITORY THMC PROCESSES

The features of the repository conceptual model include the excavated drift, the waste packages emplaced with backfill there, and the undisturbed far field (Figure 2-2). The extent and nature of the transition between the near- and far-field is somewhat gradational and evolves significantly with time. For this report, we distinguish between the excavation *damaged* zone (EDZ), where material properties have been altered, and the excavation *disturbed* zone (EdZ), where only the system variables have changed (Figure 4-1). System variables can include observable variables (e.g., strain, temperature, water content), internal variables (e.g., damage, hysteresis), or associated variables (e.g., stress, pressure) [148]. Because mechanical damage to salt will eventually heal, these zones will shrink with time; their maximum extent at early time is their typical definition.

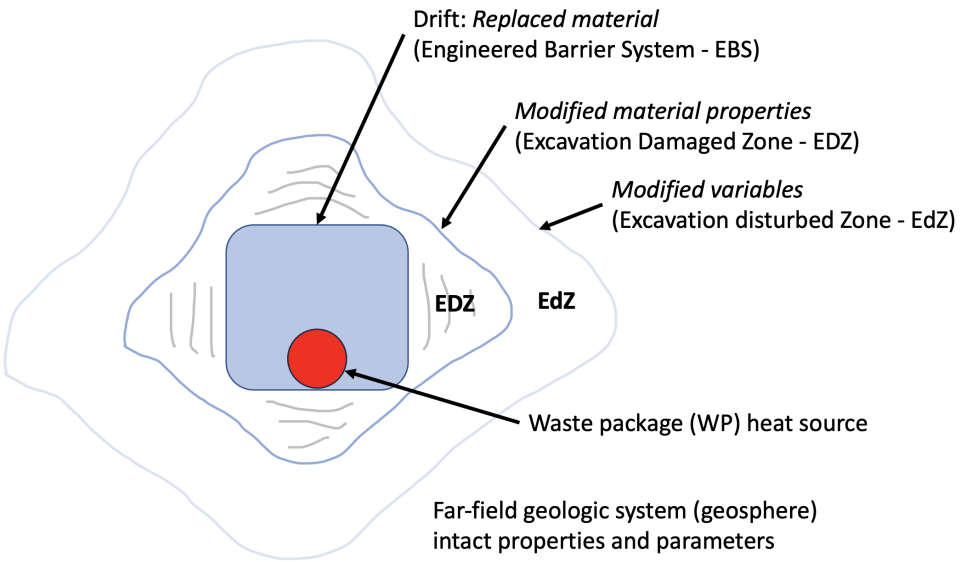

Figure 4-1. Definitions of EdZ and EDZ regions in salt repository conceptual model at early time.

The following definitions are given by Tsang et al. [268]:

- The EdZ is a zone with hydromechanical and geochemical modifications, without major changes in flow and transport properties.
- The EDZ is a zone in which hydromechanical and geochemical modifications induce significant changes in flow and transport properties. These changes can, for example, include one or more orders-of-magnitude increase in flow permeability.

We further consider multiple overlapping EDZ and EdZ may exist, as many as one for each group of processes [268, 52]. A thermal EDZ would be where the thermal properties have been modified (i.e., in the drift and areas of significant mechanical damage), and the thermal EdZ would be where only the

temperature has been perturbed from background (may extend several tens of meters into the formation during post-closure). With coupling between the processes, these definitions can become complex and time dependent.

Process	EDZ-defining Properties	EdZ-defining Variables
Thermal	thermal conductivity, heat capacity, fluid advection, porosity	temperature
Hydrological	permeability, porosity, tortuosity	fluid pressure, liquid saturation, fluid density, fluid advection
Mechanical	moduli, creep constitutive law parameters, interface slip parameters, Poisson's ratio	stress, strain, strain rate, damage
Chemical	tortuosity, porosity, fluid advection, fluid density, salinity	water activity, redox state, pH, species concentrations (solid, liquid and sorbed phases)

Table 4-1. Process-specific EDZ and EdZ.

The processes are presented here in a generic way to cover both the near field and the far field, but most processes are not equally impactful or relevant everywhere. We present the key properties and variables at a high level.

Since we cannot represent the entire subsurface in our numerical simulations, we must truncate the domain at some convenient but hopefully adequate distance from the repository. The size of the domain required increases with the time extent of the simulation. Thermal boundary conditions may need to be located much farther from the repository than hydrological or chemical boundary conditions to reduce unwanted non-physical boundary interactions. Mechanical model domains often extend to the land surface, and the effects of salt creep may accumulate and increase the lateral size of the domain needed over long periods of time.

PA simulations usually require larger domains than process model simulations. PA models have expectations regarding their extent in space (i.e., beyond the extent of the majority of the disturbance from the repository or at least beyond a legally specified compliance boundary), time (e.g., from before emplacement to the regulatory compliance time horizon), and parameter space (i.e., relevant combinations of physically plausible parameters should be considered), that are often much larger than the same expectations on process models. Setting up initial conditions, especially in simulations with coupled processes, must be considered carefully. Often an initial simulation must be performed to derive a consistent (i.e., steady-state) set of thermal, chemical, or hydrological inputs for a transient repository flow model. The initial simulation is often quiescent without the disturbance of the repository. Sometimes process models are used to define initial conditions, boundary conditions, or source terms used in PA models.

4.1. Thermal Processes

The primary thermal variable is local change in temperature, T, [K] above the background temperature (i.e., geothermal gradient) due to the energy output from radioactive waste decay and any other thermal

perturbation in the system. It is highest near the waste package immediately after emplacement, and is lowest in the far field away from the perturbation of the repository. Mechanical deformations and hydrological flow are usually slow enough to neglect mechanical heating and viscous dissipation heating. Dissolution and precipitation may be endothermic or exothermic processes, but these changes in temperature are often neglected because their effect is usually minimal, but their importance may grow if significant dissolution or precipitation is expected. In-package criticality at later times [42] could modify the thermal output and waste source term, but it is usually not included in salt repositories, because of the high chloride content in salt and brine, which would prevent neutron multiplication and criticality.

4.1.1. Heat Conduction

Heat conduction due to a temperature gradient is the dominant energy transport mechanism in the far field, where porosity and permeability are low. It is the only energy transport mechanism through nonporous salt (i.e., it does not require connected pore space),

$$\frac{1}{\alpha_T}\frac{\partial T}{\partial t} = \nabla^2 T,$$

where thermal diffusivity, $\alpha_T = k_T/(\rho C_v)$, $[\mathrm{m}^2/\mathrm{s}]$ is the ratio of thermal conductivity, k_T, $[\mathrm{W}/(\mathrm{m}\cdot\mathrm{K})]$ and specific heat capacity, C_v, $[\mathrm{J}/(\mathrm{kg}\cdot\mathrm{K})]$ times bulk density, ρ, $[\mathrm{kg}/\mathrm{m}^3]$. It is not significantly different in the mechanical EDZ and in the far field [46], but both k_T and ρC_v are much lower in the backfilled drift than in intact rock. In granular salt, thermal conduction becomes less effective because the run-of-mine salt is up to 40% porosity, resulting in lower k_T. At the same time significant thermal gradients in fluid-filled spaces may initiate convection.

Intact salt has temperature-dependent thermal conductivity; it is higher at ambient temperatures by as much as 50% compared to the temperatures expected next to heat-generating waste [260]. A simple example thermal conductivity model used for intact bedded salt is

$$k_T^{\text{intact}}(\theta) = k_{T0}/(1 + a_1\theta) \tag{4.1}$$

where θ is temperature (not change in temperature) [C], $k_{T0} = 6.0\ \mathrm{W}/(\mathrm{m}\cdot\mathrm{K})$ is the thermal conductivity at $T = 0\ ^\circ\mathrm{C}$, and $a_1 = 0.0045$ is a linear resistivity coefficient (i.e., $k_T \propto 1/\theta$). The granular salt model developed for Gorleben [21] is a modification of the intact salt model as

$$k_T^{\text{granular}}(\theta, n) = k_{T0}/(1 + a_1\theta)\cdot\left(1 - \frac{n}{n_0}\right)^{\hat{\gamma}} + \frac{n}{n_0}\cdot(b_1 + b_2\theta)\,, \tag{4.2}$$

where n is the dimensionless porosity, $n_0 = 0.35$ is the initial porosity, $\hat{\gamma} = 1.14$ is an exponent, $b_1 = 0.42$ and $b_2 = 0.0027$ are linear temperature dependence coefficients (i.e., $k_T \propto \theta$) relevant at high porosities. The relationships in Equations 4.1 and 4.2 are illustrated in Figure 4-2.

At emplacement, the granular salt near the waste packages starts at high porosity and low thermal conductivity ($\approx 0.5\ \mathrm{W}/(\mathrm{m}\cdot\mathrm{K})$), but then evolves to the thermal conductivity of intact salt during the reconsolidation process. The thermal conductivity of the backfill can go up by a factor of 10× during reconsolidation to intact properties. This is a significant benefit of crushed salt over bentonite backfill.

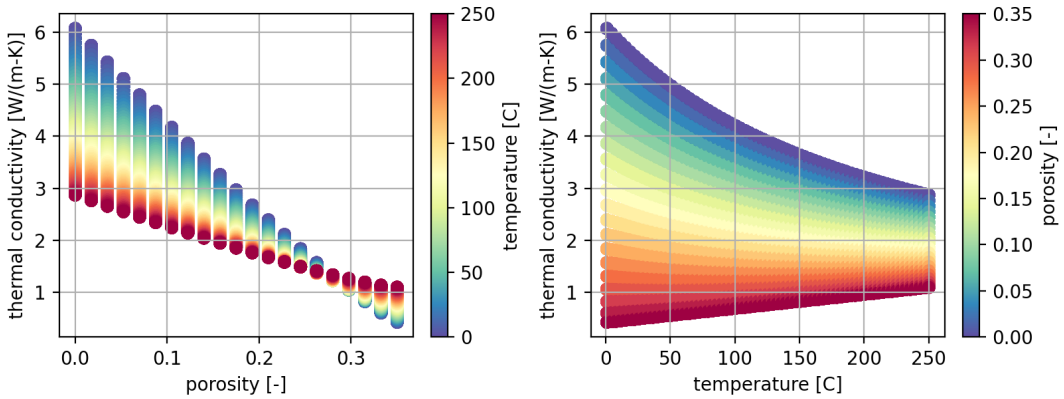

Figure 4-2. Thermal conductivity of granular salt as a function of temperature and porosity (Equation 4.2).

For numerical models, the initial conditions (before heat-generating waste emplacement) is a geothermal gradient increasing temperature with depth. Physical boundary conditions are specified-temperature near the top of the domain, and either a specified-temperature or specified heat flux at the bottom of the domain. Before the waste is emplaced, energy is being conducted up from warmer rocks at depth to the cooler surface.

The thermal boundary condition on the sides of the domain usually do not correspond to physical boundaries and are either specified temperature (type I) or specified flux (type II). If we represent them as specified temperature, we will *underestimate* impacts of the repository in the far field (since temperature is fixed there). If we represent them as specified flux or insulated, we will *overestimate* impacts of the repository in the far field (since flux is fixed there). The most physically realistic option is to make the model domain larger, until a physical boundary is reached or the impacts of the repository perturbation do not reach the model boundaries, but this could lead to very large model domains.

4.1.2. Heat Convection

Convection occurs when energy is moved by either gas- or liquid-phase transport through pore spaces. Convection, when viable, can be a far more efficient mechanism for energy transport than conduction, but it can only occur through a connected pore space, and requires a freely circulating fluid phase (gas or liquid). Heat pipes are a type of free convection cell (Figure 4-3) that is possible in the near field, when high temperatures cause boiling of brine, they drive convection of energy (i.e., internal energy + pressure × volume) away from the heat source. Convection and diffusion of energy is

$$\rho C_v \frac{\partial T}{\partial t} = k_T \nabla^2 T + \vec{u} \nabla T$$

where $\vec{u}$ is the pore velocity vector [m/s].

The pore flow velocity of brine or vapor driving convection ($\vec{u}$) varies significantly between the drift, EDZ, and the far field (see § 4.2, Hydrological Processes). In the far field there is very little connected porosity and no convection of energy. If there is any convection through the tiny pore space, it is minor compared to heat conduction through the solid salt. Convection of gas in the drift, through granular

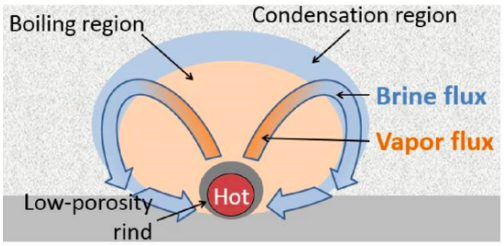

Figure 4-3. Illustration of cross-section through a heat pipe due to a hot waste package in granular salt; the boiling region (orange) is nearly constant temperature.

salt or through large open fractures, can be significant in high porosity and permeability materials. Additionally, the heat source is needed to drive free convection. A heat-pipe can form; hot vapor carries energy away from the heat source efficiently (lower temperature gradients than heat conduction), precipitating salts and reducing the porosity where the brine boils away (see § 4.4, Chemical Processes). When the vapor migrates to a cooler region, it condenses and dissolves salt (increasing the porosity).

If heat conduction is the only mechanism for thermal energy transport in the near field, the temperature at the heat source will be hotter than in a system with free convection (Figure 4-4). Convection is potentially a more efficient heat transfer process than conduction. Kuhlman [129] presented an analysis based on dimensionless parameters, which illustrated how the thermal Péclet number changes from the near to far field, illustrating how the problem goes from convection-dominated in the near field to conduction-dominated in the far field.

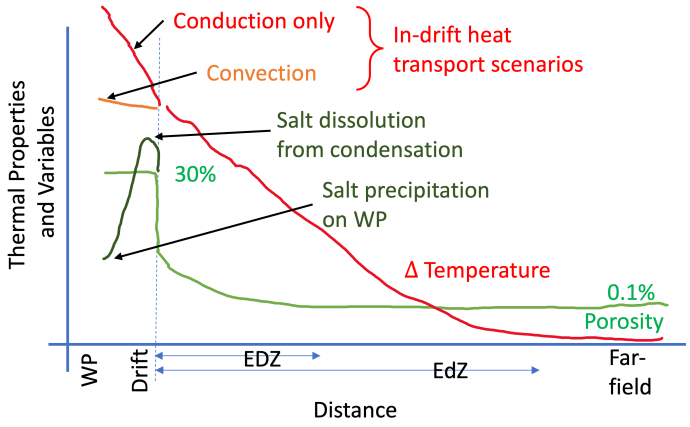

Figure 4-4. Conceptual trends in temperature under conduction and convection scenarios.

Thermal convection is most effective at high porosities, where thermal conductivity is lowest (due to the relatively low thermal conductivity of granular salt $\approx$ 0.5 W/(m $\cdot$ K) compared to intact salt $\approx$ 5.0 W/(m $\cdot$ K) – Figure 4-2). During compaction and precipitation of salt from boiling brine on the waste package, porosity and permeability of the granular salt will reduce, eventually conduction dominates over convection. As porosity reduces, the thermal conductivity of the granular salt increases (as it approaches the properties of intact salt), in part making up for loss of convection as a energy transport mechanism.

The initial condition for thermal convection is no regional liquid or gas flow, and therefore no thermal convection. Previous DOE-NE Generic Disposal Safety Assessment simulations have included minor

lateral regional hydrological flow [158, 236], but this does not convect energy because it is perpendicular to the geothermal gradient. Thermal convection is solely due to the repository perturbation. The boundary conditions applicable to the regional hydrological flow problem drive thermal convection. Even if there is some component of regional groundwater circulation to drive convection, there will be minimal regional steady-state energy convection.

4.1.3. Radiation

Radiative transfer of electromagnetic radiation only occurs in open air-filled spaces (i.e., open drifts or high porosity) for repository-relevant conditions, where the heat flux is proportional to the fourth power of difference in temperature. It can be an efficient and important energy transport mechanism where large temperature differences exist in an air-filled borehole or drift, but is not usually considered because most salt reference cases assume all openings are back-filled with porous materials. It may occur in any gaps that occur next to waste packages. Some models for heat transfer in granular salt include terms that approximately include the effects of radiation (Equation 4.2), but the impact of this is slight unless temperature differences are large [149].

4.2. Hydrological Processes

A common set of primary hydrological variables are fluid pressure (p [Pa], liquid or gas phase pressures) and the volume fraction of each phase (S [−], relative fraction of the pore space). Figure 4-5 illustrates the trends in hydrological properties and variables. In the far-field the small amount of pore space is liquid saturated (no connected gas phase) and the liquid pressure is equal to the lithostatic pressure (e.g., WIPP is at 650 m depth or 15 MPa lithostatic pressure). In the drift, the system is nearly gas saturated (limited brine) and the gas pressure is equal to atmospheric pressure (0.1 MPa) before closure. There is a very steep gradient in saturation and fluid pressure going away from the drift into the far field, which is supported by the low permeability and porosity of the salt (which themselves are changing in space across the EDZ) [257, 254, 255, 256]. If the salt were more permeable, brine would flow and dissipate the steep pressure gradient, extending the EdZ much further away from the excavation. Here, we use H^1 and H^2 to indicate single- or two-phase hydrological processes, like TH^1C or TH^2C.

Thermal expansion can drive thermal pressurization, creep closure or chemical precipitation and dissolution can reduce the free porosity, increasing pressure and liquid saturation. High pressures due to fluid pressure or thermal expansion can hydrofracture and lead to fracturing. Additionally, pressure gradients or saturation gradients can also be driven by energy flux or electric currents (i.e., Onsager coupled processes [232]) or transport can be driven by gradients in surface tension (i.e., thermo-capillary convection), but these effects are often minor and usually neglected. That being said, heat-generating radioactive waste does maintain a large temperature difference across the EBS for a long time, which may enhance the cumulative impact of otherwise minor processes.

The following subsections describe contributing driving factors or considerations in hydrological flow: pressure-driven flow, capillarity-driven flow, gravity-driven flow, and the distribution of material properties that control hydrological flow.

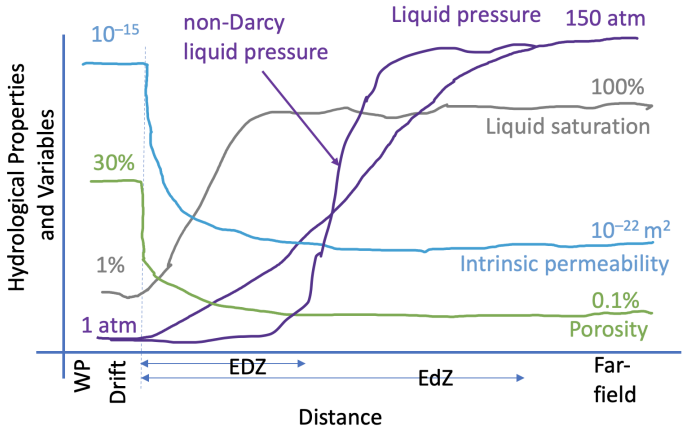

Figure 4-5. Conceptual trends in hydrological properties and variables around an excavation.

4.2.1. Pressure-driven Flow

Pressure-driven flow of fluid through a porous medium or fracture network moves fluids (i.e., gas or brine) down a pressure gradient. Flux of gas or liquid can occur if a continuous phase exists in the pore space and a pressure gradient is maintained and is described by Darcy's law,

$$\vec{u}n = \vec{q} = \frac{k k_{r,\ell}}{\mu_\ell} \nabla \left(p + \rho g z\right)$$

where $\vec{q}$ is Darcy flux (over the bulk of the whole rock) [m/s], μ_ℓ is liquid viscosity [Pa · s], $k_{r,\ell}$ and $k_{r,g}$ are the dimensionless relative permeability for liquid and gas, k is the medium intrinsic permeability [m^2], g is gravitational acceleration [m/s^2], and z is elevation above a datum [m].

Darcy's law is then combined with mass conservation to arrive at either Richards' equation for variable-saturation single-phase flow or a pair of flow equations (one for liquid and one for gas) for two-phase flow. The mixed form of Richards' equation is

$$\frac{\partial \bar{\theta}}{\partial t} = -\nabla \cdot \vec{q},$$

where $\bar{\theta}$ is the dimensionless volumetric water content. The non-linear relationship between water content and pressure and $k_{r,\ell}$ are both given by the moisture retention curve, discussed in § 4.2.2, Capillarity-driven flow.

The flow of brine or vapor varies significantly between the open drift and the far field [269]. In the far-field there is no gas flow ($k_{r,g} \rightarrow 0$, because there is no connected gas-filled porosity) and no liquid flow due to low intrinsic permeability and possibly due to non-Darcy effects. In the near field there can be significant short-range flow of both gas and liquid through the open intergranular porosity.

The absolute permeability increases near an excavation, but the relative permeability to liquid simultaneously decreases (due to decreasing liquid saturation, because brine cannot quickly flow in to fill new damage-derived porosity), therefore the relative liquid permeability reaches a maximum some distance into the salt (see § 4.2.5, Hydrological Properties and Figure 4-19). The flow of fluids is very sensitive to

changes in permeability, for a fracture network the permeability can be very sensitive to changes in stress, including thermal expansion from changes in temperature.

The initial condition for single-phase pressure-driven flow is a pressure distribution. The liquid pressure in the far field may be as high as lithostatic, since salt cannot support a deviatoric stress over geologic time. At equilibrium all the stress components are equal, and pore pressure is equal to the average stress, and should be near lithostatic (the weight of the overburden rocks). The fluid pressure in the salt can be up to lithostatic pressure, since if it were higher it would lead to hydrofracture and dissipation of pressure. Field data measured in boreholes from the underground at WIPP [218, 11, 10] indicate the far-field static formation pressure is approximately 12 to 15 MPa (hydrostatic to lithostatic pressure at a depth of 650 m).

A regional boundary condition for Darcy flow is often simulated by an imposed fluid pressure difference between two vertical sides of the domain to create uniform lateral flow. The aforementioned evidence for a lack of regional groundwater circulation in salt means either the undisturbed permeability of salt is low enough (with or without non-Darcy flow mechanisms) to prevent steady-state circulation, or the imposed gradient is too small to drive flow.

The brine saturation and pressure distribution around a deep excavation can be simulated via the relief of pressure around the excavation from the initial state, either using a hydrological model (e.g., Figure 4-6) or a coupled hydrological-mechanical model [225]. Figure 4-14 shows DECOVALEX results on the development of a two-phase flow initial condition.

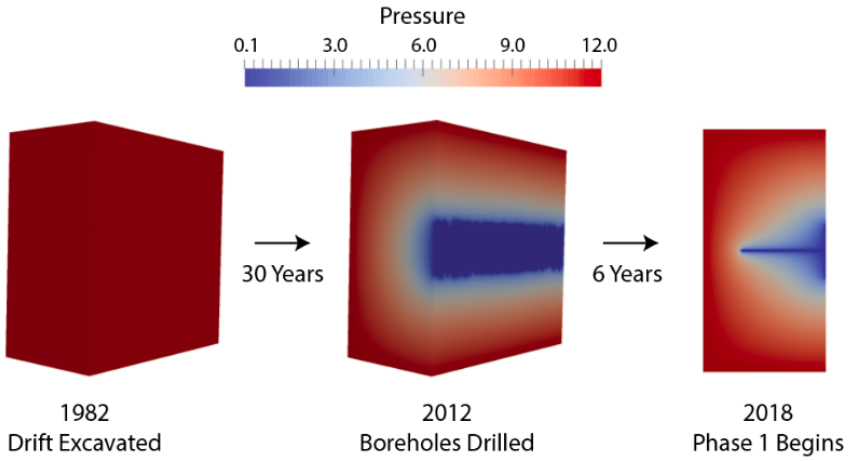

Figure 4-6. Liquid pressure evolution (in MPa) around horizontal boreholes and a drift in salt from undisturbed conditions [252].

4.2.1.1. Non-Darcy Threshold Flow

In some low-permeability rocks, non-Darcy flow has been observed [154, 153], where a threshold gradient (I shown in Figure 4-7 [m/m]) must be overcome to achieve a typical Darcy flux (i.e., flowrate is linearly proportional to pressure gradient). This threshold non-Darcy flow mechanism (sometimes called "pre-Darcy" flow) yields zero or lower regional groundwater flow than would be found by simply applying

Darcy's law with the regional gradient and permeability. One proposed non-Darcy expression for flux in terms of pressure gradient is [153]

$$\vec{q} = \frac{k k_r \rho g}{\mu_\ell} \left[\vec{i} - I \frac{\vec{i}}{|\vec{i}|} \left(1 - e^{|\vec{i}|/I} \right) \right],$$

where $\vec{i} = \nabla \left(p/\rho g + z \right)$ is the hydraulic gradient vector in terms of head [m/m] and I is the threshold gradient [m/m]. Although there is no salt-specific field data, it is conceptually consistent with geologic stability of salt deposits, which would dissolve if regional groundwater flow were significant across geologic time. This assumption was made in Germany for the Gorleben radioactive waste disposal reference case [20]. In the German safety case, there is no far-field hydrological flow beyond the permeability associated with damage from excavating the repository. The non-Darcy approach is consistent with both the US and German conceptual models of how flow in salt should be treated [240].

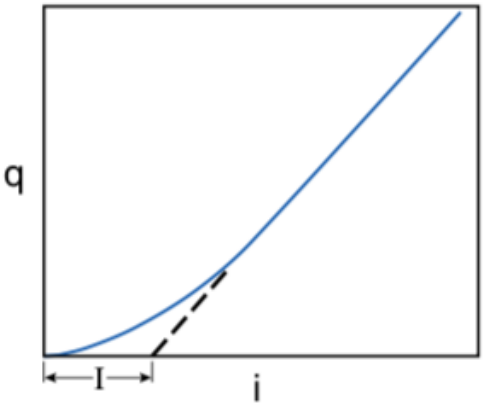

(a) Darcy flux ($|\vec{q}|$), applied gradient ($|\vec{i}|$), and threshold gradient (I).

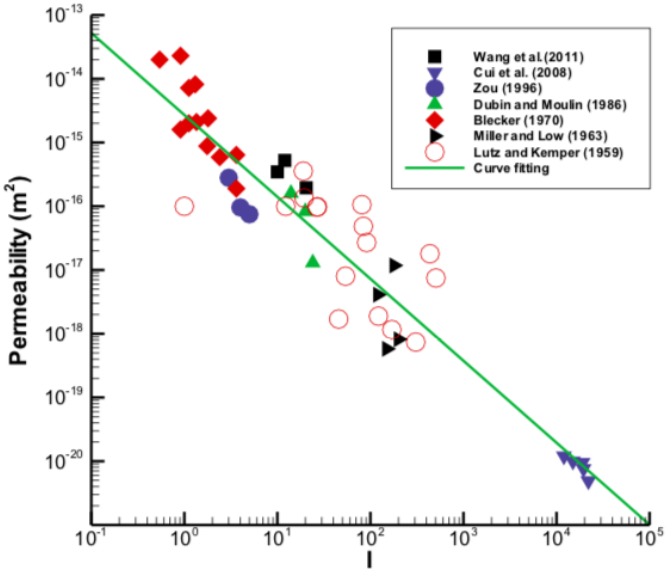

(b) Data showing estimated threshold gradient and relationship to intrinsic permeability.

Figure 4-7. Threshold non-Darcy flow characteristics [153].

Figure 4-8 illustrates the effect of non-Darcy flow at early time around a salt repository, as implemented in PFLOTRAN for the RANGERS project [240]. The definitions of the hydrological EdZ in these two cases are clearly very different (i.e., the extent of the region where the pressure and flow velocity are perturbed by the presence of the repository). Given the same initial conditions for repository and far-field pressure, saturation, and material properties (aside from the non-Darcy flow parameters), there is a marked difference predicted away from the repository. In the non-Darcy case, there is no flow outside a halo of few 10s of meters surrounding the repository (i.e., the flow magnitude is $< 10^{-11}$ m/yr), while in the Darcy case it is small but non-zero (≈ 1 μm/yr) all the way to the boundaries of the domain (beyond the extents of the Figure 4-8–up to several km). In this model the intact salt has an intrinsic permeability of 10^{-20} m^2 and the threshold gradient is estimated from the permeability with the "curve fitting" line plotted in Figure 4-7, $I = Ak^B$ ($A = 4 \times 10^{-12}$, $B = -0.78$).

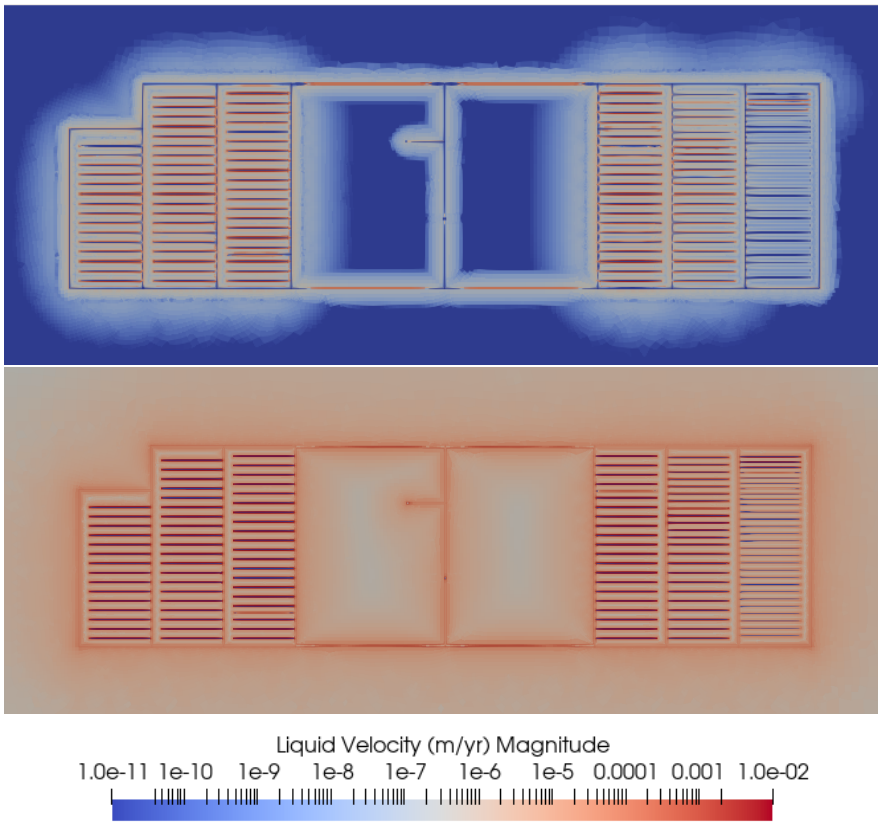

Figure 4-8. RANGERS comparison of flow velocity in salt for a horizontal slice through a repository 100 years after closure for non-Darcy (top) and Darcy (bottom) flow cases [240].

Earlier model-data validation exercises at WIPP (specifically the INTRAVAL study [145]) were interested in confirming the use of standard Darcy flow for very low permeabilities of salt [9, 146]. The WIPP portion of INTRAVAL showed that Darcy flow could be used to predict the observations of brine inflow made at WIPP [9]. Although the exercises did not require non-Darcy flow effects to explain the data, they did not definitively rule out non-Darcy flow as a possibly contributing factor. There were differences between observations and model-predicted inflow (especially in estimated parameters for the transient storage mechanisms), given the uncertainties in the observations and parameters used in the numerical models. The model-data differences were attributed to hydrological-mechanical coupling.

4.2.1.2. Thermal Pressurization

In DECOVALEX-2023 Task E, TH^1M and TH^1 numerical models were benchmarked against the McTigue analytical thermoporoelasticity solution [160, 161] around a heated borehole in an unpressurized formation [131, 133]. The exercise illustrated the difference between two popular, but quite different ways of simulating thermal expansion. First is an "unconfined" system (i.e., TH^1 models, only with the thermal expansion of fluid or equivalently allowing the solid to expand freely), and second is a "confined" system (i.e., TH^1M models, which include the expansion of the solid or equivalently confining the expansion of the solid). The two approaches resulted a difference of 38× in predicted thermal pressurization resulting in similarly different brine inflow rates to the heated borehole, due to the effects of confinement of the

surrounding rock (Figure 4-9). In the example shown, the very high pressures predicted by the TH^{1}M models would likely exceed the lithostatic load (e.g., 15 MPa at 650 m depth) and lead to hydrofracture, but this process was not included in this simple benchmarking model.

The results in Figure 4-9 clearly show the crest of a thermal pressurization "divide" or "dam," with the peak slowly moving away from the heater with time. This divide splits the direction of pressure-driven flow to be directed away from the peak pressure, either towards or away from the excavation (i.e., away from the peak). In this simplistic DECOVALEX example, there is no initial formation pressure gradient towards the excavation. In reality, the divide will be superimposed on a monotonic gradient towards the borehole (Figure 4-10). This simplistic problem also has uniform material properties and single-phase flow. Despite these limitations, the benchmark clearly illustrated the impacts that confinement has on pressure build up.

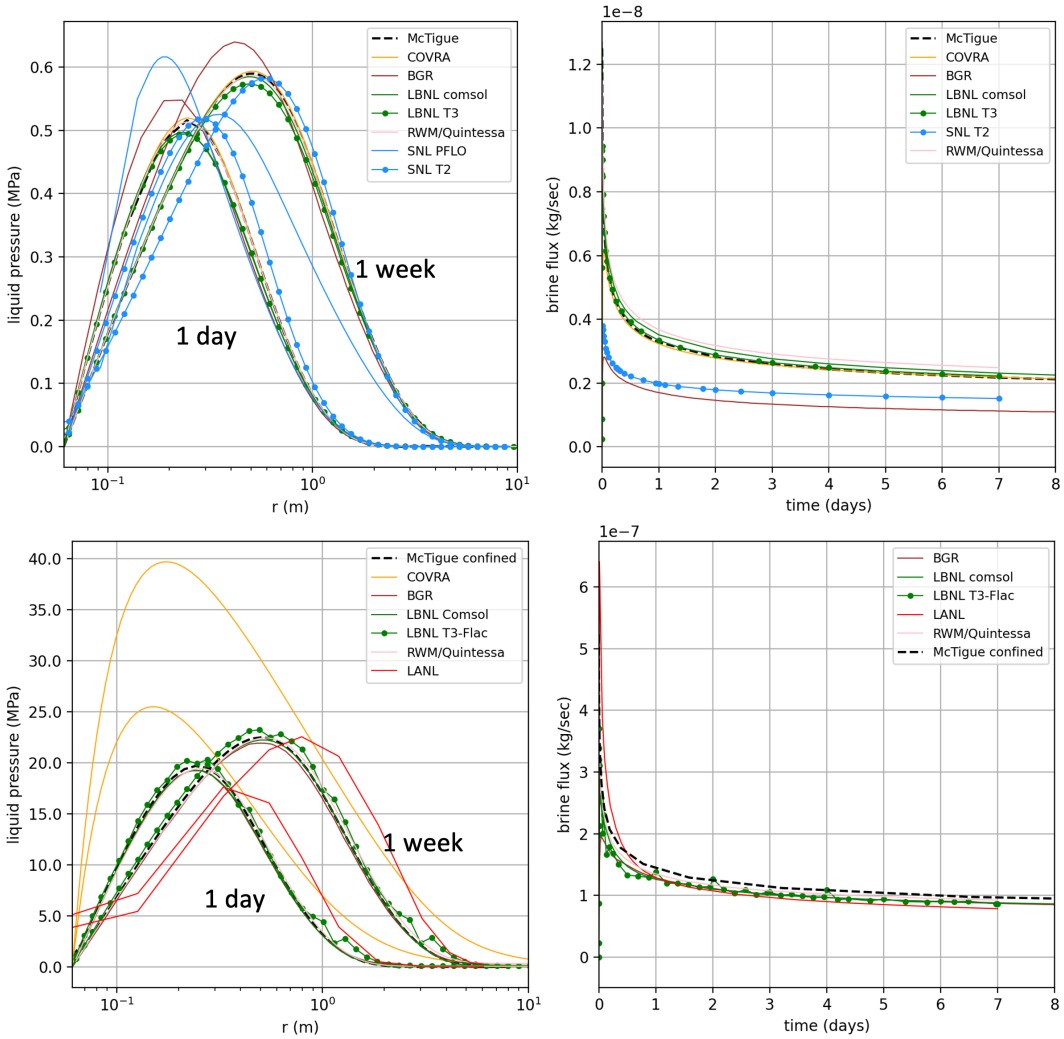

Figure 4-9. Comparison of TH^1 (top) and TH^{1}M (bottom) responses in McTigue thermoporoelasticity problem from DECOVALEX-2023 Task E. Left subplots show pressure distribution at two times as a function of distance; right subplots show predicted brine inflow through time [133].

In a repository where damage exists around boreholes or excavations, thermal pressurization may be greatest at the edge of the hydrological EDZ (Figure 4-10), if the temperature increase is large enough to cause

significant thermal expansion and pressurization of the pore fluids and the intrinsic permeability is low enough to prevent the liquid pressure from dissipating quickly. The McTigue problem (Figure 4-9) is single-phase liquid. In a two-phase flow problem (TH^2M), liquid saturation must also be high enough for thermal pressurization, or the more mobile residual gas will preferentially bleed off pressure due the higher mobility of gas in the EDZ.

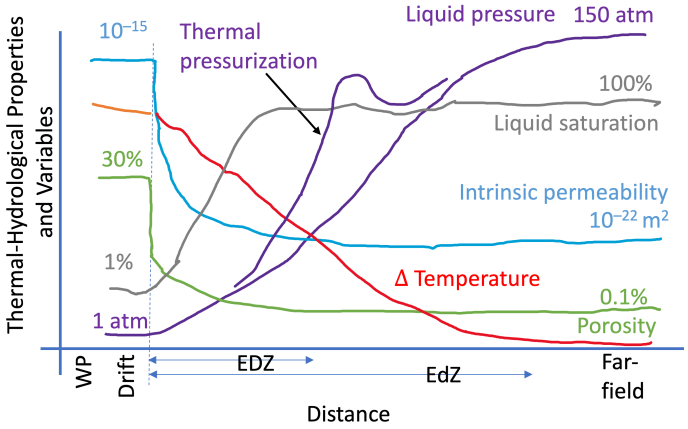

Figure 4-10. Conceptual trends in TH processes, including thermal pressurization.

If the temperature perturbation from the emplacement of waste in a repository (i.e., the thermal EdZ) extends out further than the hydrological EDZ (the region where permeability and porosity are increased due to damage) and the hydrological EdZ (to the undisturbed region where fluid pressure is nearly lithostatic and the liquid saturation is unity), the thermal pressurization could locally bring liquid pressure above lithostatic pressure, leading to hydrofracture, increase in permeability, and dissipation of the excess pressure. Therefore the hydrological EdZ is larger or approximately the same size as the region with significant thermal perturbation to cause expansion and pressure increase (i.e., the thermal EdZ), since the hydrological EDZ would grow in size due to hydraulic fracture if thermal pressurization exceeded lithostatic pressure. This is an example of the highly-coupled nature of salt; thermal diffusivity (3.5×10^{-6} m^2/s) is close in magnitude to hydraulic diffusivity (0.16×10^{-6} m^2/s) [160, Table 1].

4.2.2. *Capillarity-driven Flow*

The effect of capillarity on flow is not a separate hydrological process; it is a contributing factor in two-phase flow (H^2), but it is discussed here separately. Capillary pressure represents the pore-scale effect that surface tension in small pores or thin fractures has on the balance between gas and liquid pressures, and is given by

$$p_c = p_{\text{air}} - p_{\text{brine}},$$

where p_c is capillary pressure [Pa], and brine is the wetting fluid and air is the non-wetting fluid. The Young-Laplace equation additionally relates the capillary pressure to the air-brine surface tension on an idealized surface characterized by a single capillary radius,

$$p_c = \frac{2\gamma \cos \hat{\theta}}{R} \tag{4.3}$$

where γ is the surface tension of water [N/m], $\hat{\theta}$ is the contact angle (often considered to be small or zero, therefore $\cos\hat{\theta} \approx 1$), and R is the pore or tube radius [m].

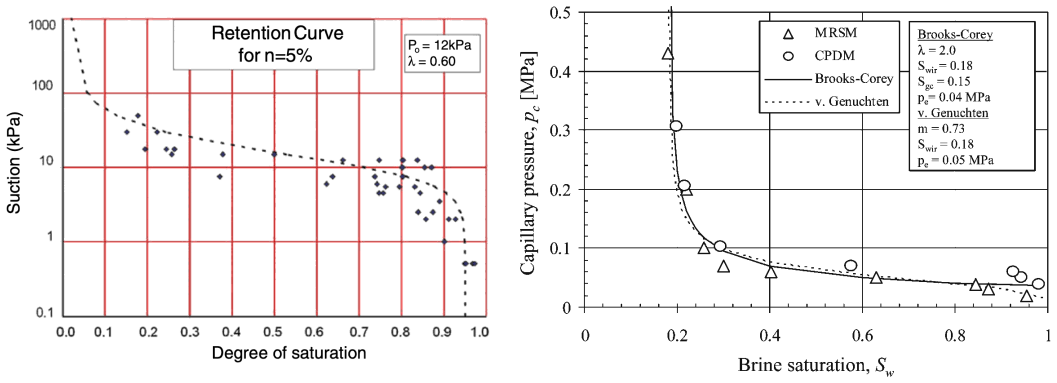

Figure 4-11. Moisture retention curve for granular salt (down to ≈ 5% porosity) [193, 41].

The capillary pressure relationship illustrated in Figure 4-11 is for reconsolidated (to ≈ 5% porosity) granular salt. The connectivity of the media is more characteristic of a porous media than fractured salt. Figure 4-12 shows capillary pressure data for a fractured anhydrite marker bed located near the disposal interval at WIPP (MB-139), which is fractured, but not strictly halite [22]. These data can be fit to relationships that can be used to predict $k_{r,\ell}$ or $k_{r,g}$ as a function of liquid saturation (e.g., see Figure 4-19). Capillarity can wick brine into a porous or fractured medium, or prevent air (i.e., the non-wetting fluid) from entering brine-saturated fractures and pores below the air-entry pressure. When the porosity gets high (i.e., an open drift or large open fracture, with large values of R in Equation 4.3), capillarity can be significantly reduced [121]; the maximum capillary pressure in an open space should be much lower than that in small pores or fractures. Reconsolidation could change the maximum capillary pressure and it may also change the shape of the moisture retention curve, but there is not significant data on this dependence (moisture retention curves are available for reconsolidated salt at two porosities [193], but these are not exhaustive).

The dryout, later re-wetting, and possible subsequent invasion of high-pressure gas into the backfill and host rock could each require different moisture retention curves (i.e., hysteresis). This is likely more important in an argillite host rock or in bentonite backfill [83, 228], and has not been considered in salt. Including the effects of hysteresis makes the numerical solution more complex, and there are few data available on salt capillary pressure curves, and there are no known data in salt for both wetting and drying.

Surface tension, and therefore capillarity, increases when salinity increases. When changing from 0 to 5 molal NaCl solution the surface tension at 25 °C increases from 72 to 81 mN/m (a 12% increase; [150]). Despite this change, salinity is often considered simplistically to be uniformly saline in a salt repository (see § 4.4, Chemical Processes). At the same time, capillarity is reduced at higher temperatures, due to the decrease in water surface tension with temperature; from 25 to 100 °C the surface tension of pure water reduces from 72 to 59 mN/m (an 18% decrease; [274]). Measurements of surface tension in different strengths of synthetic seawater at different temperatures show the combinations of these two effects [180] (Figure 4-13). Contact angles in a halite-brine system ($\hat{\theta}$ in Equation 4.3) have been observed to be near zero [259]; similar to those in a brine-silica system.

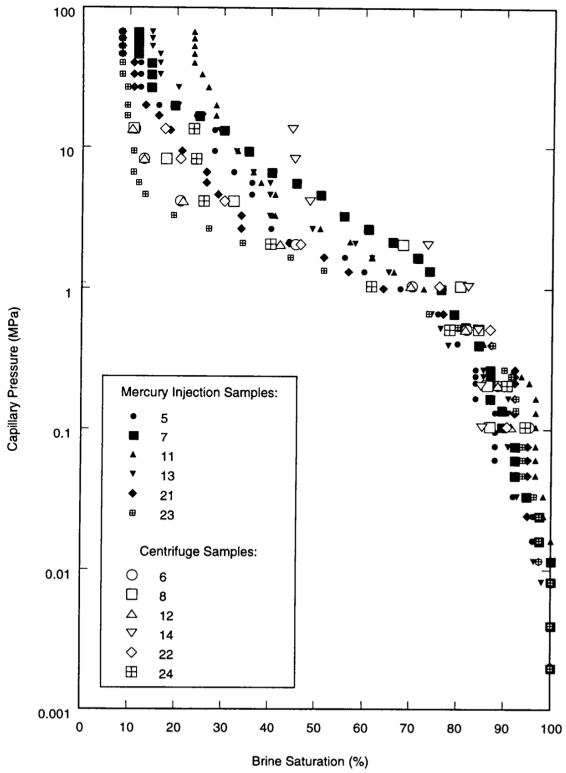

Figure 4-12. Moisture retention curve for fractured anhydrite marker beds at WIPP [105].

This reduction in surface tension with increase in temperature could lead to a release of brine in a system where the brine is held in the formation near the borehole or drift primarily by capillary forces, which would be reduced upon heating (i.e., emplacement of waste). The effect may be reduced in some part by the slight increase in brine salinity due to the temperature-dependence of salinity for NaCl, and the availability of salt to dissolve. The temperature effect on surface tension is implemented in several numerical models (e.g., PFLOTRAN, TOUGH, FEHM), but the effect salinity has on surface tension is not implemented widely, and the effect of salinity on contact angle is largely ignored for being insignificant.

Capillary effects are limited to the saturation perturbation around the excavation [129]. The saturation distribution around an excavation is related to the distribution of dilated salt which is a function of stress state and the age of the excavation. The salt is low-permeability in the far field, the mechanical damage which increases the absolute permeability and porosity near an excavation simultaneously decreases the liquid saturation near the excavation. The decrease in relative permeability in the EDZ will cancel out any increases in absolute permeability, creating a type of vapor barrier near the excavation, reducing the ability of brine to flow into an excavation (see § 4.2.5, Hydrological Properties).

In DECOVALEX-2023 Task E, a comparison was made between different modeling approaches for initializing two-phase flow models for the EDZ around a drift (i.e., the initial condition for the BATS experiment). Figure 4-14 shows the spread between model predictions for this exercise, despite the relatively strict specification of parameters and constitutive models. In this case, the EDZ was treated as a step change in properties at $r = 2.5$ m (i.e., permeability, porosity, and air-entry pressure). Some of the difference between models is due to how compressibility and storage are handled (i.e., largest effects are early time) and some is inherent to different assumptions in making non-linear two-phase flow predictions.

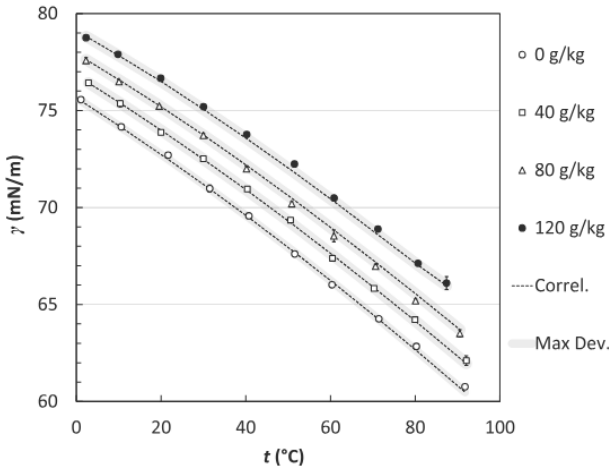

Figure 4-13. Surface tension of synthetic seawater as a function of salinity (marker type) and temperature (abscissa) [180].

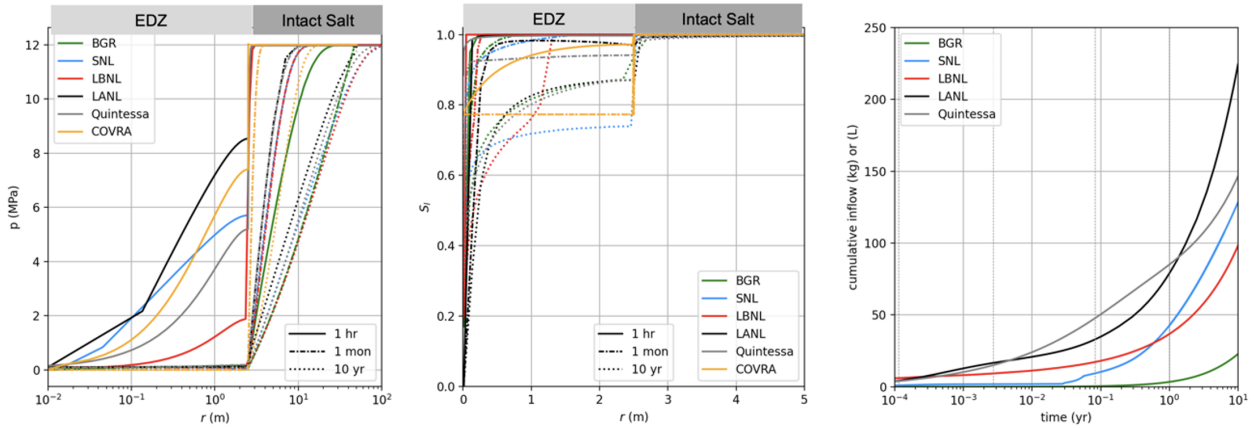

Figure 4-14. DECOVALEX-2023 Task E comparison of 1D model initializations for EDZ around a drift [133].

Additionally, as part of Task E, the Quintessa team made a comparison (Figure 4-15) of the results obtained when using different two-phase flow properties associated with data in Figures 4-11 and 4-12 (top two rows) and between using the "wetting up" and "drying down" conceptualizations (bottom row). In the drying down scenario, the EDZ region surrounding the drift has higher permeability and porosity and starts fully saturated with brine. Water then drains from the EDZ via the constant-pressure atmospheric boundary condition in the drift. In the wetting up scenario, the higher porosity and permeability EDZ region starts mostly air-filled. Water then flows into the EDZ from the intact salt. The comparison shows that even at 100 years, the two conceptualizations do not produce similar results. The simpler and more common "drying down" conceptualization results in an EDZ that is overly saturated with brine and therefore produces too much brine, especially at early time (e.g., see "DRZ rain" at WIPP [36]).

The difference between the granular (Olivella; Figure 4-11 left) and the fractured (H&C-F; Figure 4-12) capillary models results in a fairly large change in initialization (2 vs. 3 kg brine inflow per m along the axis of the drift), while the difference between the two conceptualizations results in a much larger (100×) difference in brine production. Even if the "drying down" conceptualization is only used to initialize two-phase flow models (i.e., brine inflow at early time is not assigned any physical meaning), it can have a

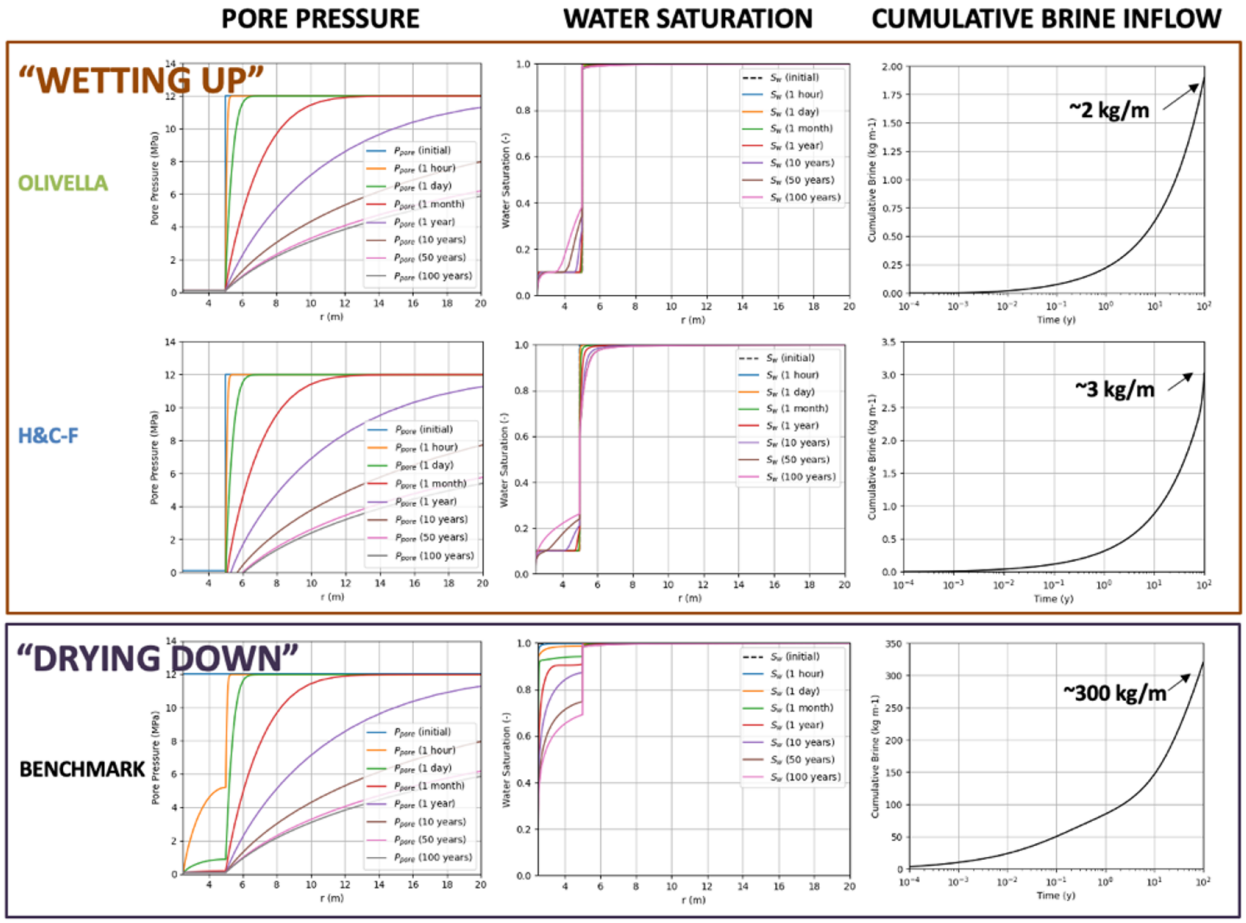

Figure 4-15. DECOVALEX-2023 Task E comparison by Quintessa for 1D model initialization in "wetting up" and "drying down" conceptualizations [133].

significant impact on the starting conditions. Two-phase flow models may require a long time to initialize (e.g., 100 years or more), and as a consequence of using the wrong initialization, the EDZ may start out too wet in PA simulations.

4.2.3. Gravity-driven Flow

The effects of gravity on flow is also not a separate process, it is a contributing factor to density-driven flow. Gravity effects become significant where two fluids of different densities exist in a pore space (i.e., gas and liquid, or brines of different ionic strengths), leading to free convection of fluid, which can then drive solute or energy convection. Changes in salinity or temperature of a single phase can also lead to significant enough density changes to drive free convection.

Multiphase or Richards' equation flow simulations can track the drainage of liquid under gravity. Only multiphase flow simulations can also track the rising of gas through a liquid-saturated medium. Coupled TH^2 models can track the effects of free convection due to thermal expansion (Figure 4-9) and coupled TH^2C models can track the impacts dissolution and precipitation of solutes has on the density of the

liquid phase (see § 4.4, Chemical Processes). Gravity can drive brine to accumulate in the EDZ below an excavation, simultaneously driving gas to rise up in the EDZ above an excavation.

In the far field, flow is essentially single-phase and brine is assumed to be of uniform density, so the initial condition does not usually involve free convection; geothermal gradients are usually too small to induce vertical convection in low-permeability media. Density effects may stabilize regional groundwater flow systems near the edge of salt deposits [207] (i.e., fresh water above saline brine is stable, but fresh water below saline is not). The density and viscosity of brine in a salt deposit may inhibit the mixing of fresh meteoric groundwater from above [75]. Breccia pipes were a hypothesized "event" FEP at WIPP, where a high-pressure fresh aquifer below the salt would suddenly and catastrophically dissolve up through the salt deposit from the bottom, driven by density (Figure 4-16). This event was then excluded through the siting process; WIPP was sited away from places where the more permeable Capitan Reef directly underlies the salt [55, 205]. The effect may also important around the edges of salt domes or at the fringes of a bedded salt deposit.

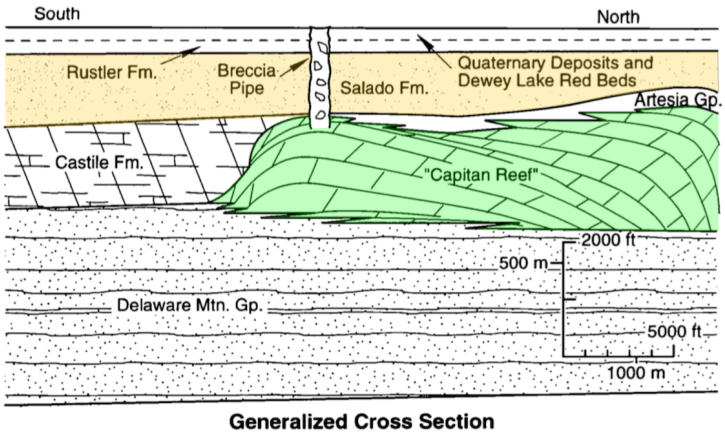

Figure 4-16. Hypothetical breccia pipe in Permian Basin [205].

In excavations at WIPP, brine is observed to accumulate in the EDZ below an excavation. The Brine Sampling and Evaluation Program at WIPP [57] established several sets of shallow vertical monitoring locations in MB-139 (a 1-m thick clay, anhydrite, and salt layer below the disposal horizon). A "water table" was observed at or near the bottom of MB-139 (Figure 4-17). Multiple low-flowrate short-duration pumping tests were performed in and between these boreholes, illustrating the connectivity of the fractures. These observations are consistent with a mostly dry EDZ surrounding the drifts, with the bottom of the EDZ (MB-139 in the floor) acting as a sump, collecting brine flowing into the EDZ surrounding rooms via gravity [137]. At WIPP, the excavations follow geologic bedding (specifically Map Unit 2, the "orange marker band"), which undulates slightly. Flow of brine is known to occur in the sump along drifts towards the regional low point, the waste handling shaft–where brine is collected and removed [137].

Heater experiments were conducted in arrays of 1-m diameter vertical boreholes in the late 1980s and early 1990s in WIPP Experimental Area Rooms A and B [177, 178]. Several of the vertical heater boreholes were also instrumented to measure brine inflow [187, 189], which encountered significant brine ($\approx$ 22 L of water collected per borehole per year [187]), which was attributed to clay layers intersecting the boreholes. The main clay layer intersecting these boreholes was Clay F, which is a relatively minor and disseminated

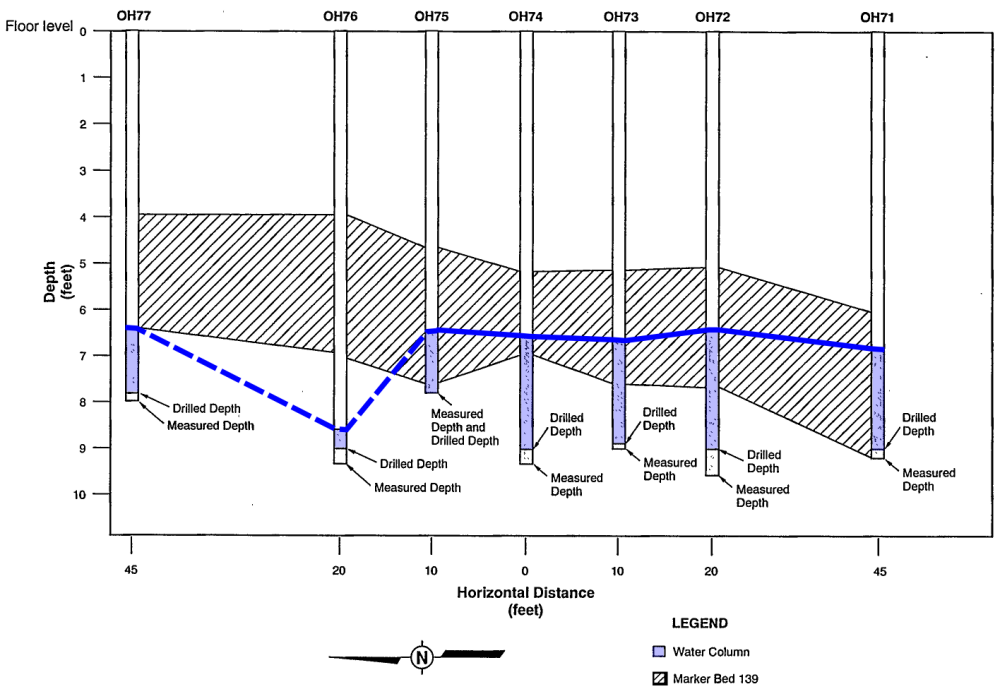

Figure 4-17. Water table observed in shallow MB-139 boreholes in the EDZ at WIPP. Modified from [57, Appendix E].

clay layer (contrasted to Clay E at the base of MB-139). In retrospect, it is likely that the brine accumulated in these heated boreholes was largely due to the "sump" effect, which is consistent with observations in other unheated vertical boreholes at WIPP (Figure 4-17).

This gravity driven collection effect is one reason to avoid disposal of waste in vertical boreholes in bedded salt (domal salt is drier). Instead, disposing into horizontal boreholes or placing waste packages on the drift floor would avoid the region that could potentially become a "sump" for brine to accumulate. Since the EDZ porosity is comprised of fractures, it does not have significant porosity (< 5%), and therefore it does not take a large volume of brine to fill the sump. A primary reason to install waste into boreholes is to take advantage of the higher thermal conductivity of intact salt (approximately 10× higher than granular salt). In domal salt, less brine would be expected, and the benefit of higher thermal conductivity near the waste package (intact vs. granular salt) may outweigh any concerns there for potential brine accumulation. In crystalline disposal concepts (e.g., Finland and Sweden), vertical disposal boreholes are used, but the bentonite backfill hydrates and swells to keep free water away from the waste packages. This is a difference between a salt disposal concept that may keep the waste packages dry as long as possible, and the crystalline concepts that maintains the waste packages in the saturated zone. Additionally, the disposal drifts could be designed with a slight slope to drain and collect brine away from the waste packages.

4.2.4. Gas Generation

Gas generation processes generally convert solid and liquid substances to non-condensable gas, increasing the gas pressure and potentially driving transport away from the repository. There are some gas pressure increases that occur without the generation of gas, but gas generation is often considered the major factor

contributing to high gas pressures at late time in PA simulations [223, 224]. High gas pressures are also a concern in argillite and crystalline repositories. Since salt repositories have the potential to be drier than argillite and crystalline repositories, they may have potential for less gas generation.

Assuming the shaft seal readily saturates with brine at some point along its length and becomes gas tight (i.e., its relative gas permeability goes to zero), gas pressures in the repository will rise. One gas pressure increase mechanism in a salt repository is creep closure of the formation during the period of reconsolidation (i.e., reduction in repository volume during the first few 100 years). Additionally, the heat from the waste will cause some minor temporary gas pressure increase due to thermal expansion of the gas in the repository (i.e., gas expansion due to Charles' Law). Finally, the main source of gas pressure rise is associate with gas generation (i.e., increase in the number of moles of gas).

Gas generation is a source term of gas in two-phase TH^2 models (e.g., TOUGH2, PFLOTRAN, FEHM). Gas generation may be dependent on the local conditions (e.g., temperature and liquid saturation), but sometimes it is simply specified at an expected rate regardless of local conditions. While Richards' approximation [215] can be used to simulate migration of liquid brine due to gravity and capillary effects, this approximation cannot be used to simulate the effects that may arise due to the accumulation of gas pressure from closure, thermal effects, or gas generation. Explicit two-phase flow of liquid and gas is needed to understand the accumulation and effects of elevated gas pressure in a repository.

4.2.4.1. Gas Generation Mechanisms

Gas can be generated in a repository via several mechanisms, and excessive gas generation can create high gas pressures in the repository during later post-closure [88, 181]. Primary gas pressure mechanisms include:

- anoxic corrosion of metals (i.e., Fe, Cu, Al) in the presence of brine, producing H_2 or H_2S;
- microbial metabolism of cellulose (i.e., wood), plastic, and rubber, producing CO_2 or CH_4;
- radiolysis of water, producing H_2 and O_2; and
- generation of gaseous daughter products during radioactive decay, producing $^4He^{2+}$ and Rn from alpha decay or producing Kr and Xe during spontaneous fission.

Anoxic corrosion gas generation can happen with copper, aluminum, or iron, all resulting in the production of H_2 or H_2S gas. Although aluminum and copper metal are more reactive in brine than iron, there is expected to be small amounts of them in the repository. There should be significantly more iron in a repository for spent fuel (e.g., low-carbon steel), so this is the main reaction considered [261]. Gas generation from iron corrosion can be written as [29, 28]

$$Fe + (x + 2)H_2O_{(\ell)} \rightarrow Fe(OH)_2 \cdot xH_2O + H_{2(g)},$$

where liquid water is a reactant and gaseous hydrogen is a product, leading to the large increase in volume (assuming a relatively small volume difference between the reactant and product solid phases). If the reactant water is instead vapor, the associated change in volume will be much less significant (i.e., less pressure generated). Pressure from generation rates are significantly less in a vapor-limited (i.e., "humid")

environment, compared to a system with excess water [54] (see § 4.4.4, Corrosion). Anoxic corrosion strongly depends on the availability liquid water.

Microbial gas generation [74] is expected to be limited in a salt spent-fuel and high-level waste repository because 1) there are limited amounts of cellulose, plastic, and rubber (i.e., the WIPP PA considers these significant for its waste stream), and 2) there are limited number of halophilic microbes that can thrive in a halite environment where the activity of water is < 0.75 [183]. Microbial gas generation strongly depends on the availability and activity of liquid water. Microbes (if viable) may also consume excess gas, especially H_2 . Any halophilic microbes that consume H_2 could reduce excess gas pressure from anoxic metal corrosion.

Radiolysis of water will occur in the presence of ionizing radiation, but is generally a slow process, and does not contribute significantly to the overall gas pressure compared to the expected gas generation rates of anoxic corrosion [62]. Radiolysis strongly depends on the availability of water.

The generation of ^{4}He or radon from alpha decay or krypton and xenon from spontaneous fission are a minor source of gas pressure that is independent of the availability of liquid water. The process will occur in a dry, intact spent fuel cask, and also occurs during surface storage [98, 97].

4.2.4.2. Consequences of High Gas Pressure

Excessive gas pressure can lead to hydrofracture (and increase in porosity and permeability) if gas pressure exceeds the least principle stress, believed to be close to the lithostatic stress in the far-field [283]. Even if the gas pressure does not lead to hydrofracture, it will slow down or even reverse creep closure of openings, by reducing the deviatoric stresses [240], and it can change patterns of brine migration that would otherwise exist [54]. At closure, brine flow is largely directed from the far-field to the low-pressure excavation, while increased repository pressure could stop or reverse this trend.

Gas permeation into brine-filled pores allows the gas to migrate into the formation (i.e., to develop interconnected gas pathways). This process would be limited by the air-entry pressure characteristic of the formation. Media that are fully saturated with brine are impermeable to gas, until the capillary forces resisting the penetration of gas into the medium have been overcome and a network of interconnected gas pathways are established. The gas-threshold and air-entry pressures ($p_{gt} = p_e + p_\ell$, where p_{gt} is gas-threshold pressure, p_e is the air-entry pressure, and p_ℓ is the liquid or formation pressure) are important parameters related to two-phase flow behavior. Air-entry pressure is the pressure required for air to enter a liquid-saturated sample [53]. It can be estimated through laboratory or field experiments, but is often empirically related to permeability or pore/fracture aperture (Figure 4-18). Lower permeability materials tend to have high air-entry pressure, since both are related to the pore radius or fracture aperture. Reconsolidation of salt should change the air-entry pressure, which can affect the moisture retention curve too.

Field tests were conducted in boreholes at WIPP to estimate the air-entry pressure of anhydrite interbed MB-138 [218, Appendix E]. These experiments were mostly unsuccessful, but one test found the air-entry pressure to be much lower (≈ 0.2 MPa) than the lithostatic stress (15 MPa), indicating gas would likely invade the formation well before it builds up to a pressure that could lead to hydraulic fracturing. This value estimated from field testing is also lower than that predicted by the correlation in Figure 4-18.

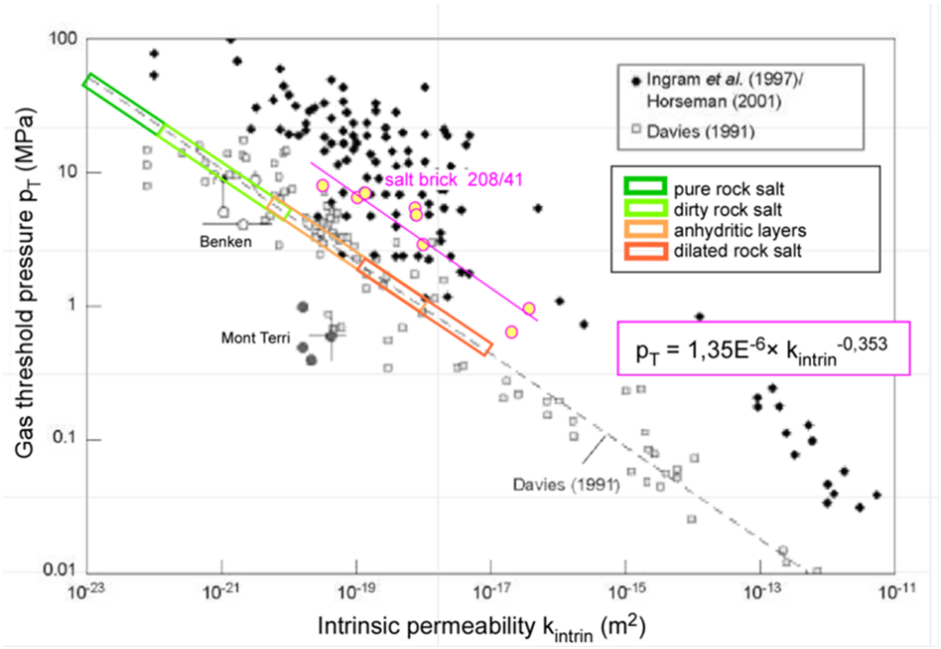

Figure 4-18. Relationship between permeability and gas-threshold pressure in salt [231].

Some of the generated gas will dissolve into the formation brine (reducing the total volume and pressure), as the air pressure rises in the repository. The solubility will depend on the species of gas that generated (noble gases, H_2, CO_2, or O_2), total pressure, and temperature. The solubility of air, H_2, or noble gases in brine are mostly known as a function of temperature and total pressure, and can be found in the literature [49, 68, 123]. Two-phase flow simulators (e.g., PFLOTRAN, TOUGH2, FEHM) can track the dissolution of gas into the liquid phase, and the diffusion of dissolved gas, if the relevant solubility data are available for the gases of interest. Hydrogen may also react with minerals or microbes, reducing the gas pressure [275].

4.2.5. Hydrological Properties

Permeability, porosity, tortuosity, and the moisture retention curve are hydrological properties that vary significantly from the drift, across the EDZ, to the far field.

Intrinsic permeability and porosity increase significantly around an excavation over their very low, undisturbed far-field values [132]. The intrinsic permeability of the EDZ can be several orders of magnitude higher than the far field, and the porosity of the EDZ can be a factor of 10 or 20 higher than the far field (Figure 4-19).

Figure 4-19 shows possible distributions of porosity, permeability, saturation, and relative permeabilities for gas and liquid phases around an excavation, extending the power-law approach of Kuhlman [132] to two-phase flow. First, porosity is assumed to vary like

$$n(r) = \max(n_{\text{drift}} \, (r/r_0)^{-\eta} \, , n_{\text{far}}),$$

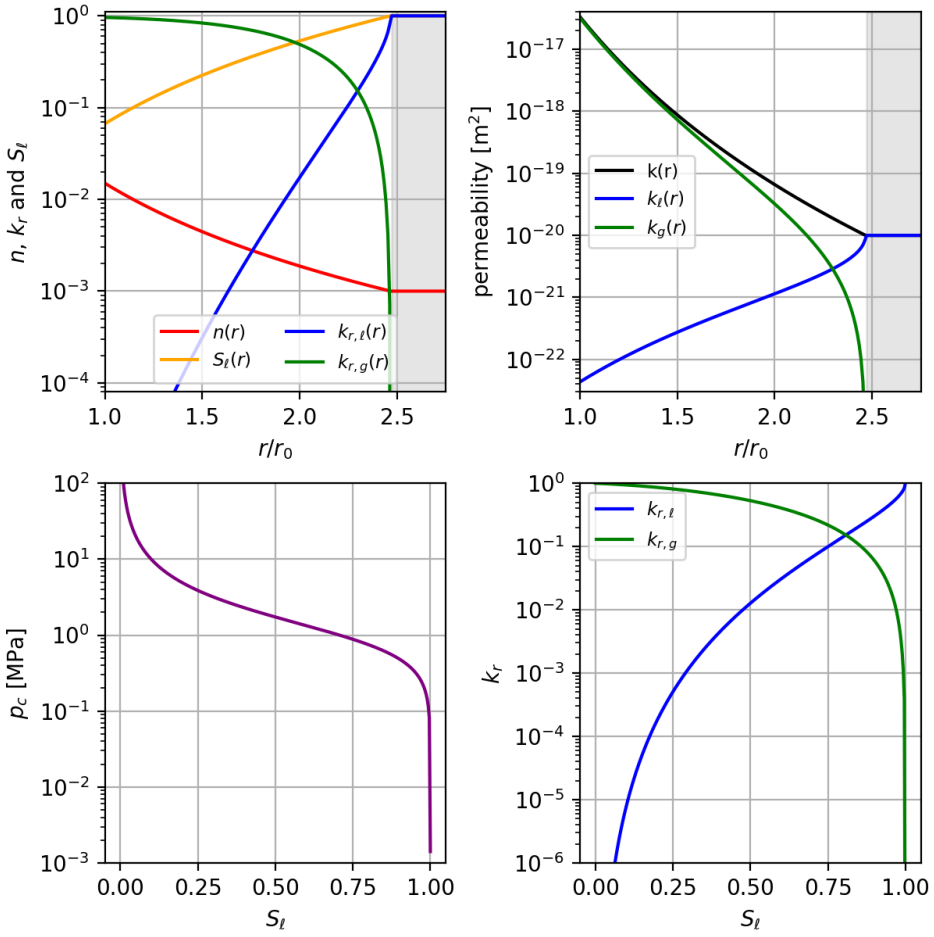

Figure 4-19. Permeability, porosity, and relative permeability predicted across an EDZ, assuming power-law porosity and permeability, and two-phase flow properties. Gray areas indicate intact salt.

where r is the radial distance away from the center of the drift [m], r_0 is the drift radius, $n_{\text{far}} = 0.001$ is the far-field porosity, $n_{\text{drift}} = 0.015$ is the porosity at the drift wall, and $\eta = 3$ is a dimensionless power-law exponent. Next, the permeability is assumed to follow

$$k(r) = \texttt{max}(k_{\text{drift}}\,(r/r_0)^{-\eta\cdot\beta}\,, k_{\text{far}}),$$

where $k_{\text{far}} = 10^{-20}$ is the far-field permeability [m^2], k_{drift} is selected to make $k(r)$ continuous at the outer edge of the EDZ, and $\beta = 3$ is another dimensionless exponent; permeability is related to porosity as $k(r) = n(r)^\beta$. Then, the liquid saturation is assumed to be

$$S_\ell(r) = n_{\text{far}}/n(r),$$

where all new damage-derived porosity is assumed to be air-filled. This is consistent with the "wetting up" conceptual model in Figure 4-15. Lastly, the capillary pressure model and the relative permeability models are based on the data for fractured marker bed core (Figure 4-12). The values used here are just for illustration of trends.

Figure 4-19 shows the liquid permeability ($k_\ell = k \cdot k_{r,\ell}$) is highest at the far edge of the EDZ and the gas permeability ($k_g = k \cdot k_{r,g}$) is almost equal to the intrinsic permeability across most of the EDZ. The

EDZ behaves somewhat like a vapor barrier does in a landfill cover design, to keep out liquid water. This observation, along with the gravity drive of brine to the "sump" of EDZ fractures below the room, would then lead to collection of brine from the far field, *mostly along the outer edge of the EDZ*. In reality, some brine is also released inside the EDZ due to various sources (i.e., not all brine originates from the far field, see § 3.2, Brine Migration) and mine ventilation removes some moisture from the salt, too.

During drift closure and healing of the damage associated with the excavation, the porosity will be reduced, eventually back to the undisturbed state. Permeability will also be reduced during healing, but the relationship between porosity and permeability is not always a simple linear relationship (even on log-log scale; [138]). Sometimes a small change in porosity can lead in a huge change in permeability, depending on the connectivity of the porosity. Permeability in the EDZ surrounding a room is also directional, with fractures preferentially forming parallel to the drift walls (Figure 4-1).

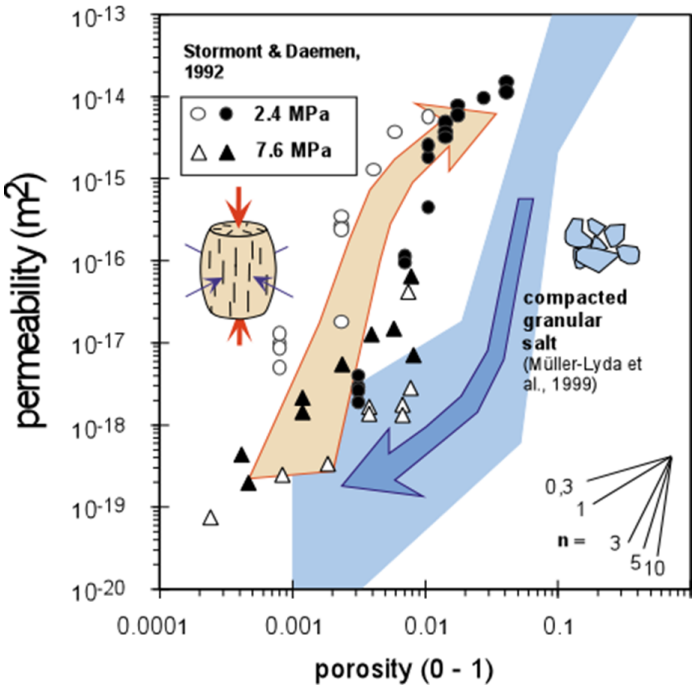

Figure 4-20. Porosity-permeability data for dilating (orange) and reconsolidating (blue) salt [203]. Slopes of power-law exponents shown in inset.

Porosity holds a special place among the parameters in the THMC problem, because it can be changed by several processes and it controls the extent of convection through the domain. Mechanical damage (i.e., volumetric strain) and healing can increase or decrease the porosity, along with chemical precipitation and dissolution. Permeability is often given simply as a power-law relation to porosity (e.g., Figure 4-20, [138]). Tortuosity is often a function of porosity and phase saturation. Capillary pressure distributions have been shown to depend on porosity [121]. Heat conduction and mechanical deformation are the primary processes that do *not* exclusively rely on porosity, since they are effective through the solid matrix, as well as the open pore space. Heat convection, radiation, hydrological processes, and chemical processes all depend explicitly on a connected gas- or liquid-filled porosity.

Porosity in undisturbed salt is associated with very small inter-granular apertures (Figure 4-21), which tend to be dominated by surface forces (e.g., held or influenced by electrostatic forces associated with

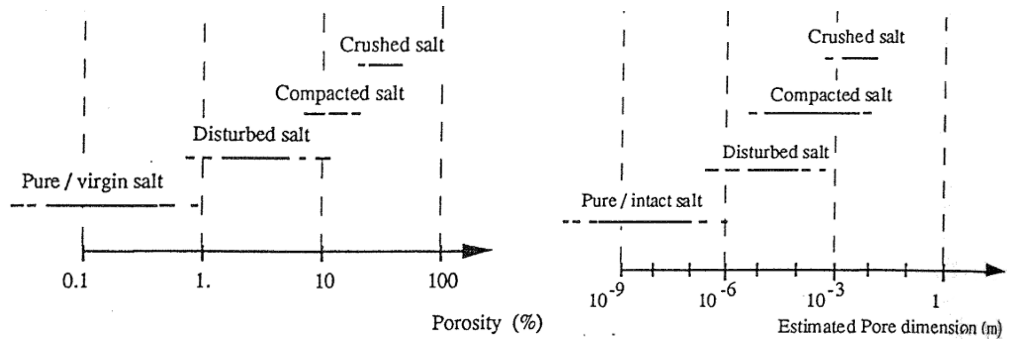

Figure 4-21. Porosity and pore size around a salt excavation [47].

the mineral phase). A large number of small pores and tight fractures contribute significantly to the specific surface area (surface area per volume [1/m]). Granular salt backfilled in the excavation behaves much more like a traditional porous medium, with pores, pore throats, and significant connectivity. Microfractures added to the salt due to excavation or heating/cooling damage tend to be planar structures, which only have an aperture and roughness, with lower overall connectivity. The connectivity of porosity is captured implicitly in the relationship of porosity to permeability and tortuosity. A non-zero porosity can be associated with a zero permeability or tortuosity, if the porosity is disconnected (Figure 3-2c)

A pore distribution conceptual model (e.g., bundle of capillaries, parallel fractures, or fractal pore networks [66, 229]) can be used to derive the moisture retention curves and tortuosity factors. Porosity is an important variable that impacts anything occurring exclusively in the pore space, the pore model and pore-size distribution and further constrain this important backbone of hydrological processes, discriminating between granular and fracture-based media [138] (Figure 4-20). As mechanical deformation (i.e., damage and healing or hydrofracture) or chemical processes (i.e., precipitation and dissolution) occur in the salt, the porosity changes, ideally the permeability, pore distribution, and specific surface area should also change.

Dissolution and precipitation only occur in the smaller liquid-filled pores in a two-phase medium, preferentially changing these smaller pores while leaving larger air-filled pores unchanged. Mechanical deformation may occur differently in gas-filled pores compared to liquid-filled pores, based on impacts of fluid-assisted deformation and pressure solution [107, 108, 281] and the effects that soil matric potential has on effective stress [293]. The air-entry pressure or gas-threshold pressures have been shown to be correlated to the formation permeability [53] and porosity (larger pores have lower air-entry pressures). Further, the maximum capillary pressure of a formation that changes porosity significantly (i.e., during dissolution and precipitation) has been shown to be a function of porosity as well [121].

The evolution of the natural salt and EDZ are important, but we must also consider the evolution and hydrological stability of the EBS components. Cement seals are an integral component of the EBS in a salt repository. They would be placed at the ends of a seal of granular salt. The granular salt will be used to provide long-term sealing function in a repository, that will take over the sealing function from the cement abutments before the failure of the cement sealing elements (i.e., their accumulation of damage and increase in permeability) due to loading and creep, depending on whether the seals are brittle or can creep (i.e., made with granular salt as aggregate). Cement seal exposure tests have been conducted as part of the Small-Scale Seal Performance Tests at WIPP [258, 270], but mostly from the point of view of the hydrological isolation provided by the seals. Seals need to guarantee immediate strength to hold

against convergence of the host rock, and seals need to have a specified minimum permeability at early time (e.g., 10^{-18} m^2). Full-scale drift sealing demonstrations have been conducted at Morsleben [291], with extensive in situ monitoring and sampling of the seal-salt interface. Asse has seen significant isolation of mined regions by filling and sealing mined areas with Sorel cement backfill [71], to both slow down overall salt-dome convergence and plug potential pathways for migration of brine within the facility.

4.3. Mechanical Processes

Rheology is the field of study of flowing materials that exhibit both fluid and solid characteristics, including salt [152]. The mechanical deformation of salt results from the configuration of and time rate of change in stress and strain around an excavation, including damage accumulation, creep closure, thermal expansion, hydrofracture, and healing [113, 44, 112]. The primary mechanical variables are stress [σ, Pa], strain [ϵ, m/m], and strain rate [$\dot{\epsilon}$, 1/s].

There are several modes in which salt deformation takes place [117]:

- cataclastic fracture of intact salt or salt grains;
- intergranular movement (e.g., grain rotation in granular salt);
- intergranular dislocation and gliding (i.e., damage-free creep); and
- diffusive mass transfer in liquid films (i.e., pressure solution).

Unlike many other rocks and geomaterials, salt readily creeps at ambient temperatures and pressures (rather than only at conditions found in the Earth's mantle). At ambient conditions (298 K), salt is at 28% of its melting point (1074 K). Unlike metals, which also experience dislocation creep, pressure solution is a significant micro-mechanical deformation process in salt [23]. Like salt, water ice creeps and experiences grain-boundary melting, which is analogous to pressure solution [285, 126].

Elastic stress-strain behavior is (at the speed of elastic wave propagation, $\approx 4.5\,km/s$ [100]), rate-independent, and reversible. In salt elastic deformation is often a relatively small strain component compared to the magnitude of strain associated with long-term creep closure of excavations, although a non-trivial amount of early elastic deformation can happen when a room is first excavated due to the significant stresses at depth [213]. Plastic damage is initially irreversible, rate-independent, and accumulates when the material exceeds its yield strength (i.e., based on stress state). Viscoelastic creep is an initially irreversible and time-dependent change that relates the deformation rate to the stress state [121]. All damage in salt is eventually reversible, through creep closure of porosity and healing or suturing of salt across closed micro- and macro-fractures.

Most laboratory creep testing is concerned with characterizing steady-state creep behavior, rather than the early transient creep phase, or the tertiary phase usually seen just before failure (Figure 4-22). During viscoplastic creep the rock slowly and continuously deforms under a constant differential stress, like a very viscous fluid (effective viscosity of halite at repository conditions is about 3×10^{-8} Pa · s [76]).

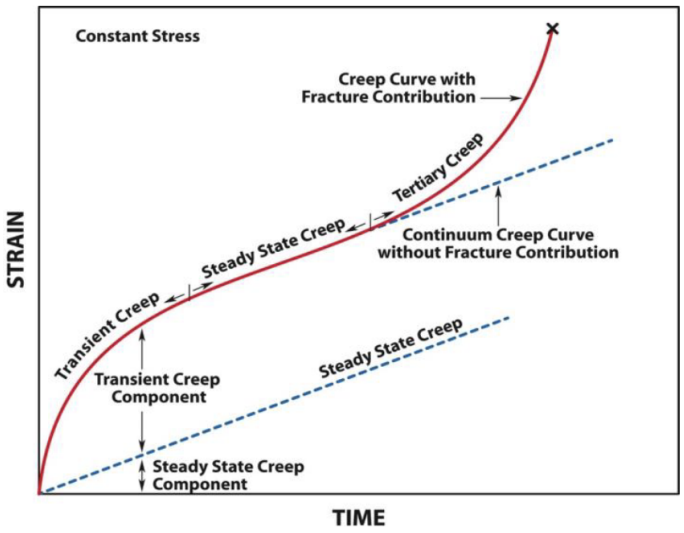

Figure 4-22. Illustration of different stages of salt creep [93]. Elastic response at $t = 0$ not included.

4.3.1. Salt-Specific Constitutive Models

Early transient phases of creep are characterized by micro-mechanisms that lead to strain hardening (i.e., concave down part of red curve in Figure 4-22) and later tertiary phases are dominated by micro-mechanisms that lead to strain softening (i.e., concave up part of red curve in Figure 4-22) [93]. The macroscopically observed transient and steady-state creep stages are due to multiple simultaneous small-scale processes (e.g., dislocation multiplication, dislocation movement [glide, cross slip, and climb], pressure solution creep, recrystallization/healing [93]), active at different pressures, temperatures, relative humidity, and strain rates [175, 39, 210]. Hot salt creeps faster than cold salt and its temperature dependence is often related to an exponential Arrhenius term, and small amounts of moisture speed up salt creep (i.e., enough liquid to make continuous films that enable the pressure solution mechanism) [80]. It seems the different micro-mechanical deformation mechanisms should contribute in different ways to the macroscopic system variables of volumetric strain (i.e., porosity), tortuosity, permeability, specific surface area, and the moisture retention curve, but this is currently not accounted for in models.

Not all combinations of stresses applied to the salt result in permanent damage, or an increase in porosity. The dilatancy boundary delineates stresses that result in damage from those that do not. Figure 4-23a shows two different dilatancy boundaries in salt, the red one for triaxial tests where the maximum principal stress (σ_1) is axial and the green one for triaxial tests where σ_1 is radial (also called an "extension" test). The abscissa ($I_1 = \sigma_1 + \sigma_2 + \sigma_3$) is the first stress invariant (hydrostatic or confining stress), and the ordinate is the square root of the second deviatoric stress invariant, proportional to octahedral shear stress, more specifically $J_2 = \frac{1}{6}\left[(\sigma_1 - \sigma_2)^2 + (\sigma_2 - \sigma_3)^2 + (\sigma_3 - \sigma_1)^2\right]$ [90]. Conditions above these curves (higher deviatoric stress for the same confining stress) result in dilatancy or the accumulation of microfracture damage. Still larger deviatoric stresses can result in failure ("F" curve in Figure 4-23b). Conditions below the dilatancy boundary are isochoric (constant volume) and do not result in accumulation of microfracture damage, and lead to the eventual closure of fractures and healing [203, 233]. Damage tends to accumulate near excavations in unconfined regions, where I_1 is relatively low and J_2 is relatively high. Further from the excavations, the salt tends to be damage free, due to lower deviatoric stresses and

higher confining stresses.

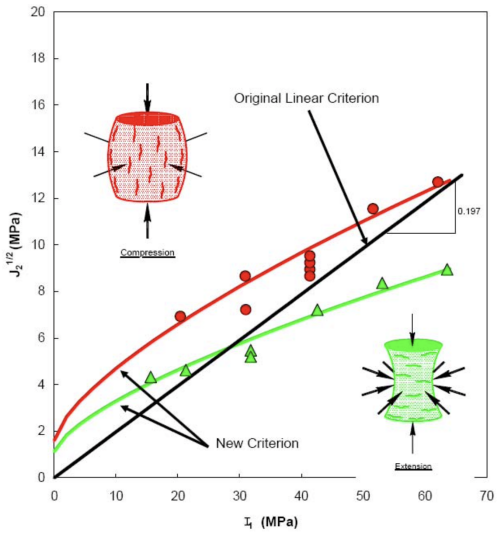

(a) Dilatancy boundaries for compressional and extensional tests [100].

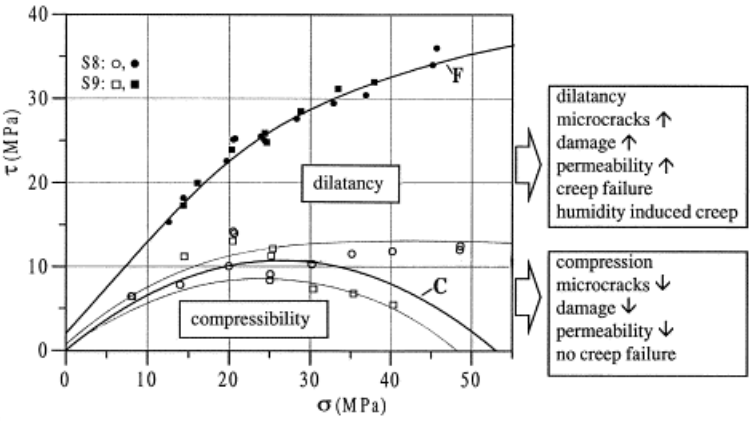

(b) Failure (F) and compressibility (C) boundary separating domains "compressibility" and "dilatancy" for salt [109].

Figure 4-23. Dilatancy boundaries for laboratory triaxial tests in salt.

Testing of bedded Salado Formation salt in Germany as a part of the historical "Joint Project III" international collaboration observed a constancy of the dilatancy boundary with respect to temperature (over the range $20 \leq T \leq 100\,^{\circ}\mathrm{C}$) and strain rate ($10^{-6} \leq \dot{\epsilon} \leq 10^{-4}\,1/\mathrm{s}$) [230, 67]. This constancy then supports the relevance of the dilatancy boundaries determined in the laboratory to field conditions. Figure 4-23b also shows a region of compressibility ("C"), where healing occurs.

The repository relevant geomechanical problem is typically a static balance of forces ($\sum_i F_i = 0$), ignoring inertial terms ($\sum_i ma_i$) due to the very slow speed of mechanical movements (except during fast events like rockfalls [212] or to track propagation of elastic waves like acoustic emissions). The geomechanical problem then maps forces and the corresponding stresses onto strains and displacements through a constitutive law (e.g., Hooke's law) [209]. Viscoelastic effects are included through stress-strain rate relationships. Versions of these constitutive laws can include the effects of changes in temperature (i.e., thermoelasticity [195]), pore pressure (i.e., poroelasticity [279]), or both (i.e., thermoporoelasticity [48, 234]). Mathematically, thermoelasticity and poroelasticity have analogous formulations; changes in pore pressure or temperature have analogous effects on stress [279].

The isotropic elastic response (i.e., generalized Hooke's law) for primary direction stress in terms of strains in the same direction, other primary direction stresses, pore pressure, and temperature is

$$\sigma_1 = E\epsilon_1 + \nu\left(\sigma_2 + \sigma_3\right) + \alpha p + bKT, \tag{4.4}$$

where stress, pore pressure, p, [Pa], and temperature are changes from an initial value (i.e., not absolute values), E is Young's modulus [Pa], K is the bulk modulus [Pa], ν is Poisson's dimensionless ratio, α is the dimensionless Biot-Willis coefficient, and b is the coefficient of volumetric expansion [1/K]. This constitutive behavior is a link between the kinematic (i.e., displacement or strain) and dynamic (i.e., forces

or stresses) responses of the system. The poroelastic and thermoelastic responses are dynamic contributions (i.e., stresses derived from changes in temperature or pore fluid pressure).

The generally non-Newtonian viscous steady-state response of strain rate to deviatoric stress (i.e., steady-state creep rate), can be given by the Norton power law [152]

$$\dot{\epsilon}_{\text{norton}} = A_0 e^{-Q/R\theta} (\sigma_1 - \sigma_3)^n, \tag{4.5}$$

where n is an empirical exponent, $\Delta\sigma = \sigma_1 - \sigma_3$ is the differential stress [Pa], A_0 is a material-dependent parameter analogous to viscosity with an exponential Arrheneius temperature-dependence term (θ in K), Q is an activation energy [J/mol], and R is the universal gas constant ($R = 8.314$ J/(mol $\cdot$ K), balancing the dimensions of typical activation energy). Equation 4.5 has the form of Newtonian viscosity for $n = 1$.

For viscoplastic materials, different combinations of spring (elastic), dashpot (viscous), and sliding block (perfectly plastic) elements can be combined in parallel and in series to result in more complex and physically realistic constitutive models (e.g., Kelvin or Burgers [72]). The effect of changes in fluid pressure or temperature are associated with the elastic element, and combined with viscous elements to result in time-dependent thermal-poro-viscoelastic models.

The mechanical properties of the salt (i.e., Young's modulus, bulk modulus, shear modulus, Poisson ratio and creep constitutive law properties) may change smoothly as a function of damage across the EDZ to the far field [148]. Some constitutive models include this (e.g., Lux-Wolters), but other constitutive models (e.g., Munson-Dawson) do not [209, 210].

4.3.2. Modeling Repository Mechanical Processes

We differentiate between mechanical models with infinitesimal-deformation elastic behavior and large-strain behavior, with and without with creep constitutive laws. We also consider the difference between purely mechanical models, and models with thermomechanical coupling, poroelastic coupling, or both. Some modeling approaches approximated the deformation of a salt, brine, and gas system as being made up solely of different fluids.

FEHM and PFLOTRAN both have some ability to simulate infinitesimal mechanical deformation (e.g., include effects of thermal expansion of the solid phase on the changes in fluid pressure, as shown earlier in Figure 4-9), but are not considered viable mechanical models for long-term salt simulation without the ability to simulate creep and large deformation (e.g., closure of drifts). Sierra Mechanics, FLAC, and OpenGeoSys have the ability to handle large deformations. Salt often requires complex constitutive laws, that are not commonly used for other rock types [296, 210, 89]. Not all geomechanical simulators capable of large strains are also useful for salt. TOUGH-FLAC has been developed to accommodate large deformations and use modern salt constitutive models [227, 18, 264].

Predictions of simultaneous flow of salt, brine, and gas at WIPP was once cleverly treated in an approximate manner using a three-phase hydrological flow model (i.e., TOUGH2 EOS8 for liquid, gas, and "dead oil"), by changing the viscosity and density of the oil phase to that of salt [76]. Although it captures some characteristics of salt behavior (i.e., viscoelastic creep), the elastic response is only in terms

of pressure (i.e., I_1); the shear response of the medium is neglected. Fluids cannot sustain shear stresses without continuously straining.

The mechanical initial condition for a repository is usually an undisturbed state (i.e., just before the excavation is made), with the overburden stress and self-weight of the rocks being the primary driving force. Since salt cannot support differential stress long-term (i.e., creep will dissipate any differential stress), salt tends to be in a hydrostatic stress state far from interfaces or excavations. Mining out the underground excavation for the repository leads to a large differential stress perturbation that creates the EDZ and drives creep closure [213]. Figure 4-24 shows how the distribution of radial and hoop stresses around an excavation lead to the development of the EDZ (i.e., dilation or porosity) at three different times. In the uppermost panel (earliest time, immediately after excavation) the differential stress ($\sigma_\theta - \sigma_r$) is maximum at the drift wall. This exceeds the dilatancy boundary, resulting in plastic damage (gray bar in subsequent panels), which tends to grow with time.

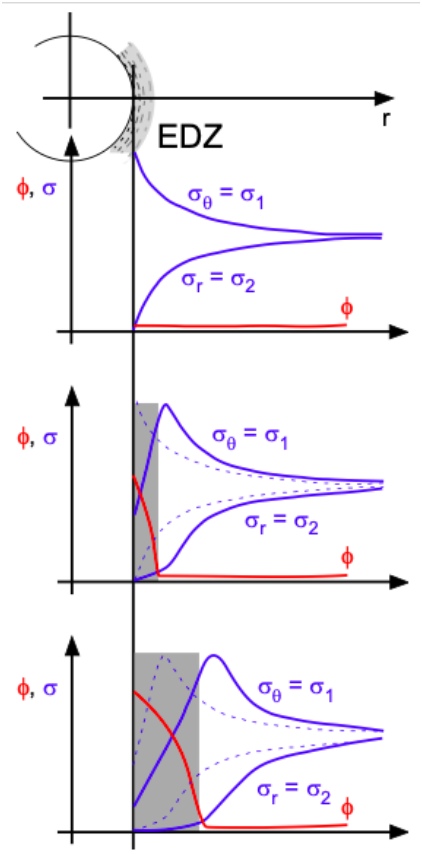

Figure 4-24. Temporal evolution of radial (r) and azimuthal (θ) components stress and strain (porosity, ϕ) contributing to the EDZ (gray) around an idealized circular 2D salt excavation [202].

Granular salt in a backfilled drift has quite different mechanical properties from intact salt and requires using a different constitutive law from the intact or EDZ salt [35, 194], but eventually the backfilled salt will also reconsolidate to the properties of intact salt in the far field [175]. Consistent mechanical constitutive laws should be used for intact, damaged, and reconsolidating salt, since in reality these different types of salt exist on a continuum, and they should smoothly evolve from one type another, during repository post-closure. Granular salt is used as a backfill material in the EBS because it is readily available (i.e., does

not need to be brought in from another location) and it will evolve back into the same material as the host rock with time. While the exact details regarding the timing of the reconsolidation of granular salt are complex, it is generally understood that the process will ultimately happen [50, 79, 96]. Drift closures and shaft seals include granular salt seals, along with other complimentary components (see § 2.3, Engineered Barrier Systems).

4.3.3. Creep at Low Deviatoric Stresses

It has become clearer in the last ten years, pressure-solution deformation mechanism is very important in salt at low deviatoric stresses (i.e., low von Mises effective stress or octahedral shear stress). Field creep rates will be significantly underestimated if steady-state laboratory creep test results at large deviatoric stress ($\gg$ 8 MPa) are extrapolated to low stress levels (Figure 4-25). Despite most laboratory testing being done at higher differential stresses, low differential stresses are expected to exist over a large volume of rock surrounding the repository for a long period of time.

At higher differential stresses, behavior is often described by a Norton power law (i.e., Equation 4.5; a straight line on a log-log plot) with $n = 6$ to 7, but at lower stresses, pressure solution requires a unit slope in this model [250]. Pressure solution is a pore-scale MC coupled process [23, 281]. Excess chemical potential drives dissolution of asperities that are stress concentrations, and diffusion of brine in thin films allows migration of excess concentrations to precipitate at regions of lower chemical potential. Small grains or crystals experience faster pressure solution creep than large-diameter grains. Pressure-solution creep can be described using a Newtonian viscosity model [152]

$$\dot{\epsilon}_{\text{ps}} = B_0 e^{-Q/R\theta} \left(\frac{\sigma_1 - \sigma_3}{\theta D^3} \right) \tag{4.6}$$

where B_0 is a material parameter with an Arrhenius term (like Equation 4.5), and D is a grain size [m]. Pressure solution is relatively a more important mechanism in fine-grained (small D) salt than in coarse-grained salt [251]. Pressure solution is more grain-size dependent than temperature-dependent at repository relevant conditions (see large difference in responses at high deviatoric stress for different temperature curves in Figure 4-25). The Arrhenius temperature dependence in B is balanced to some amount by the θ in the denominator of Equation 4.6. A very fine-grained backfill could be engineered to speed up pressure solution creep (the effect of grain size is not shown in Figure 4-25).

Given that a large volume of the salt surrounding an excavation will be in this low deviatoric stress regime, the effect of pressure-solution creep can be significant at the field scale and over long times. This raises the possibility of waste package sinking over the life of the repository (given their high temperatures and their high density compared to salt), essentially the reverse of the buoyancy effect that leads to the creation of salt domes. Recent modeling at LBNL has shown that even with a range of behaviors for creep that includes the pressure-solution mechanism, negligible sinking of waste packages is expected (< 2 m) over 10^4 years [265].

4.3.4. Shearing on Discrete Layers

In bedded salt, thin clay layers or other interfaces between different materials (e.g., salt and anhydrite) can slip, which relieves shear stresses, and impacts the predicted damage or closure rate around an excavation.

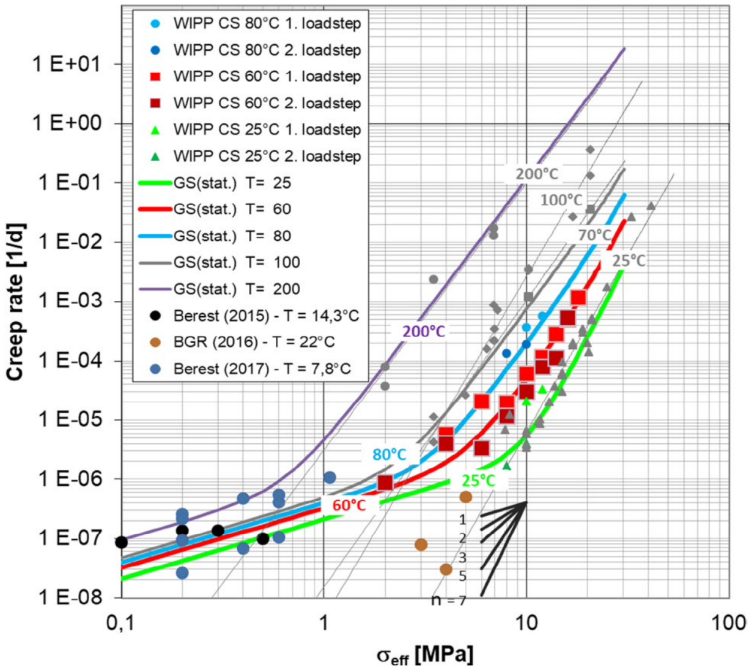

Figure 4-25. Comparison of creep strain rate at high and low deviatoric stresses [15]. Norton creep law (Equation 4.5) exponent visualized in bottom inset.

The Mohr-Coulomb shear stress criteria with pore pressure effects [12] can be given

$$\sigma_c = \tau - \mu\,(\sigma_n - p) \tag{4.7}$$

where all the factors are relative (i.e., changes); τ is the change in shear stress on the plane in the expected slippage direction [Pa], σ_n is the change in normal stress on the plane [Pa], p is the change in pore fluid pressure on the plane [Pa], μ is the dimensionless coefficient of friction, and σ_c is the change in Coulomb failure stress [Pa]. Positive values of σ_c indicate the plane is closer to slipping, whereas negative values indicate stress changes that move the plane further from slipping. The interface is assumed to be stiff in its normal direction, but the plane can slip if shear stresses dominate over normal stresses, which are further reduced by pore pressure. There are not significant data available to characterize the slipping properties of in-situ clay layers in bedded salt [211, 246], therefore a nominal value ($\mu = 0.2$) has been used at WIPP [176], based on engineering judgment (although many silicate rocks have $\mu \approx 0.7$ [34]). Mechanical simulations at WIPP also have not taken fluid pore pressure effects into account.

Elevated pore pressure in clay layers reduces the effective normal stress that otherwise clamps the layer and prevents sliding [12]. In the far field, the clay has pore pressure approaching the lithostatic stress (see § 3.1, Brine Types). Far from the excavation, where both σ_n and p nearly equal lithostatic stress, Equation 4.7 indicates the layer is "floating" (effectively no normal stress preventing slip) and may slip easily, but shear stresses in salt in the far field are also very small or zero, so there are no stresses tending to drive slip. Clay layers closer to the repository excavation have lower pore pressure (brine from clay is the first to bleed off – Table 3-1), but they will also have higher shear stresses, associated with the excavation. The clay layer may be in a critically stressed state [297]. Thermal pressurization could also increase slip on clay layers by increasing the pore pressure in the clay layers, reducing effective normal stress.

Sobolik investigated the apparent static and dynamic friction coefficients for different man-made clay layers in salt [246, 247]. It is difficult to sample an undamaged clay layer in core, because it is a preferential weakness that often fails during drilling. The nature of the interface depends strongly on whether the surfaces on either side of the clay layer are smooth or comprised of rough and possibly interlocking salt crystals. Smooth surfaces are found with some clay layers at WIPP (e.g., clay layers associated with anhydrite layers which do not have large crystals like halite, e.g., Clay E), while other clay layers are associated with rough, interlocking crystal surfaces (e.g., Clay F, where large halite crystals may penetrate the clay from either side).

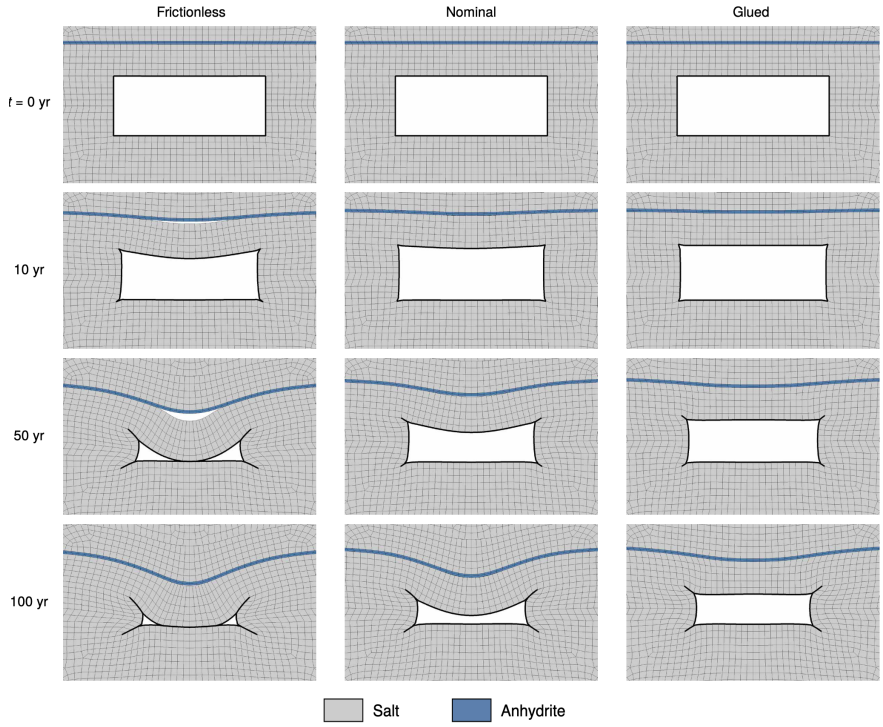

Figure 4-26. Model predictions of open-room closure evolution at WIPP for different slip behaviors [211].

Figure 4-26 shows mechanical predictions (not including pore pressure or gas-generation effects) of open-room closure at WIPP for three different types of discrete anhydrite and clay layer behavior [211]. A clay layer is often associated with the bottom of anhydrite layers in the Salado Formation. In this simulation, "frictionless" indicates $\mu = 0$ for the anhydrite layer, "glued" indicates there is no slippage ($\mu = \infty$), and "nominal" is $\mu = 0.2$, as has been used in most WIPP simulations.

Discrete layers can allow stresses to redistribute, resulting in different predictions of early time ($\leq$ 100 years) closure. Domal salt does not have significant continuous layering; slipping on clay layers is mostly a bedded or pillow salt phenomenon. Figure 4-26 shows visible separation at layers for the frictionless case. In reality, there would likely be discrete failure and roof falls, rather than continuous deformation. Discrete fracturing and failure are difficult behaviors to capture in large-scale models, especially over long time periods [212].

4.3.5. Development of Damage and Fracture Closure

Coupled THM models can be used to predict the distribution of microfracture damage (i.e., porosity) due to creating an excavation (i.e., a borehole or drift), heating, or changes in pore pressure. The creation of and distribution of porosity as well as the directionality of porosity (i.e., permeability or tortuosity) are critical to those processes that require pore space for convection (advection of solutes or heat or diffusion of solutes). Plastic damage is often implemented as an isotropic scalar quantity (Figures 4-27 and 4-24). In reality, microfracturing or dilation results in oriented fractures (i.e., with the fracture normal preferentially along σ_3), which contributes to directional permeability and diffusion [148].

The distribution and accumulation of damage around an excavation is a function of the lithostatic stress, the orientation of the stress tensor near the excavation (fractures open perpendicular to σ_3 – Figure 4-28a), the size and shape of the excavation (i.e., rounded vs. rectangular excavation – Figure 4-27), and any geologic heterogeneity associated with the salt (e.g., lettered clay layers or anhydrite marker beds at WIPP, also shown in Figure 4-27). Not only do fractures and granular pores have different porosity-permeability relationships (Figure 4-20), but properly aligned fractures are far more compressible than pores typical of reconsolidated granular salt [51].

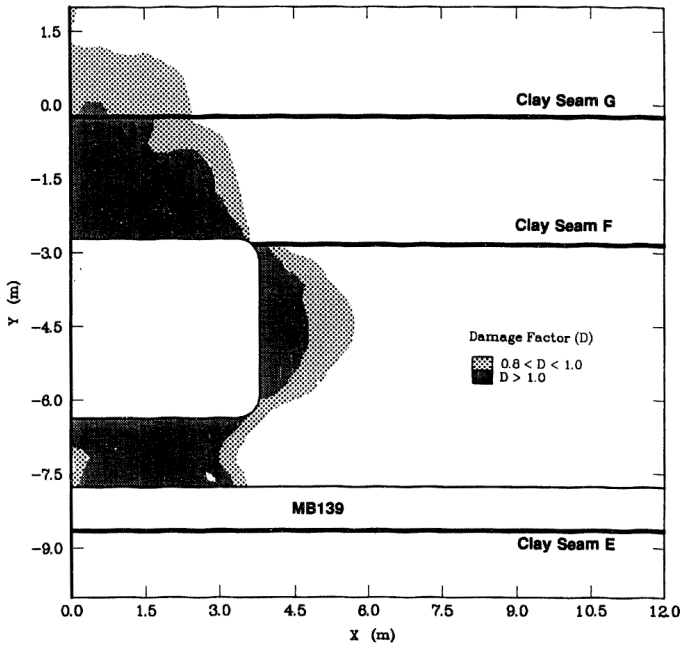

Figure 4-27. Model predicted damage around rectangular excavations, including effects of non-salt clay layers and marker beds [273].

The effect of accumulated damage on gas permeability around the N-1100 drift at WIPP was characterized by Stormont [24] using specified-pressure (70 kPa) gas flowrate tests (Figure 4-29). The log-spaced contours of flowrate in this figure effectively quantify damage magnitude, which is highest in the anhydrite marker bed (MB-139) below the floor of the excavation. At these low gas working pressures, some regions without measurable gas flowrate may have had open fractures that were filled or at least blocked with brine, and therefore low-pressure gas did not flow into them (i.e., the low-pressure gas system is sensitive to the relative gas permeability, not the absolute permeability). Higher gas pressures may have been

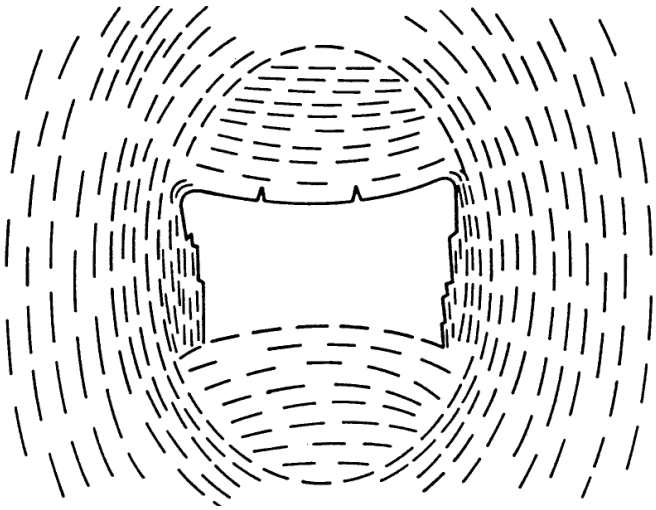

(a) Mostly azimuthal cracking around mined openings at Asse, due to excavation stress relief [24, 84].

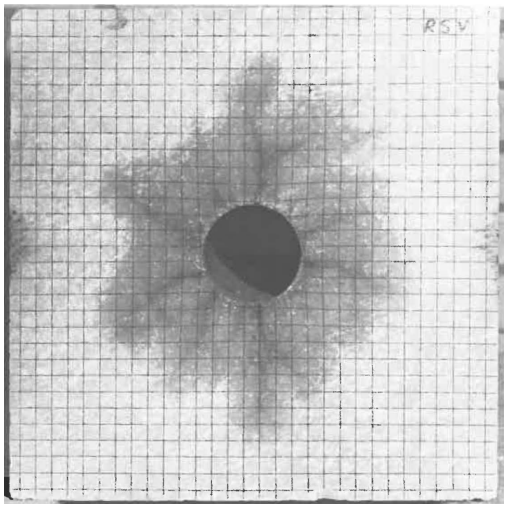

(b) Radial cracking (highlighted by staining) observed at cool-down after heating [221].

Figure 4-28. Fracturing in salt; σ_3 was perpendicular to the fractures when created.

less susceptible to relative permeability effects, but they may also have mechanically opened the aperture of the fractures, changing their absolute permeability.

The distribution of higher gas flowrate regions corresponds well to the envisioned fracture distribution (Figure 4-28a) and the areas of higher model-predicted damage for WIPP disposal rooms (Figure 4-27). Gas flow can be used to probe the extent of damage and fracturing in the EDZ in salt. Other methods have also been successfully used to delineate the EDZ, including ultrasonic wave velocity [103] and electrical resistivity tomography [40, 24, 119].

4.3.5.1. Thermal Expansion Feedback to Hydrological Properties

Heating leads to thermal expansion. Due to this non-uniform constrained thermal expansion, stresses will be induced in the salt in the area being heated. The increased stresses may close some fractures (depending on their orientation to the stress state and the geometrical configuration). Closing fractures may only reduce the porosity slightly, but it may reduce the permeability significantly. As illustrated in Figure 4-20, granular salt will result in a relatively small change in permeability from a small change in porosity (e.g., from 3% to 2% porosity leads to a factor of approximately 2 change in permeability – blue arrow). While in fractured salt, the same change in temperature might result in a similar change in porosity, but a larger change in permeability (e.g., 1% to 0.5% porosity leads to 2-3 orders of magnitude change in permeability – orange arrow).

Figure 4-28b shows radial fracturing observed around a borehole in a lab heater test [221]. The test showed a sharp increase in ultrasonic wave travel time upon the start of cooling, indicating damage was imparted when heating ended. Staining after the experiment revealed the radial cracking pattern seen in Figure 4-28b. Large hoop stress set up around the borehole during heating, and during the rapid after-test cooling the drop in hoop stress allowed radial fractures to develop. In the fields of geothermal energy production

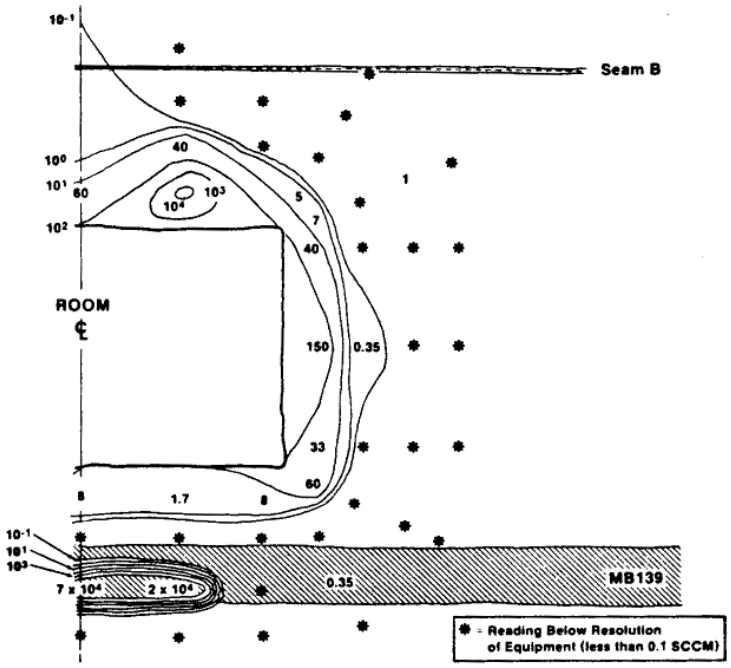

Figure 4-29. WIPP gas flowrate contours (SCCM is standard cm^3/min) from constant-pressure 1-m long packer-isolated intervals; stars indicate no flow [24].

and carbon sequestration, "thermal shock" is known to occur in rocks after cyclic heating and cooling, and is known change to the hydrological properties of rocks [106, 17, 295]. To a lesser degree, different thermal expansion coefficients for different materials can also lead to microfracturing during large temperature changes (heating or cooling). This differential expansion and contraction can occur at boundaries between different macroscopic layers in evaporite deposits (e.g., contributing further to movement on layers, as discussed in § 4.3.4, Shearing on Discrete Layers), or at grain/material boundaries associated with smaller-scale heterogeneities (e.g., as shown in X-ray tomograms in Figure 3-1).

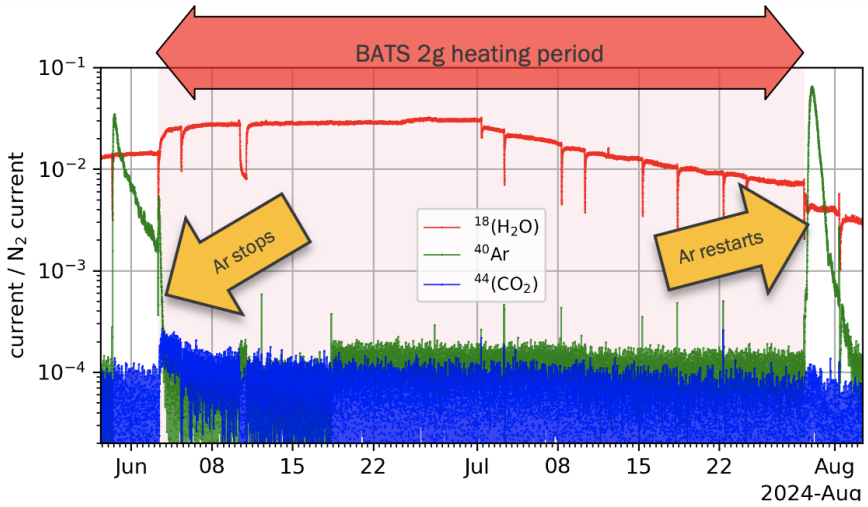

Figure 4-30. BATS 2g breakthrough of Ar (green line) from D borehole to HP borehole that is stopped by heating and restarts after cooling [141].

The BATS 2 field experiment showed similar development of radial fractures from damage associated with cooling in earlier tests (as seen in the lab experiment by Roest & Gramberg [221]), the experiment also demonstrated repeated opening and closing of the fractures by heating and cooling.

In the BATS 2 heater experiments [139, 141], argon was pressurized behind an inflatable packer in a satellite borehole (D) parallel to the heated borehole (HP). After three heating/cooling cycles (BATS 2a-BATS 2c), it was observed subsequently that pressurizing the gas in the satellite packer borehole while the heater was off resulted in rapid breakthrough of Ar (i.e., breakthrough of tracer gas along radial fractures emanating from the central heated borehole, connecting up with the parallel tracer borehole, 10 cm away). Figure 4-30 shows gas concentrations in the heated HP borehole gas stream (measured on an in-drift quadrupole mass spectrometer). Once damage had been imparted to the rock from repeated heating and cooling cycles, gas breakthrough in later heater tests stopped soon after the heater was turned back on and restarted once the heater was turned off. Even after 8 weeks of heating, there was no breakthrough while the salt was hot.

In a repository, fractures in the EDZ (Figure 4-28a) would be closed due to emplacement of heat-generating radioactive waste, through thermal expansion of the EDZ and increased stresses due to confined thermal expansion. In a repository, decay heat should not experience an abrupt shutdown, like at the end of a heater test. Cesium-90 and strontium-137 are significant components of radioactive waste, with half lives of approximately 30 years. On this time scale, any slight change in devaitoric stress due to thermal contraction from incremental cooling will likely be dissipated via viscoplastic creep, rather than result in fracturing.

Previous field experiments have attempted to reduce the thermal shock that occurs at cool down after a heater test by reducing the temperature in steps (i.e., at Avery Island [127], at Asse [222], or in a laboratory salt block test [102, 264]), but even relatively small steps lead to shocks and damage at each small change (e.g., Figure 4-31). Brine is often produced to the heated borehole at the end of heating, due to the fracturing imparted from rapid cool down. The rate of change in temperature at the source may be more important than the absolute value of the change in temperature.

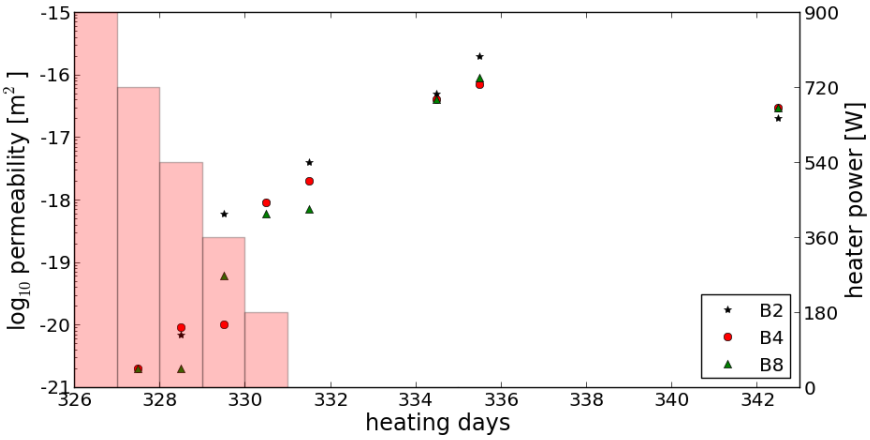

Figure 4-31. Daily stepwise reduction in heater power (bars) at end of Avery Island heater test, plotted against gas permeability through time (dots) [127].

4.4. Chemical Processes

The primary variables relevant to chemical dissolution and precipitation reactions and liquid-phase transport are concentration or activity of dissolved components (including dissolved radionuclides) in the liquid and solid phases (mostly halite, but $\approx 5\%$ anhydrite, polyhalite, and clay may exist locally).

As was mentioned earlier for mechanical processes, changes to porosity may change relationships to moisture retention curves, permeability, and tortuosity. Typically, these parameters are only related to porosity through simple power-law relationships, with porosity being the main variable changed. Pressure-solution is a pore-scale MC coupling, and is one of the main deformation mechanisms in salt, especially at low deviatoric stresses.

At WIPP, primary fluid inclusions (i.e., intragranular) have a different chemical and isotopic composition than intergranular brine or clay porosity produced to boreholes in the salt [69, 135]. The composition of fluid inclusions has been observed to change after thermomigration [38, 37].

Water vapor from hot regions (above the boiling point) can migrate and condense at cooler locations and dissolve salt (Figure 4-3). This new brine derived from dissolved salt is observed to be quite different composition from native brine [135], since it is more closely related to the highly soluble solid minerals present (e.g., halite) than to the highly concentrated bitterns associated with fluid inclusions–brine with elevated concentrations of species that do not readily precipitate, e.g., Br^- and Li^+. Given these differences, the contributions of these different water types can be distinguished in samples from boreholes given major ion analyses and geochemical modeling [135, 163].

As a primary effect, condensing water vapor will dissolve salt (increasing porosity) and boiling brine will precipitate salt (reducing porosity). As a lesser secondary effect, the minerals in the geologic salt deposits have solubility limits that are functions of temperature (Figure 4-32). Heating salt permeated with Na-Cl brine will dissolve more salt into the brine (increase porosity a bit) while cooling a hot salt-brine system will precipitate salts (decreasing porosity a bit). These changes in porosity due to dissolution and precipitation can also drive change in fluid pressure or liquid saturation.

Many evaporite salts (e.g., halite or sylvite) are very soluble and are essentially not kinetically limited at time scales relevant to other repository flow processes. PFLOTRAN, FEHM, and TOUGH2-EWASG have the capability to simulate an equilibrium (i.e., not kinetically limited) soluble matrix [6, 25], accounting for mass balance of both water and soluble solid.

We distinguish here between geochemical modeling capabilities in chemical transport models, in increasing order of complexity:

- simulation of advecting, diffusing, and sorbing tracer transport with possible radioactive decay of non-interacting solutes (C_{TRACER} – feasible in large 3D domains);
- simulation of dissolving and precipitating salt, which modifies the porosity, permeability, and tortuosity ($C_{PPT/DIS}$ – possible in large 3D domains, but more effective in 2D or smaller domains);
- simulation of "full chemistry" of the dissolved and solid species in the system (e.g., Na^+, Cl^-, and pH), using thermodynamic and kinetic data to predict dissolution and precipitation of minerals, and requiring a framework that can predict activities in high ionic strength solutions (C_{FULL} – typical in only 0D or 1D models [118]).

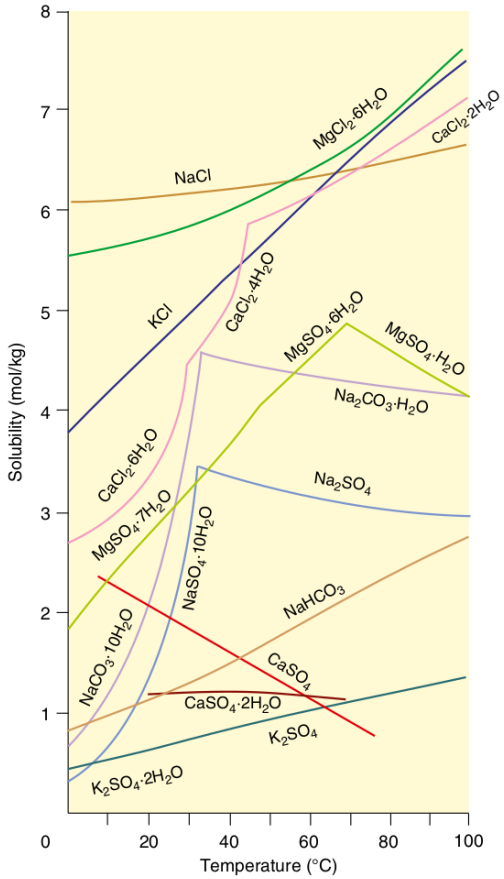

Figure 4-32. Solubility of minerals during evaporation of seawater with temperature [282].

THC models that include full chemistry information, which is needed for waste package corrosion or cementitious material degradation, are the most complex geochemical models. These models are typically only simulated in simplified 0D or 1D configurations (i.e., at the waste package or under representative repository-wide conditions). Fully coupled THMC process models may be used to screen processes for inclusion in PA simulations, and may ultimately be incorporated into PA simulations through multi-scale coupling (e.g., source term to near-field coupling or near-field to far-field coupling), reduced order modeling, or surrogate modeling. Elevated temperatures may change solubilities (Figure 4-32), kinetic dissolution rates, or equilibrium constants in full chemical reactions. Dissolution and precipitation can also lead to changes in temperature, if the reactions are endothermic or exothermic (but this is often considered insignificant).

4.4.1. Reactive Transport

Reactive transport includes transport of dissolved species in the liquid phase, allowing species to react with each other and the solid phase during movement [253]. The reaction-advection-diffusion equation is a set of N reactions (one for each species), with each equation taking the form

$$\frac{\partial c_i}{\partial t} = D_{\text{eff},i}\nabla^2 c_i + \vec{u}\nabla c_i + R_i$$

where c_i is molar concentration [$\mathrm{mol/m^3}$] of species i, $D_{\mathrm{eff},i} = D_{\mathrm{bulk},i}T^*$ is the effective diffusion coefficient of species i in a porous or fractured medium [$\mathrm{m^2/s}$], T^* is a dimensionless tortuosity coefficient ($0 \leq T^* \leq 1$, specifically "diffusional tortuosity" in [43]), $D_{\mathrm{bulk},i}$ is the free-water molecular diffusion coefficient for species i [$\mathrm{m^2/s}$], and R_i is a reaction term that accounts for radioactive decay, ingrowth, dissolution, precipitation, and reactions [$\mathrm{mol/(m^3 \cdot s)}$].

The equations of state for the viscosity, density, enthalpy, surface tension (Figure 4-13), and vapor pressure for brine must be used in place of the more typical equations for pure water [7, 249, 64, 63, 180], to represent the hydrological system for a brine, rather than fresh water. Viscosity of both fresh water and brine are a strong function of temperature, potentially increasing the mobility of brine upon heating. The density of both fresh water and brine are also functions of temperature (see § 4.2.3, Gravity-driven Flow). The vapor pressure of water is also a function of salinity, which results in elevated boiling point for brine compared to fresh water (≈ 8 °C at 1 atm [70]).

Hyper-saline pore fluids in salt systems tend to reduce potential solute-transport issues like colloid-assisted transport of actinides [157, 14]. In a strong brine, the electric double layer is much thinner which reduces the electrostatic attraction and repulsion forces at the pore scale (e.g., membrane effects). While the thin electric double layer results in less colloid transport, it also results in less sorption of radionuclides to the salt itself [289]. One of the benefits of bentonite is its high sorption capacity for dissolved actinides leached from waste forms. The soluble portions of the halite do not provide much sorption, while some sorption may be provided by geologic clay or anhydrite layers within evaporite deposits. This is one of the reasons bentonite has been proposed as an additive to granular salt backfill (but the sorption properties of bentonite hydrated by high ionic strength brines may be different from that in fresh water).

Gas-phase reactive transport is also possible (e.g., oxidation and reduction of metal waste packages), but often is not considered in porous media subsurface simulations. Commonly, the gas phase is treated in a simpler manner than the liquid phase (e.g., single component of air), since most chemical reactions of interest happen in the liquid phase. Gas transport of radionuclides is possible (e.g., krypton or xenon daughter products, carbon-14 in CO_2, and radon from alpha decay), but it has not been considered in previous US PA simulations, because of the short half-lives of most gaseous radionuclides.

Reactive transport of solutes in the liquid phase in salt formations is complicated by the high ionic strengths in hyper-saline evaporite brines. To accurately predict mineral solubility and speciation at high ionic strengths and elevated temperatures require an activity model that accounts for more complex ion interactions, such as the Pitzer approach [200, 201]. Both EQ3/6 [290] and TOUGH-REACT [294] have Pitzer capabilities, allowing full chemistry in high ionic strength systems.

The 0D geochemical model EQ3/6 [290] has been used to predict speciation of actinides in WIPP brines at ambient conditions as part of WIPP Compliance Recertification Application [62], and by DOE-NE to predict ion concentrations and solid precipitants during the evaporation process at elevated temperatures [135]. Figure 4-33 shows the predicted evolution of precipitated salts (top) during the process of evaporation (proceeding from left to right, increasing degree of evaporation) and concentration at elevated temperatures (50 °C). In this situation, the solid phases remain in contact with the solution, and therefore control the solution chemistry (i.e., geochemical "divides" occur when some minerals appear or disappear from the solid phase [8, 282]). This is the expected behavior inside a heated borehole, except additional brine may flow in during the evaporation process.

The thermodynamic databases require consistent data across a range of temperatures and for the dissolved and mineral components of interest. The Nuclear Energy Agency maintains reference thermodynamic databases for low ionic strength solutions. Thermodynamic databases relevant to high ionic strength systems have been developed for the WIPP project [62], but not for elevated temperatures. Prediction of precipitation and dissolution of minerals also requires information on kinetic precipitation and dissolution rates for minerals of interest, possibly with different forward and backward rates as a function of temperature.

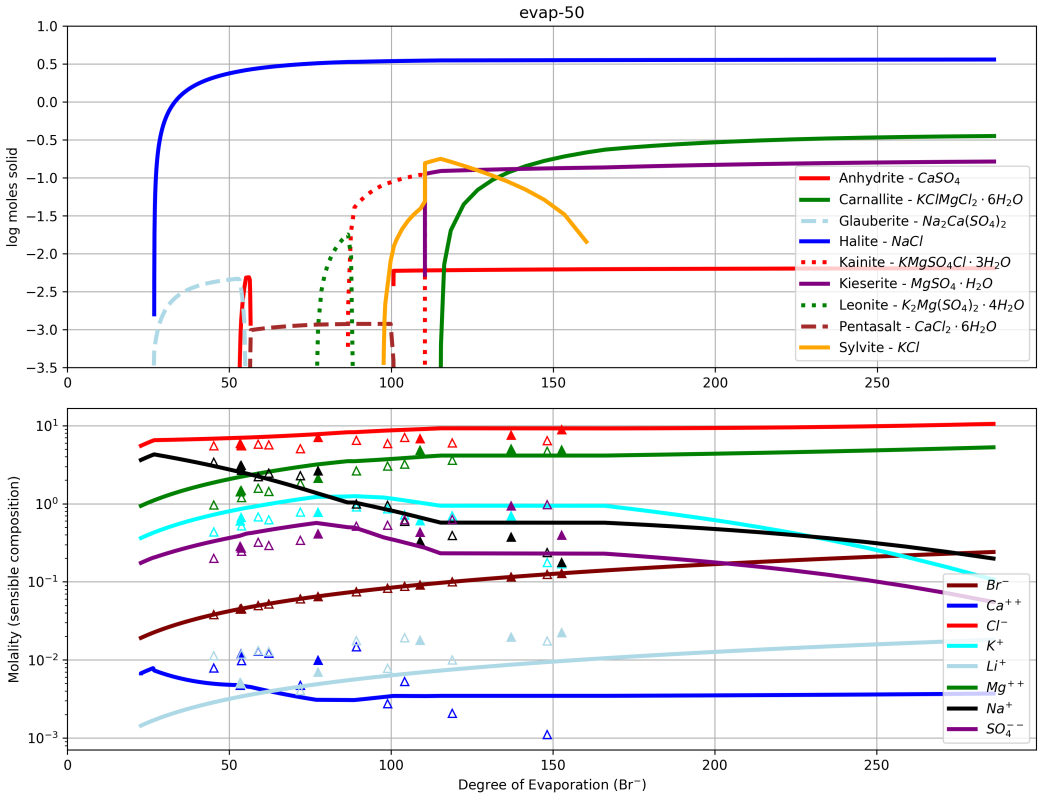

Figure 4-33. Brine evaporation at 50 °C; precipitated phases (top) and solution composition (bottom). Experimental observations are symbols. Degree of Evaporation represents concentration of Br above seawater [135].

4.4.2. Water-salt Interactions

In most chemical modeling of salt systems (e.g., TOUGH-EWASG, FEHM, PFLOTRAN) where porosity is created and destroyed through precipitation and dissolution, variation in composition of the brine and solid salt are not explicitly tracked. The solid is considered to be pure halite, and the brine only a saturated Na-Cl brine [6]. The distribution of different minor minerals found in bedded salt deposits or in native brine collected from boreholes are usually not considered (except in some C_{FULL} simulations [135]). As a first approximation, this approach is more realistic than treating the salt as non-reactive, but the different minerals and components in the brine should be considered in a reactive transport simulation (even if the exact spatial distribution of minerals is unknown) – especially one with significant heating and vapor transport.

If a humid vapor is passed over a multi-mineralic salt deposit, depending on the relative humidity, some minerals will hygroscopically pull water from the air (i.e., water will condense from the air onto the mineral (i.e., deliquesce) and if enough condensation occurs, it can dissolve the mineral). Figure 4-34 shows the different equilibrium relative humidity associated with common evaporite minerals associated with concentrating seawater; it shows halite has an equilibrium relative humidity of $\approx$ 75%. This is the steady-state humidity in a borehole or room in salt with minimal ventilation [116]. Other more soluble minerals will deliquesce at even lower relative humidity, such as sylvite (KCl), carnallite ($KMgCl_6 \cdot 6H_2O$), bischofite ($MgCl_2 \cdot 6H_2O$), and tachyhydrite ($CaMg_2Cl_6 \cdot 12H_2O$). While these minerals beyond halite only exist in small amounts in WIPP salt, they will preferentially dissolve from moisture removed directly from humid air (i.e., in the air-saturated portion of the porosity), and can change the composition and physical properties (e.g., density and viscosity) of brines around a heat source.

Figure 4-34 also shows how brines at different points along the evaporation curve have increasing specific gravity (relative density of brine to fresh water). As a brine is heated to evaporation near a heat source, it may tend to sink because of density contrast with surrounding brine (see § 4.2.3, Gravity-driven Flow). Furthermore, the temperature dependence of halite solubility in brine can lead to increases in permeability and porosity around a heat source, as the salt further dissolves into the heated brine (which would also only occur in the brine-saturated porosity).

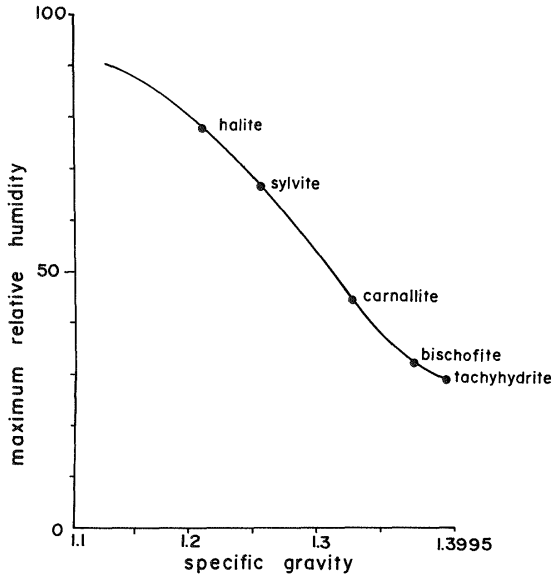

Figure 4-34. Critical relative humidity and brine specific gravity during concentration of brine by evaporation (moving down and right) [248].

Man-made engineered components like cements are key components of a salt repository. They must be designed in a chemically compatible manner with the salt minerals and with any brine produced from the salt. There are few geochemical compatibility experiments that used relevant materials and brine under conditions expected for disposal of heat-generating waste. Since corrosion of the cement seals could lead to premature failure of key sealing components, chemical exposure tests regarding the long-term stability of salt concrete or Sorel cement should be conducted. Some predictions of stability are based on geochemical modeling [240], these prediction are useful, but they may not take into account complex metastable phases present during the expected transient evolution of the system.

4.4.3. Chemical Transport Properties

Hydraulic tortuosity is a measure of how long an effective flow path is through the pore space of a porous medium, and most significantly impacts diffusive transport (i.e., it relates the effective diffusion coefficient to the free-water or molecular diffusion coefficient) [43]. In the far field the intergranular salt porosity is not well-connected and therefore the effective diffusion coefficient is very low (i.e., essentially zero), as evidenced by compositionally different brines being juxtaposed by a few m or cm in evaporite deposits over geologic time [218]. Setting the tortuosity to zero or a very small value is necessary to stop diffusion from occurring, even if the permeability is zero, or the brine flux is limited by non-Darcy effects (§ 4.2.1.1). The porosity may not be zero, but if it is disconnected, the permeability and the tortuosity should go to zero before the porosity does. In the near field the increased porosity and permeability are associated with tortuosity values that allow gas- or liquid-phase diffusion. Most generally, tortuosity is a tensor [185] with different values in the principle directions (like permeability), related to the nature of connectivity of a porous medium, which is a transport-centric description of the pore-space, beyond the information conveyed by just the scalar porosity value.

Little data are available on the tortuosity numerical values in salt environments of the near- and far-field, and no information is available on how tortuosity changes with mechanical damage and healing of the excavations or chemical dissolution and precipitation in pore spaces. Fluegge et al. [73] presented results of laboratory diffusion experiments (cesium through brine) in re-compacted granular salt (2% porosity). One result showed tortuosity values close to unity (i.e., effective diffusion coefficient nearly equal to free-water diffusion coefficient), but other data possibly show the effects of precipitation and dissolution in the sample. In numerical models, often it is assumed tortuosity is a simple power-function of porosity and phase saturation [162]. More data on effective tortuosity of liquid and gas phases in granular, damaged, and intact salt would be useful for parameterization of both process and PA models. Since it controls the magnitude of diffusion component of transport.

The existence of an open pore or fracture network (i.e., connected intergranular porosity) in the salt is required for convection of solute. The following list mentions how the different brine types correspond to different porosity types, and how they can participate in transport processes under different conditions.

- intergranular salt porosity derived from dilation (i.e., fractures and secondary fluid inclusions):
  - open and connected porosity (low confining stress environment): brine is mobile under ∇p, solutes mobile under ∇c, fractures are directional and highly compressible
  - closed porosity (higher confining stress; reconsolidated or healed): brine is immobile under ∇p, solutes immobile under ∇c (tortuosity $\rightarrow$ 0), brine mobile through salt crystals under ∇T, decrepitation and release of water vapor at high T, possible reconfiguration of porosity connectivity at high pressure and temperature (i.e., dihedral angle)
- intergranular porosity contributions from non-salt components (e.g., clay, anhydrite): behaves like intergranular porosity in salt without decrepitation or thermomigration, and without dynamic dissolution and creep
- intergranular porosity derived from reconsolidated granular salt: brine is mobile under ∇p, solute mobile under ∇c, pores are isotropic and poorly compressible

- intragranular salt porosity (within crystals, not connected; mostly primary fluid inclusions): brine is immobile under ∇p, solute immobile under ∇c, mobile under ∇T through salt crystals, and decrepitation and release of water vapor at high T
- hydrous minerals: are always immobile, unless exceeding dehydration temperature, then they produce water vapor.

4.4.4. Corrosion of Metals in Brine

Corrosion of metal waste packages can be one of the main drivers of gas generation in a salt repository (see § 4.2.4, Gas Generation). Corrosion can also lead to breach and failure of waste packages, allowing brine to access the waste form. Dissolution of the waste form (i.e., spent fuel rods) within any brine is complex. The process depends on the dissolved species in the hot brine, waste package components (e.g., effect of overpack, canister, and spacers), and the waste form itself (e.g., UO_2 fuel rods and cladding) [289, 118]. If there is liquid brine at the waste packages, there can be corrosion, depending on the metals and brines present.

Several *in-situ* experiments were conducted at WIPP related to corrosion of waste package materials under the Waste Package Performance Tests program [270]. The largest experiment was the Materials Interface Interactions Test that involved placing 1845 "pineapple slice" shaped samples of proposed waste package materials, waste form materials, geologic samples, and backfills into heated brine-filled boreholes in the floor of Room J at WIPP for 0.5, 1, 2, and 5 years of exposure [172, 170]. Coupons of materials were supplied by a range of countries and programs. The coupons were exposed to hot (90 °C) NaCl brine. None of the titanium test samples showed any evidence of corrosion, while mild steel and 304L stainless steels showed uniform corrosion [167]. There were some issues interpreting the leachate data collected in this test, possibly compounded by the large amount of salt precipitation that occurred. More recent corrosion work in Germany supports the statements of impressive performance of titanium alloys and Hastelloy (a corrosion-resistant superalloy) in salt repository brines [242, 243, 241].

Waste packages can be designed with corrosion-resistant materials or coatings to prevent release, or they can be designed with corrosion allowances (i.e., thick overpacks of cheap sacrificial material). Both approaches have been considered [45, 168], but the details of a design would depend on whether costs, early-time performance, or late-time performance were the primary optimization target.

When corrosion-resistant materials are used for waste packages in a repository, it is not the very low general corrosion rate that is the most relevant to the breach and ultimate failure of the waste package, but instead localized corrosion processes [289]. The most important process leading to a breach is a potentially faster and more localized corrosion process, such as crevice and pitting corrosion or stress-corrosion cracking, which are an ongoing area of active research [30]. From the point of view of gas generation, it is the lower general corrosion rate that may be most important, as it is potentially applied over a much larger surface area. Localized processes are only occurring over small fractions of the canister surface.

Historically, laboratory exposure tests were conducted using autoclaves and representative metals with salts [169]. Before testing began in the WIPP underground, preliminary field tests were conducted in potash mines near WIPP [171]. Waste package exposure tests were also conducted on WIPP remote-handled waste packages (placed into horizontal boreholes in the drift wall), and contact-handled waste

packages (drums stacked in the drift) [168]. While useful demonstrations, these exposure tests can be difficult to extrapolate to long times expected in a repository. They exposure tests are at least confirmatory about the general processes that are important in a brine/metal system, during the early months and years of emplacement. Corrosion rates should be estimated and bounded for relevant conditions. Corrosion rates can be bounded by the amount of brine expected to be present next to a hot waste package. The best strategy is to keep the waste packages dry, since corrosion is very slow or non-existent in a dry salt system.

5. SUMMARY AND DISPOSAL CONCEPT

This report has presented the processes (thermal, hydrological, mechanical, and chemical) that are relevant to a deep geological repository for radioactive waste. Most of these processes are derived from the perturbation associated with the radioactive waste or the creation of the repository excavation. In salt, there are many interactions between the processes, and they often have non-linear constitutive behaviors.

Processes depending on porosity	**Processes changing porosity**
hydrological advection	mechanical damage (dilatancy/healing)
advection: heat convection	chemical (dissolution/precipitation)
advection: reactive transport	hydrological (hydrofracture)
radiative heat transfer	thermal expansion (stress changes)
Properties related to porosity	**Processes occurring even without porosity**
permeability	heat conduction
tortuosity	geomechanical deformation
moisture retention curve	
air-entry or gas-threshold pressure	
specific surface area	

Table 5-1. Porosity dependence of processes.

To summarize previous sections, Table 5-1 lists processes that depend on porosity (top left) and those that modify porosity (top right). When chemical or thermal-chemical processes modify the porosity, how does this get updated in the mechanical model? In a loosely coupled THMC model, multiple processes can change the porosity and it is updated in the next time step (requiring very small time steps). Not all porosity (e.g., fracture porosity, granular porosity, intergranular fluid inclusions, intragranular fluid inclusions) has the same equivalent transport behavior (Figure 4-20), and therefore porosity/permeability, porosity/tortuosity, and porosity/pore distribution relationships can be changed in different ways depending on whether a change to porosity was made by the mechanical model, the chemical model, or the hydrological model (Table 5-1, bottom left). Different micro-mechanisms of mechanical deformation may even have different impacts on different transport properties (e.g., pressure solution tends to reduce asperities in pores reducing specific surface area, while shear fracturing will increase connectivity, increasing specific surface area).

The hydrological problem has a large change in material properties across the hydrological EDZ and a large change in variables across the hydrological EdZ (Figures 4-5 and 4-19). Other processes (mechanical, chemical, or thermal) tend to have smaller associated damaged zones than the hydrological problem. The mechanical process results in dilatancy or changes in porosity that impact the hydrological model, but

this damage is typically not considered to have a large impact on the mechanical properties themselves (except where failure is explicitly accounted for in mechanical constitutive models).

The processes in a salt repository can be grossly divided into those that require porosity and those that do not. Mechanical deformation and heat conduction do not require a connected porosity (Table 5-1, lower right), and therefore are effective into the far field. The processes that require a connected porosity can either operate in air-filled porosity or brine-filled porosity, which can both exist in the backfilled drift, in the EDZ around the drift, but they will not be effective into the far field.

5.1. Notes on a New Salt Disposal Concept

Building on the things learned in the international collaborations of BATS, DECOVALEX, KOMPASS, and RANGERS, we present some notes on a disposal concept for heat generating waste in a salt repository. We acknowledge that there have been several historical salt disposal concepts, or partial disposal concepts that any new repository concept should knowingly be built upon. The history of radioactive waste disposal programs are complex both in the US [155] and internationally [186, 3] and salt has been studied for a long time. In rough chronological order, salt disposal concepts and attempts are:

- (1965–1967) Project Salt Vault disposal concept for solidified reprocessing waste in vertical boreholes in bedded salt in Kansas [26, 159];
- (1971–current) Morsleben facility for low- and intermediate-level radioactive waste in a re-purposed domal salt mine in Germany (Endlager für Radioaktive Abfälle Morsleben, ERAM), currently licensed for decommissioning and closure [13, 292];
- (1981–current) currently operating DOE-EM WIPP repository for disposal of non-heat generating defense-derived transuranic waste in the bedded Salado Formation [61];
- (1982–1988) US Office of Nuclear Waste Isolation salt disposal concept for borehole disposal and in-drift self-shielded waste packages at the bedded salt Deaf Smith site in Texas [45, 190];
- (2011–2013) Gorleben disposal concept for spent fuel in a salt dome in Germany; Vorläufige Sicherheitsanalyse Gorleben, VSG (Preliminary Safety Assessment for the Gorleben Site) [174, 173, 276];
- (2011–2019) DOE Office of Nuclear Energy Generic Disposal Safety Assessment and Integrated Waste Management reference cases for disposal of large, hot dual-purpose canisters in a generic bedded salt formation [95, 91, 245]; and
- (2020–2025) Centrale Organisatie Voor Radioactief Afval (COVRA) preliminary disposal concept and conditional safety case for high-level waste in a salt dome in the Netherlands (COPERA [4, 5], building on OPERA [99]).

In a generic salt repository for "hot" radioactive waste (i.e., above brine boiling temperature at the waste package surface), the region around the waste packages will dry out. While drying out, additional water associated with clay, fluid inclusions, and hydrous minerals may also become mobile (see § 3.1, Brine Types). Only a small amount of brine will enter the EDZ from the far field, due to the low intrinsic permeability of intact salt and due to the low relative permeability to brine inside the EDZ (see Figure 4-19).

Thermal expansion in the EDZ and host rock leads to closing some fractures, reduction of brine viscosity and the creation of a thermal pressurization "dam" or "divide" (see Figures 4-9 and 4-10) driving some near-field brine towards the excavation, while simultaneously driving brine on the far side of the divide away from the excavation [264].

Depending on the EDZ extent and presence of non-salt layers, brine may accumulate in the damage region (i.e., sump) beneath the drift (see § 4.2.3, Gravity-driven flow). Waste should not be emplaced into vertical boreholes, if brine collected into a sump would be a problem. It could increase corrosion or gas generation.

Boiling and evaporation of brine with salt precipitation on or near the waste package will reduce porosity and increase thermal conductivity. Condensation of water in cooler regions away from the heat source will increase porosity there due to dissolution of salt. At a slower rate, creep closure will eventually re-consolidate granular salt backfill to low porosity and permeability, and will also close and heal the EDZ associated with mined openings (see § 4.1.2, Heat Convection).

The combination of heat and creep closure will create a relatively dry, low-porosity, low-permeability zone around the waste packages [19]. Corrosion is less in dry salt than in brine-saturated salt. Gas generation is also less at a dry waste package than in one immersed in brine.

Generically, in a salt repository with hot radioactive waste surrounded by reconsolidating granular salt backfill, we expect the following nominal behavior or base scenario:

1. decay heat from radioactive waste will dry out the backfill by the waste in the short term (months to years – the hotter the waste the quicker the backfill dries out);
2. accelerated reconsolidation of hot granular salt backfill will eliminate porosity and permeability near the waste (decades to hundreds of years—this is the primary focus of the KOMPASS and MEASURES ongoing international collaborative efforts [164] and LBNL's modeling efforts with TOUGH-FLAC [226]). While dry salt creeps slower than damp salt (moisture activates the pressure-solution mechanism), the faster creep at elevated temperature will mostly make up for this (see Figure 4-25 in § 4.3.3, Creep at Low Deviatoric Stress);
3. after peak decay heat from the waste has passed (≈1,000 years), the near-waste area will be dry, low porosity, and impermeable, slowing down late-time resaturation of the waste packages with brine derived from the far field [239, 240]; and
4. a dry system does not have: waste packages corrosion, mobile radionuclides, nor gas generation (most gas generation mechanisms depend on available water, see § 4.2.4, Gas Generation).

Variant scenarios (i.e., off normal) in a safety assessment might include deviations from these expected behaviors [134]. For example, some of the waste packages may be cooler, and creep closure may be slower near them and not fully eliminating pore space around them. There may be some residual permeability near the cooler waste in the system after the peak decay heat has passed, and therefore there may be enough moisture at cooler waste packages to drive corrosion and gas generation.

It is possible to develop a salt repository disposal concept that relies solely upon the ability of the geologic salt formation to provide complete containment of the waste in the far field, without taking credit for the more complex processes in the EBS and EDZ near the waste packages, including rapid closure of porosity, the drying out of the salt, or the expected low levels of gas generation in a dry salt system. Some TH PA

models may use simplistic initialization schemes (i.e., drying down vs. wetting up – Figure 4-15) and therefore may significantly overestimate brine availability at repository closure as a conservatism. The waste packages temperature may be lower at early time due to convection processes and the reconsolidation of granular salt would reduce the porosity of the salt with consolidation. Granular salt reconsolidation and precipitation of salt due to boiling may reduce porosity and therefore eliminate convection, but conduction simultaneously increases as porosity reduces (Figure 4-2).

The conservative approach (as used in the WIPP license application [61]), uses a simpler bounding conceptual model to avoid the need for complex predictions associated with some processes in the EBS and EDZ. For example, WIPP assumes the waste packages fail mechanically at closure and regulatory-specified human intrusions ensure the repository is flooded with brine in most scenarios. As an alternative, investigating and striving to understand and predict these complex in-drift and early-time processes, can produce a safety case for a repository in salt that is more physically realistic and has a larger safety margin between the expected performance and the regulatory limit than a simpler safety case built upon many conservatisms.

Understanding the processes that make up the base and variant scenarios is the first step towards making a defendable safety case for a future repository in salt. In undisturbed geologic salt systems, the ultralow permeability and porosity of salt [10] provides the natural barrier to contain radioactive waste over PA relevant time scales (10^4 to 10^6 years). However, physically realistic near-field conditions (e.g., fluid pressures, liquid saturation, and chemical composition) and processes (e.g., brine and gas flow, waste package corrosion, precipitation and dissolution of salt, thermal expansion and contraction of salt and brine, and salt creep) are more complex to account for in disturbed scenarios (i.e., off-normal scenarios like early waste package failure or inadvertent human intrusion). The current state of the salt at repository construction, considering both EDZ and far-field intact salt, are the initial conditions for long-term PA simulations.

Based on ideas presented here, a salt disposal concept could incorporate the following EBS features:

- Avoid vertical borehole waste package emplacement in bedded salt, since gravity tends to accumulate any brine that flows into a repository to the sump in the floor, which the boreholes will intersect. In-drift disposal with granular salt is likely optimal for cooler waste forms and horizontal in-borehole disposal would be optimal for hotter waste forms. These disposal geometries avoid the worst of the sump phenomenon (thus avoiding an early-time phenomenon, in the first years after excavation – see § 4.2.3, Gravity-driven Flow). Access and emplacement drift infrastructure could also be sloped to intentionally collect brine in areas away from waste.
- Designing the repository layout for higher temperatures at the waste package (higher density of waste emplacement or larger waste packages with more fuel in each) may lead to some simplifications or improvements to the disposal reference case. Bedded salt be heated up to 200 °C, without getting too close to the decrepitation temperature, and domal salt can get even hotter (see § 3, Brine Types). Higher temperatures tend to speed up creep closure and lead to drier salt near the waste packages. Drier salt means less corrosion, less gas generation, and less transport. If the salt dries out and becomes impermeable (i.e., isolated porosity), it would take a very long time for any brine to get to the waste packages.
- If needed to take advantage of the high thermal conductivity of intact salt in repository design, the waste packages should either be emplaced in horizontal boreholes, or be emplaced in notches or

grooves cut into the floor of the drift. Granular salt has lower thermal conductivity than intact salt. The hottest waste forms should maximize the contact area where the metal canister makes direct thermal connection with intact salt. Higher thermal conductivity will lower the peak temperatures at the waste packages, compared to surrounding waste packages completely in granular salt (see § 4.1, Thermal Processes). It is possible free convection could set up in coarse granular salt, effectively increasing the heat transfer (also reducing peak temperature at the waste package). To ensure convection, the backfill may require some changes to the run-of-mine granular salt to optimize the grain size distribution, increasing its permeability.

- Chemically salt-compatible cementitious seals, where the EDZ is mined out before installation or grouted after installation, should be emplaced for immediate strength and low-permeability at the ends of granular salt drift seals and the bottom of granular salt in shaft seals. These cement seals only need to hold until the granular salt backfill has reconsolidated to the properties of intact salt ($< 10^3$ years), see § 2.3, EBS. Using granular salt as aggregate in cementitious seals may also give them more ability to creep and deform without brittle fracture (keeping permeability low).
- High-porosity non-salt (e.g., silica gravel) region at bottom of shaft should be included to absorb infiltration and gas pressure without rapid creep closure (important at later time, once the repository closes and there is some pressurization due to creep closure and gas generation – see § 4.2.4, Gas Generation).

The salt engineered barrier system is made of saline cements and granular salt, so it doesn't share much overlap with crystalline and argillite disposal concepts, which rely almost exclusively on bentonite to fill gaps and seal fractures. Research, development, and optimization of EBS components specific to salt repositories is an area that could continue to benefit from future investment and continued international collaborations.

This page intentionally left blank.

REFERENCES

[1] Murad AbuAisha and Joël Billiote. A discussion on hydrogen migration in rock salt for tight underground storage with an insight into a laboratory setup. *Journal of Energy Storage*, 38:102589, 2021.

[2] E. H. Ahrens and T. F. Dale. Data report on the Waste Isolation Pilot Plant Small-Scale Seal Performance Test, Series F grouting experiment. Technical Report SAND93–1000, Sandia National Laboratories, Albuquerque, NM, March 1996.

[3] Maarten Arensten and Rinie van Est, editors. *The Future of Radioactive Waste Governance: Lessons from Europe*. Springer, 2022.

[4] Bartol, Vuorio, Neeft, Verhoef, McCombie, and Chapman. COPERA Salt 2024: A conditional safety case and feasibility study. Technical report, COVRA, 2024.

[5] Jeroen Bartol and Marja Vuorio. Safety assessment for a geological disposal facility in domal salt: the Dutch case. *Geomechanics for Energy and the Environment*, page 100645, 2025.

[6] Alfredo Battistelli, Claudio Calore, and Karsten Pruess. The simulator TOUGH2/EWASG for modeling geothermal reservoirs with brines and non-condensible gas. *Geothermics*, 26(4):437–464, 1997.

[7] Michael Batzle and Zhijing Wang. Sesmic properties of pore fluids. *Geophysics*, 57(11):1396–1408, 1992.

[8] M. Bąbel and B. C. Schreiber. *Treatice on Geochemistry*, chapter Geochemistry of Evaporites and Evolution of Seawater, pages 483–560. Elsevier, second edition, 2014.

[9] R. L. Beauheim, A. Ait-Chalal, G. Vouille, S.-M. Tijani, D. F. McTigue, C. Brun-Yaba, S. M. Hassanizadeh, G. M. van der Gissen, H. Holtman, and P. N. Mollema. INTRAVAL phase 2 WIPP 1 test case report: Modeling of brine flow through halite at the Waste Isolation Pilot Plant site. Technical Report SAND97–0788, Sandia National Laboratories, Albuquerque, NM, May 1997.

[10] R. L. Beauheim and R. M. Roberts. Hydrology and hydraulic properties of a bedded evaporite formation. *Journal of Hydrology*, 259(1):66–88, 2002.

[11] R. L. Beauheim, R. M. Roberts, T. F. Dale, M. D. Fort, and W. A. Stensrud. Interpretation of brine-permeability tests of the Salado Formation at the Waste Isolation Pilot Plant site: Second interim report. Technical Report SAND92–0533, Sandia National Laboratories, Albuquerque, NM, 1993.

[12] N. M. Beeler, R. W. Simpson, S. H. Hickman, and D. A. Lockner. Pore fluid pressure, apparent friction, and Coulomb failure. *Journal of Geophysical Research*, 105(B11):25533–25542, 2000.

[13] Joachim Behlau and Gerhard Mingerzahn. Geological and tectonic investigations in the former Morsleben salt mine (Germany) as a basis for the safety assessment of a radioactive waste repository. *Engineering Geology*, 61(2–3):83–97, 2001.

[14] Lyacine Bennacer, Nasre-Dine Ahfir, Abdellah Alem, and HuaQing Wang. Coupled effects of ionic strength, particle size, and flow velocity on transport and deposition of suspended particles in saturated porous media. *Transport in porous media*, 118(2):251–269, 2017.

[15] Pierre Bérest, Hakim Gharbi, Benoit Brouard, Brückner, Kerry DeVries, Grégoire Hévin, Gerd Hofer, Christopher Spiers, and Janos Urai. Very slow creep tests on salt samples. *Rock Mechanics and Rock Engineering*, 52:2917–2934, 2019.

[16] C. Betters, J. Vornlocher, T. Paronish, D. Crandall, J. Moore, and K. L. Kuhlman. Computed tomography scanning and geophysical measurements of the Salado Formation from boreholes at the Waste Isolation Pilot Plant. Technical Report NETL-TRS-1-2020, National Energy Technology Laboratory, Morgantown, WV, January 2020.

[17] O. O. Blake, D. R. Faulkner, R. H. Worden, P. J. Armitage, and A. A. Espie. Effect of thermal shock on the permeability and seismic wave velocity of the caprock and reservoir during CO_2 injection. *International Journal of Greenhouse Gas Control*, 118:103691, 2022.

[18] L. Blanco Martín, J. Rutqvist, J. T. Birkholzer, R. Wolters, M. Rutenberg, J. Zhao, and Karl-Heinz Lux. Comparison of two modeling procedures to evaluate thermal-hydraulic-mechanical processes in a generic salt repository for high-level nuclear waste. In *48th US Rock Mechanics / Geomechanics Symposium*, number ARMA 14–7411. American Rock Mechanics Association, June 2014.

[19] Laura Blanco-Martín, Jonny Rutqvist, Alfredo Battistelli, and Jens T. Birkholzer. Coupled processes modeling in rock salt and crushed salt including halite solubility constraints: Application to disposal of heat-generating nuclear waste. *Transport in Porous Media*, 124:159–182, 2018.

[20] W. Bollingerfehr, D. Buhmann, W. Filbert, S. Keller, J. Krone, A. Lommerzheim, J. Mönig, S. Mrugalla, N. Müller-Hoeppe, J. R. Weber, and J. Wolf. Status of the safety concept and safety demonstration for an HLW repository in salt. Technical Report TEC-15–2013-AB, Federal Ministry for Economic Affairs and Energy (BMWi), Peine, Germany, 2013.

[21] W. Bollingerfehr, W. Filbert, S. Dorr, P. Herold, C. Lerch, P. Burgwinkel, F. Charlier, B. Thomauske, G. Bracke, and R. Kilger. Endlangerauslegung und -optimierung. Technical Report GRS-281, Gesellschaft für Anlagen- und Reaktorsicherheit (GRS) GmbH, 2012.

[22] David J. Borns. Marker Bed 139: A study of drillcore from a systematic array. Technical Report SAND85–0023, Sandia National Laboratories, Albuquerque, NM, 1985.

[23] David J. Borns. Rates of evaporite deformation: The role of pressure solution. Technical Report SAND85–1599, Sandia National Laboratories, Albuquerque, NM, July 1987.

[24] David J. Borns and John C. Stormont. An interim report on excavation effects studies at the Waste Isolation Pilot Plant: The delineation of the disturbed rock zone. Technical Report SAND87–1375, Sandia National Laboratories, Albuquerque, NM, 1988.

[25] S. M. Bourret, P. J. Johnson, G. A. Zyvoloski, S. P. Chu, D. J. Weaver, S. Otto, H. Boukhalfa, F. A. Caporuscio, A. B. Jordan, and P. H. Stauffer. Experiments and modeling in support of generic salt repository science. Technical Report LA-UR-16–27329, Los Alamos National Laboratory, Los Alamos, NM, September 2016.

[26] R. L. Bradshaw and W. C. McClain. Project Salt Vault: A demonstration of the disposal of high-activity solidified wastes in underground salt mines. Technical Report ORNL-4555, Oak Ridge National Laboratory, Oak Ridge, TN, 1971.

[27] R. L. Bradshaw and Florentino Sanchez. Migration of brine cavities in rock salt. *Journal of Geophysical Research*, 74(17):4209–4212, 1969.

[28] L. H. Brush, J. W. Gardner, and L. J. Storz. Development of a gas-generation model for the Waste Isolation Pilot Plant. Technical Report SAND93–1145C, Sandia National Laboratories, Albuquerque, NM, 1993.

[29] L. H. Brush, M. A. Molecke, R. E. Westerman, A. J. Francis, J. B. Gillow, R. H. Vreeland, and D. T. Reed. Laboratory studies of gas generation for the Waste Isolation Pilot Plant. Technical Report SAND92–2160C, Sandia National Laboratories, Albuquerque, NM, 1992.

[30] C. R. Bryan, A. W. Knight, B. L. Nation, R. M. Katona, E. K. Karasz, T. J. Montoya, D. M. Brooks, N. W. Porter, L. N. Gilkey, J. M. Taylor, and R. F. Schaller. Understanding and predicting stress corrosion cracking of SNF dry storage canisters. In *International High Level Radioactive Waste Management Conference*, number SAND2022–15755C, Albuquerque, NM, 2022. Sandia National Laboratories, American Nuclear Society.

[31] C. Bube, V. Metz, E. Bohnert, K. Garbev, D. Schild, and B. Kienzler. Long-term cement corrosion in chloride-rich solutions relevant to radioactive waste disposal in rock salt - Leaching experiments and thermodynamic simulations. *Physics and Chemistry of the Earth, Parts A/B/C*, 64:87–94, 2013.

[32] Stuart Buchholz, Evan Keffeler, Karla Lipp, Kerry DeVries, and Francis Hansen. Proceedings of the 10th US/German workshop on salt repository researh, design, and operation. Technical Report SAND2019–9998R, Sandia National Laboratories, Albuquerque, NM, 2019.

[33] B. M. Butcher. The advantages of a salt/bentonite backfill for Waste Isolation Pilot Plant disposal rooms. Technical Report SAND90–3074, Sandia National Laboratory, Albuquerque, NM, 1991.

[34] J. Byerlee. *Rock Friction and Earthquake Prediction*, chapter Friction of Rocks, pages 615–626. Number 6 in Contributions to Current Research in Geophysics. Birkhäuser, 1978.

[35] G. D. Callahan. Crushed salt constitutive model. Technical Report SAND98–2680, Sandia National Laboratories, Albuquerque, NM, 1999.

[36] Florie Caporuscio, John Gibbons, Chunghong Li, and Eric Oswald. Salado flow conceptual models final peer review report. Technical report, US Department of Energy Carlsbad Field Office, March 2003.

[37] Florie A. Caporuscio, Hakim Boukhalfa, Michael C. Cheshire, and Mei Ding. Brine migration experimental studies for salt repositories. Technical Report LA-UR-26603, Los Alamos National Laboratory, Los Alamos, NM, August 2014.

[38] Florie A. Caporuscio, Hakim Boukhalfa, Michael C. Cheshire, Amy B. Jordan, and Mei Ding. Brine migration experimental studies for salt repositories. Technical Report LA-UR-13–27240, Los Alamos National Laboratory, Los Alamos, NM, September 2013.

[39] N. L. Carter and F. D. Hansen. Creep of rocksalt. *Tectonophysics*, 92(4):275–333, 1983.

[40] Hang Chen, Jiannan Wang, Linqing Luo, Shawn Otto, Jon Davis, Kristopher L. Kuhlman, and Yuxin Wu. Electrical resistivity changes during heating experiments unravel heterogeneous thermal-hydrological-mechanical processes in salt formations. *Geophysical Research Letters*, 51(14):e2024GL109836, 2024.

[41] Y. Cinar, G. Pusch, and V. Reitenbach. Petrophysical and capillary properties of compacted salt. *Transport in Porous Media*, 64(2):199–228, 2006.

[42] Justin B. Clarity, Kaushik Banerjee, L. Paul Miller, Santosh Bhatt, and Mathew W. Swinney. Dual purpose canister reactivity and groundwater absorption analyses. Technical Report ORNL/SPR-2020/1724; FCRD-UFD-2014-000520-Rev. 06., Oak Ridge National Laboratory, Oak Ridge, TN, 2020.

[43] M. Ben Clennell. *Developments in Petrophysics*, chapter Tortuosity: a guide through the maze, pages 299–344. Number 122. Geological Society, 1997.

[44] François Henri Cornet. *Elements of Crustal Geomechanics*. Cambridge University Press, 2015.

[45] Westinghouse Electrical Corporation. Engineered waste package conceptual design: Defense high-level waste (Form 1), commercial high-level waste (Form 1), and spent fuel (Form 2) disposal in salt. Technical Report AESD-TME-3131, Office of Nuclear Waste Isolation, September 1982.

[46] Ph. Cosenza. *Coupled Effects Between Mechanical Behavior and Mass Transfer Phenomena in Rock Salt*. PhD thesis, Ecole Polytechnique, 1996.

[47] Ph. Cosenza and M. Ghoreychi. Coupling between mechanical behavior and transfer phenomena in salt. In M. Ghoreychi, editor, *3rd Conference on Mechanical Behavior of Salt*, pages 271–293. Trans Tech Publications, 1993.

[48] Olivier Coussy. *Poromechanics*. John Wiley & Sons, 2004.

[49] Randall T. Cygan. The solubility of gases in NaCl brine and a critical evaluation of available data. Technical Report SAND90–2848, Sandia National Laboratories, Albuquerque, NM, January 1991.

[50] Oliver Czaikowski, Larissa Friedenberg, Klaus Wieczorek, Nina Müller-Hoeppe, Christian Lerch, Ralf Eickemeir, Ben Laurich, Wenting Liu, Dieter Stührenberg, Kristoff Svensson, Kornelia Zemke, Christoph Lüdeling, Till Popp, James Bean, Melissa Mills, Benjamin Reedlunn, Uwe Düsterloh, Svetlana Lerche, and Jaun Zhao. KOMPASS - Compaction of crushed salt for the safe containment. Technical Report GRS-608, Gesellschaft für Anlagen- und Reaktorsicherheit (GRS) GmbH, August 2020.

[51] Christian David, Teng-Fong Wong, Wenlu Zhu, and Jiaxiang Zhang. Laboratory measurements of compaction-induced permeability change in porous rocks: Implications for the generation and maintenance of pore pressure excess in the crust. *Pure and Applied Geophysics*, 143(13):425–456, 1994.

[52] C. Davies and F. Bernier, editors. *Impact of the Excavation Disturbed or Damaged Zone (EDZ) on the Performance of Radioactive Waste Geological Repositories*, number EUR 21028 EN, Brussels, Belgium, 2005.

[53] P. B. Davies. Evaluation of the role of threshold pressure in controlling flow of waste generated gas into bedded salt at the Waste Isolation Pilot Plant. Technical Report SAND90–3246, Sandia National Laboratories, Albuquerque, NM, 1991.

[54] P. B. Davies, L. H. Brush, and F. T. Mendenhall. Assessing the impact of waste-generated gas from the degradation of transuranic waste at the Waste Isolation Pilot Plant (WIPP): An overview of strongly coupled chemical, hydrological, and structural processes. Technical Report SAND91-0707C, Sandia National Laboratories, Albuquerque, NM, 1991.

[55] Peter B. Davies. Assessing deep-seated dissolution-subsidence hazards at radioactive-waste repository sites in bedded salt. *Engineering Geology*, 27(1–4):467–487, 1989.

[56] C. De Las Cuevas and J. J. Pueyo. The influence of mineralogy and texture in the water content of rock salt formations. Its implications in radioactive waste disposal. *Applied Geochemistry*, 10(3):317–327, 1995.

[57] D. E. Deal, R. J. Abitz, D. S. Belski, J. B. Case, M. E. Crawley, C. A. Givens, P. P. James Lipponer, D. J. Milligan, J. Myers, D. W. Powers, and M. A. Valdivia. Brine sampling and evaluation program 1992–1993 report and summary of BSEP data since 1982. Technical Report DOE-WIPP 94–011, Westinghouse Electric Corporation, Carlsbad, NM, 1995.

[58] D. E. Deal, R. J. Abitz, J. Myers, J. B. Case, D. S. Belski, M. L. Martin, and W. M. Roggenthen. Brine sampling and evaluation report, 1990 program. Technical Report DOE-WIPP 91–036, IT Corporation and Westinghouse Electrical Corporation, 1991.

[59] D. E. Deal and J. B. Case. Brine sampling and evaluation program - Phase I report. Technical Report DOE/WIPP-87–008, IT Corporation, June 1987.

[60] D. E. Deal, J. B. Case, R. M. Deshler, P. E. Drez, J. Myers, and J. R. Tyburski. Brine sampling and evaluation program - Phase II report. Technical Report DOE/WIPP-87–010, IT Corporation, December 1987.

[61] DOE CBFO. Title 40 CFR Part 191 Compliance Certification Application. Technical Report DOE/CAO 1996–2184, US Department of Energy Office of Environmental Management Carlsbad Field Office, October 1996.

[62] DOE CBFO. Title 40 CFR Part 191 Compliance Recertification Application 2019 for the Waste Isolation Pilot Plant. Technical Report DOE/WIPP-19-3609, Rev. 0, US Department of Energy Office of Environmental Management Carlsbad Field Office, March 2019.

[63] Thomas Driesner. The system H_2O-NaCl. Part II: Correlations for molar volume, enthalpy, and isobaric heat capacity from 0 to 1000 °C, 0 to 5000 bar, and 0 to 1 X_{NaCl}. *Geochimica et Cosmochimica Acta*, 71(20):4902–4919, 2007.

[64] Thomas Driesner and Christoph A. Heinrich. The system H_2O-NaCl. Part I: Correlation formulae for phase relations in temperature-pressure-composition space from 0 to 1000 °C, 0 to 5000 bar, and 0 to 1 X_{NaCl}. *Geochimica et Cosmochimica Acta*, 71(20):4880–4901, 2007.

[65] Oliver B. Duffy, Michael R. Hudec, Frank Peel, Gillian Apps, Alex Bump, Lorena Moscardelli, Tim P. Dooley, Naiara Fernandez, Shuvahit Bhattacharya, Ken Wisian, and Mark W. Shuster. The role of salt tectonics in the energy transition: An overview and future chanllenges. *Tektonika*, 1(1), 2023.

[66] F. A. L. Dullien. *Porous Media: Fluid Transport and Pore Structure*. Academic Press, second edition, 1992.

[67] U. Düsterloh, K. Herchen, K. H. Lux, K. Salzer, R. M. Günther, W. Minkley, A. Hampel, J. G. Argüello, and F. Hansen. Joint Project III on the comparison of constitutive models for the mechanical behavior of rock salt III. Extensive laboratory test program with argillaceous salt from WIPP and comparison of test results. In Roberts, Mellegard, and Hansen, editors, *Mechanical Behavior of Salt VIII*, pages 13–21. Taylor & Francis, 2015.

[68] William C. Eichelberger. Solubility of air in brine at high pressures. *Industrial and Engineering Chemistry*, 47(10):2223–2228, 1955.

[69] Daniel L. Eldridge, Melissa M. Mills, Hayden B. D. Miller, Shawn Otto, Jon E. Davis, Eric J. Guiltinan, Thom Rahn, Kristopher L. Kuhlman, and Philip H. Stauffer. Measuring the stable isotope composition of water in brine from halite fluid inclusions and borehole brine seeps using cavity ring-down spectroscopy. *ACS Earth and Space Chemistry*, 9(1):16–30, 2024.

[70] Mohamed L. Elsayed, Wei Wu, and Louis C. Chow. High salinity seawater boiling point elevation: Experimental verification. *Desalination*, 504:114955, 2021.

[71] Hans-Joachim Engelhard, Lutz Teichmann, and Joachim Adelt. Drift seals at the Asse II salt mine - A summary of more than a decade of experience. In *Waste Management Symposium*, number 21207, 2021.

[72] William N. Findley, James S. Lai, and Kasif Onaran. *Creep and Relaxation of Nonlinear Viscoelastic Materials*. Dover, 1989.

[73] J. Flügge, S. Herr, T. Lauke, A. Meleshyn, R. Miehe, and A. Rübel. Diffusion in the pore water of compacted crushed salt. Technical Report GRS-421, Gesellschaft für Anlagen- und Reaktorsicherheit (GRS) GmbH, 2016.

[74] A. J. Francis, J. B. Gillow, and M. R. Giles. Microbial gas generation under expected Waste Isolation Pilot Plant repository conditions. Technical Report SAND96–2582, Sandia National Laboratories, Albuquerque, NM, March 1997.

[75] G. Freeze, E. Stein, P. V. Brady, C. Lopez, D. Sassani, K. Travis, and F. Gibb. Deep borehole disposal safety case. Technical Report SAND2019–1915, Sandia National Laboratories, Albuquerque, NM, 2019.

[76] G. A. Freeze, K. W. Larson, and P. B. Davies. A summary of methods for approximating salt creep and disposal room closure in numerical models of multiphase flow. Technical Report SAND94–0251, Sandia National Laboratories, Albuquerque, NM, October 1995.

[77] Geoff Freeze, S. David Sevougian, Kristopher L. Kuhlman, Michael Gross, Jens Wolf, Dieter Buhmann, Jeroen Bartol, Christi Leigh, and Jörg Mönig. Generic FEPs catalogue and salt knowledge archive. Technical Report SAND2020–0013186, Sandia National Laboratories, Albuquerque, NM, November 2020.

[78] Daniela Freyer. *Cementitious Materials*, chapter Magnesia building material (Sorel cement) - from basics to applications, pages 311–332. De Gruyter, 2017.

[79] Larissa Friedenberg, Jeroen Bartol, James Bean, Steffen Besse, Hans de Bresser, Jibril B. Coulibaly, Oliver Czaikowski, Uwe Düsterloh, Ralf Eickemeir, Ann-Kathrin Gartzke, Suzanne Hangx, Kyra Jantschik, Ben Laurich, Christian Lerch, Svetlana Lerche, Wenting Liu, Christoph Lüdeling, Melissa M. Mills, Nina Müller-Hoeppe, Bart van Oosterhout, Till Popp, Ole Rabbel, Michael Rahmig, Benjamin Reedlunn, Abram Rogalski, Christopher Rölke, Nachinzorig Saruulbayar, Christopher J. Spiers, Kristoff Svensson, Jan Thiedau, and Kornelia Zemke. KOMPASS-II compaction of crushed salt for safe containment - Phase 2. Technical Report GRS-751, Gesellschaft für Anlagen- und Reaktorsicherheit (GRS) GmbH, January 2024.

[80] L. H. Gevantman. Physical properties data for rock salt. NBS Monograph 167, US Department of Commerce, Washington, DC, January 1981.

[81] Axel Gillhaus, Fritz Crotogino, Daniel Albes, and Leo Van Sambeek. Compilation and evaluation of bedded salt cavern characteristics important to successful cavern sealing and abandonment. Part I: Worldwide bedded salt deposits and bedded salt cavern characteristics. Technical Report 2003–5-SMRI, Solution Mining Research Institute, Encinitas, CA, 2006.

[82] Earnest F. Gloyna and Tom D. Reynolds. Permeability measurements of rock salt. *Journal of Geophysical Research*, 66(11):3913–3921, 1961.

[83] Laura Gonzalez-Blanco, Enrique Romero, Paul Marschall, and Séverine Levasseur. Hydromechanical response to gas transfer in deep argillaceous host rocks for radioactive waste disposal. *Rock Mechanics and Rock Engineering*, 55:1159–1177, 2021.

[84] J. Gramberg and J. P. A. Roest. Cataclastic effects in rock salt laboratory and in situ measurements. Technical Report EUR 9258 EN, European Commission on Nuclear Science and Technology, Brussels, Belguim, 1984.

[85] Eric J. Guiltinan, Kristopher L. Kuhlman, Jonny Rutqvist, Mengsu Hu, Hakim Boukhalfa, Melissa Mills, Shawn Otto, Douglas J. Weaver, Brian Dozier, and Philip H. Stauffer. Temperature response and brine availability to heated boreholes in bedded salt. *Vadose Zone Journal*, 19(1):e20019, 2020.

[86] Rahim Habibi, Shokrollah Zare, Amin Asgari, Mrityunjay Singh, and Saeed Mahmoodpour. Coupled thermo-hydro-mechanical-chemical processes in salt formations for storage applications. *Renewable and Sustainable Energy Reviews*, 188:113812, 2023.

[87] G. Ronald Hadley. Theoretical treatment of evaporation front drying. *International Journal of Heat and Mass Transfer*, 25(10):1511–1522, 1982.

[88] B. Haijtink. Project on effects of gas in underground storage facilities for radioactive waste (PEGASUS project). Technical Report EUR 16746 EN, European Commission, 1996.

[89] A. Hampel, J. G. Argüello, F. D. Hansen, R. M. Günther, K. Salzer, W. Minkley, Karl-Heinz Lux, K. Harchen, U. Düsterloh, A. Pudewills, S. Yildirim, K. Staudtmeister, R. Rokahr, D. Zapf, A. Gährken, C. Missal, and J. Stahlmann. Benchmark calculations of the thermo-mechanical behavior of rock salt – results from a US-German Joint Project. In *47th US Rock Mechanics / Geomechanics Symposium*, number ARMA 13–456. American Rock Mechanics Association, 2013.

[90] Francis D. Hansen. The disturbed rock zone at the Waste Isolation Pilot Plant. Technical Report SAND2003–3407, Sandia National Laboratories, Albuquerque, NM, 2003.

[91] Francis D. Hansen, Kristopher L. Kuhlman, and Steve Sobolik. Considerations of the differences between bedded and domal salt pertaining to disposal of heat-generating nuclear waste. Technical Report SAND2016–6522R, Sandia National Laboratories, Albuquerque, NM, July 2016.

[92] Francis D. Hansen, Walter Steininger, and Enrique Biurrun. Proceedings of 4th US/German Salt Repository Workshop. Technical Report FCRD-UFD-2014–000335, US-DOE Office of Nuclear Energy Used Fuel Disposition Campaign, Albuquerque, NM, December 2013.

[93] Frank D. Hansen. Micromechanics of isochoric salt deformation. In *Proceedings of the 48th American Rock Mechanics Association Meeting*, number ARMA 14-7012, 2014.

[94] Frank D. Hansen and M. Kathryn Knowles. Design and analysis of a shaft seal system for the Waste Isolation Pilot Plant. *Reliability Engineering & System Safety*, 69(1-3):87–98, 2000.

[95] Frank D. Hansen and Christi D. Leigh. Salt disposal of heat-generating nuclear waste. Technical Report SAND2011–0161, Sandia National Laboratories, Albuquerque, NM, January 2011.

[96] Frank D. Hansen, Till Pop, Klaus Wieczorek, and Dieter Stührenberg. Granular salt summary: Reconsolidation principles and applications. Technical Report SAND2014–16141R, Sandia National Laboratories, Albuquerque, NM, July 2014.

[97] E. Hardin, L. Price, E. Kalinina, T. Hadgu, A. Ilgen, C. Bryan, J. Scaglione, K. Banerjee, J. Clarity, R. Jubin, V. Sobes, R. Howard, J. Carter, T. Severynse, and F. Perry. Summary of investigations on technical feasibility of direct disposal of dual-purpose canisters. Technical Report FCRD-UFD-2015–000129 Rev. 0, Sandia National Laboratories, Albuquerque, NM, 2015.

[98] E. L. Hardin, D. J. Clayton, R. L. Howard, J. M. Scaglione, E. Pierce, K. Manegee, M. D. Voegele, H. R. Greenberg, J. Wen, T. A. Buscheck, J. T. Carter, T. Severynse, and W. M. Nutt. Preliminary report on Dual-Purpose Canister disposal alternatives (FY13). Technical Report FCRD-UFD-2013–000171 Rev. 1, Sandia National Laboratories, Albuquerque, NM, 2013.

[99] J. Hart, J. Prij, G.-J. Vis, D.-A. Becker, J. Wolf, U. Noseck, and D. Buhmann. Collection and analysis of current knowledge on salt-based repositories. Technical Report OPERA-PU-NRG221A, COVRA, 2015.

[100] C. G. Herrick, B. Y. Park, M. Y. Lee, and D. J. Holcomb. Estimating the extent of the disturbed rock zone around a WIPP disposal room. In *Proceedings of the 43rd American Rock Mechanics Association Meeting*, number SAND2009–1416C, 2009.

[101] H. H. Hess, J. N. Adkins, W. B. Heroy, W. E. Benson, M. K. Hubbert, J. C. Frye, R. J. Russell, and C. V. Theis. The disposal of radioactive waste on land, report of the committee on waste disposal of the division of Earth Sciences. Technical Report Publication 519, National Academy of Sciences - National Research Council, Washington, DC, 1957.

[102] Jacque J. Hohlfelder. Salt Block II: Description and results. Technical Report SAND79–2226, Sandia National Laboratories, Albuquerque, NM, 1980.

[103] David J. Holcomb, Terry MacDonald, and Robert D. Hardy. Using ultrasonic waves to assess the disturbed rock zone (DRZ) in an alcove corner excavated in salt at the WIPP (Waste Isolation Pilot Plant). Technical Report SAND2001–3055C, Sandia National Laboratories, Albuquerque, NM, 2002.

[104] M. B. Holness and S. Lewis. The structure of the halite-brine interface inferred from pressure and temperature variations of equilibrium dihedral angles in the halite-H_2O-CO_2 system. *Geochimica et Cosmochimica Acta*, 61(4):795–804, 1997.

[105] Susan M. Howarth and Tracy Christian-Frear. Porosity, single-phase permeability, and capillary pressure data from preliminary laboratory experiments on selected samples from Marker Bed 139 at the Waste Isolation Pilot Plant (3 volumes). Technical Report SAND94–0472, Sandia National Laboratories, Albuquerque, NM, 1997.

[106] Jianjun Hu, Heping Xie, Cunbao Li, and Qiang Sun. Effect of cyclic thermal shock on granite pore permeability. *Lithosphere*, 2021(5):4296301, 2021.

[107] Mengsu Hu, Carl I. Steefel, and Jonny Rutqvist. Microscale mechanical-chemical modeling of granular salt: Insights for creep. *Journal of Geophysical Research: Solid Earth*, 126(12):e2021JB023112, 2021.

[108] Mengsu Hu, Carl I. Steefel, Jonny Rutqvist, and Benjamin Gilbert. Microscale THMC modeling of pressure solution in salt rock: Impacts of geometry and temperature. *Rock Mechanics and Rock Engineering*, 56(10):7071–7089, 2023.

[109] Udo Hunsche and Andreas Hampbel. Rock salt – The mechanical properties of the host rock material for a radioactive waste repository. *Engineering Geology*, 52(3–4):271–291, 1999.

[110] L. D. Hurtado, M. K. Knowles, V. A. Kelley, T. L. Jones, J. B. Ogintz, and T. W. Pfeifle. WIPP shaft seals system parameters recommended to support compliance calculations. Technical Report SAND97–1287, Sandia National Laboratories, Albuquerque, NM, 1997.

[111] IAEA. The safety case and safety assessment for the disposal of radioactive waste. Technical Report SSG-23, SGI/PUB/1553, International Atomic Energy Agency, Vienna, Austria, 2012.

[112] Martin P. A. Jackson and Michhael R. Hudec. *Salt Tectonics: Principles and Practice*. Cambridge, 2017.

[113] J. C. Jaeger and N. G. W. Cook. *Fundamentals of Rock Mechanics*. Chapman and Hall, third edition, 1979.

[114] K. Jantschik, O. Czaikowski, H. C. Moog, and K. Wieczorek. Investigating the sealing capacity of a seal system in rock salt (DOPAS Project). *Kerntechnik*, 81(5):571–585, 2016.

[115] G. H. Jenks. Effects of temperature, temperature gradients, stress, and irradiation on migration of brine inclusions in a salt repository. Technical Report ORNL-5526, Oak Ridge National Laboratory, Oak Ridge, TN, 1979.

[116] A. L. Jensen, R. L. Jones, E. N. Lorusso, and C. L. Howard. Large-scale brine inflow data report for Room Q prior to November 25, 1991. Technical Report SAND92–1173, Sandia National Laboratories, Albuquerque, NM, 1993.

[117] Malcom K. Jenyon. *Salt Tectonics*. Elsevier Applied Science, 1986.

[118] James Jerden, Eric Lee, Vineeth Kumar Gattu, and William Ebert. Fuel Matrix Degradation Model development update: Alloy corrosion rates and hydrogen generation. Technical Report ANL/CFCT-19/12, Argonne National Laboratory, September 2019.

[119] Norbert Jockwer and Klaus Wieczorek. ADDIGAS: Advective and diffusive gas transport in rock salt formations, Final Report. Technical Report GRS-234, Gesellschaft für Anlagen- und Raktosicherheit (GRS), Cologne, Germany, 2008.

[120] K. S. Johnson and S. Gonzales. Salt deposits in the United States and regional geologic characteristics important for storage of radioactive waste. Technical Report Y/OWI/SUB-7414/1, Office of Waste Isolation, Oak Ridge, TN, 1978.

[121] P. J. Johnson, G. A. Zyvoloski, and P. H. Stauffer. Impact of a porosity-dependent retention function on simulations of porous flow. *Transport in Porous Media*, 127(1):211–232, 2019.

[122] Amy B. Jordan, Hakim Boukhalfa, Florie A. Caporuscio, Bruce A Robinson, and Philip H. Stauffer. Hydrous mineral dehydration around heat-generating nuclear waste in bedded salt formations. *Environmental Science & Technology*, 49(11):6783–6790, 2015.

[123] Halla Kerkache, Hai Hoang, Pierre Cézac, Guillaume Gallieéro, and Salaheddine Chabab. The solubility of H_2 in NaCl brine at high pressures and high temperatures: Molecular simulation study and thermodynamic modeling. *Journal of Molecular Liquids*, 400:124497, 2024.

[124] M. K. Knowles and C. L. Howard. Field and laboratory testing of seal materials proposed for the Waste Isolation Pilot Plant. Technical Report SAND95–2082C, Sandia National Laboratories, Albuquerque, NM, 1996.

[125] M. Kathryn Knowles, David Borns, Joanne Fredrich, David Holcomb, Ronald Price an David Zeuch, Timothy Dale, and R. Scott Van Pelt. Testing the disturbed zone around a rigid inclusion in salt. In *Proceedings of the 4th Conference on the Mechanical Behavior of Salt*, pages 1–17, Rotterdam, 1996. A.A. Balkema.

[126] M. Krabbendam. Sliding of temperate basal ice on a rough, hard bed: creep mechanisms, pressure melting, and implications for ice streaming. *The Cryosphere*, 10(5):1915–1932, 2016.

[127] Wayne B. Krause. Avery Island brine migration tests: Installation, operation, data collection, and analysis. Technical Report ONWI-190(4), Office of Nuclear Waste Isolation, Columbus, OH, 1983.

[128] Kristopher L. Kuhlman. Historic testing relevant to disposal of heat-generating waste in salt. *Radwaste Solutions*, 20(4):22–28, 2013.

[129] Kristopher L. Kuhlman. Summary results for brine migration modeling performed by LANL, LBNL, and SNL for the Used Fuel Disposition program. Technical Report SAND2014–18217R, Sandia National Laboratories, Albuquerque, NM, 2014.

[130] Kristopher L. Kuhlman. Processes in salt repositories. Technical Report SAND2019–6441R, Sandia National Laboratories, Albuquerque, NM, 2019.

[131] Kristopher L. Kuhlman. DECOVALEX-2023 Task E final report. Technical Report LBNL-2001625, Lawrence Berkeley National Laboratory, Berkeley, CA, 2024.

[132] Kristopher L. Kuhlman. Generalized solution for double-porosity flow through a graded excavation damaged zone. *Mathematical Geosciences*, 56:1739–1762, 2024.

[133] Kristopher L. Kuhlman, Jeroen Bartol, Steven J. Benbow, Michelle Bourret, Oliver Czaikowski, Eric Guiltinan, Kyra Jantschik, Richard Jayne, Simon Norris, Jonny Rutqvist, H. Shao, H. Tounsi, and C. Watson. Synthesis of results for Brine Availability Test in Salt (BATS) DECOVALEX-2023 Task E. *Geomechanics for Energy and the Environment*, 39:100581, 2024.

[134] Kristopher L. Kuhlman, Jeroen Bartol, Alexander Carter, Andree Lommerzheim, and Jens Wolf. Scenario development for safety assessment in deep geologic disposal of high-level radioactive waste and spent nuclear fuel: A review. *Risk Analysis*, 44(8):1850–1864, 2024.

[135] Kristopher L. Kuhlman, Carlos M. Lopez, Melissa M. Mills, Jessica M. Rimsza, and David C. Sassani. Evaluation of spent nuclear fuel disposition in salt (FY18). Technical Report SAND2018–11355R, Sandia National Laboratories, Albuquerque, NM, 2018.

[136] Kristopher L. Kuhlman and Bwalya Malama. Brine flow in heated geologic salt. Technical Report SAND2013–1944, Sandia National Laboratories, Albuquerque, NM, March 2013.

[137] Kristopher L. Kuhlman and Bwalya Malama. Assessment of contaminated brine fate and transport in MB139 at WIPP. Technical Report SAND2014–16153, Sandia National Laboratories, Albuquerque, NM, 2014.

[138] Kristopher L. Kuhlman and Edward N. Matteo. Porosity and permeability: Literature review and summary. In *Mechanical Behavior of Salt IX*, Hannover, Germany, 2018. Federal Institute for Geosciences and Natural Resources.

[139] Kristopher L. Kuhlman, Melissa Mills, Richard Jayne, Edward Matteo, Courtney Herrick, Martin Nemer, Yongliang Xiong, Charles Choens, Matthew Paul, Christine Downs, Phil Stauffer, Hakim Boukhalfa, Eric Guiltinan, Thom Rahn, Shawn Otto, Jon Davis, Daniel Eldridge, Aiden Stansberry, Jonny Rutqvist, Yuxin Wu, Haffsa Tounsi, Mengsu Hu, Sebastian Uhlemann, and Jiannan Wang. Brine Availability Test in Salt (BATS) FY23 update. Technical Report SAND2023–08820R, Sandia National Laboratories, Albuquerque, NM, August 2023.

[140] Kristopher L. Kuhlman, Melissa Mills, Richard Jayne, Edward Matteo, Courtney Herrick, Martin Nemer, Yongliang Xiong, Robert Choens, Matthew Paul, Phil Stauffer, Hakim Boukhalfa, Eric Guiltinan, Thom Rahn, Doug Weaver, Brian Dozier, Shawn Otto, Jonny Rutqvist, Yuxin Wu, Mengsu Hu, Sebastian Uhlemann, and Jiannan Wang. Brine Availability Test in Salt (BATS) FY21 update. Technical Report SAND2021–10962R, Sandia National Laboratories, Albuquerque, NM, August 2021.

[141] Kristopher L. Kuhlman, Melissa M. Mills, Richard S. Jayne, Edward N. Matteo, Courtney G. Herrick, R. Charles Choens, Matthew J. Paul, Phiip H. Stauffer, Eric Guiltinan, Thom Rahn, Shawn Otto, Jon Davis, Daniel Eldridge, Jonny Rutqvist, Yuxin Wu, Mengsu Hu, Hang Chen, and Jiannan Wang. Brine Availability Test in Salt (BATS) FY24 update. Technical Report SAND2024–12338R, Sandia National Laboratories, Albuquerque, NM, August 2024.

[142] Kristopher L. Kuhlman, Melissa M. Mills, and Edward N Matteo. Consensus on intermediate scale salt field test design. Technical Report SAND2017–3179R, Sandia National Laboratories, Albuquerque, NM, March 2017.

[143] Kristopher L. Kuhlman and S. David Sevougian. Establishing the technical basis for disposal of heat-generating waste in salt. Technical Report FCRD-UFD-2013–000233, US-DOE Office of Nuclear Energy Used Fuel Disposition Campaign, Albuquerque, NM, 2013.

[144] Kristopher L. Kuhlman, Steve Wagner, Dwayne Kicker, Ross Kirkes, Coutney Herrick, and David Guerin. Review and evaluation of Salt R&D data for disposal of nuclear waste in salt. Technical Report FCRD-UFD-2012–000380, US-DOE Office of Nuclear Energy Used Fuel Disposition Campaign, Carlsbad, NM, September 2012.

[145] Alf Larsson. The international projects INTRACOIN, HYDROCOIN, and INTRAVAL. *Advances in Water Resources*, 15(1):85–87, 1992.

[146] Alf Larsson, Karin Pers, Kristina Skagius, and Björn Dverstorp. The international INTRAVAL project: Phase 2, summary report. Swedish Nuclear Power Inspectorate (SKI), 1997.

[147] Patrice Lebrun, Joël Billiote, Michael Deveughèle, and Jean-Michel Le Cléac'h. Local increase in rock salt porosity by coalescence of fluid inclusions during a thermal loading. *Comptes Rendus de l'Academie des Sciences, Serie 2, Sciences de la Terre et des Planetes*, 320(7):555–561, 1995.

[148] Jean Lemaitre. How to use damage mechanics. *Nuclear Engineering and Design*, 80(2):233–245, 1984.

[149] C. Lerch. Realistic modeling in R&D project KOMPASS – generic and/or specific. In *Tenth US/German Workshop on Salt Repository Research, Design, and Operation*, 2019.

[150] Philippe Leroy, Arnault Lassin, Mohamed Azaroual, and Laurent André. Predicting the surface tension of aqueous 1:1 electrolyte solutions at high salinity. *Geochimica et Cosmochimica Acta*, 74(19):5427–5442, 2010.

[151] S. Lewis and M. Holness. Equilibrium halite-H_2O dihedral angles: High rock-salt permeability in the shallow crust? *Geology*, 24(5):431–434, 1996.

[152] Shi-Yuan Li and Janos L. Urai. Rheology of rock salt for salt tectonics modeling. *Petroleum Science*, 13:712–724, 2016.

[153] H. H. Liu. Non-Darcian flow in low-permeability media: Key issues related to geological disposal of high-level nuclear waste in shale formations. *Hydrogeology Journal*, 22:1525–1534, 2014.

[154] Hui-Hai Liu and Jens Birkholzer. On the relationship between water flux and hydraulic gradient for unsaturated and saturated clay. *Journal of Hydrology*, 475:242–247, 2012.

[155] T. F. Lomenick. The siting record. Technical Report ORNL/TM-12940, Oak Ridge National Laboratory, Oak Ridge, TN, 1996.

[156] Christoph Lüdeling, Dirk Naumann, and Wolfgang Minkley. Investigation of fluid transport in rock salt under repository-relevant conditions - the PeTroS project. In *Mechanical Behavior of Salt X*, pages 1–12, 2022.

[157] Einat Magal, Noam Weisbrod, Yoseph Yechieli, Sharon L. Walker, and Alexander Yakirevich. Colloid transport in porous media: Impact of hyper-saline solutions. *Water Research*, 45:3521–3532, 2011.

[158] P. E. Mariner, W. P. Gardner, G. E. Hammond, S. D. Sevougian, and E. R. Stein. Application of generic disposal system models. Technical Report SAND2015–10037R, Sandia National Laboratories, Albuquerque, NM, 2015.

[159] William C. McClain and A. L. Boch. Disposal of radioactive waste in bedded salt formations. *Nuclear Techology*, 24(3):398–408, 1974.

[160] D. F. McTigue. Thermoelastic response of fluid-saturated rock. *Journal of Geophysical Research*, 91(B9):9533–9542, 1986.

[161] D. F. McTigue. Flow into a heated borehole in porous, thermoelastic rock: Analysis. *Water Resources Research*, 26(8):1763–1774, 1990.

[162] R. J. Millington and J. P. Quirk. Permeability of porous solids. *Transactions of the Faraday Society*, 57:1200–1207, 1961.

[163] Melissa M. Mills, K. Kuhlman, E. Matteo, C. Herrick, M. Nemer, J. Heath, Y. Xiong, M. Paul, P. Stauffer, H. Boukhalfa, E. Guiltinan, T. Rahn, D. Weaver, B. Dozier, S. Otto, J. Rutqvist, Y. Wu, J. Ajo-Franklin, and M. Hu. Salt heater test (FY19). Technical Report SAND2019–4814R, Sandia National Laboratories, Albuquerque, NM, 2019.

[164] Melissa M. Mills, Kristopher L. Kuhlman, Richard S. Jayne, Jibril B. Coulibaly, and Benjamin Reedlunn. Salt international collaborations FY24 update. Technical report, Sandia National Laboratories, Albuquerque, NM, 2024.

[165] Melissa M. Mills, Kristopher L. Kuhlman, Richard S. Jayne, Jörg Melzer, Till Popp, Tuanny Cajuhi, Larissa Friedenberg, Oliver Czaikowski, and Neel Gupta. Proceedings of the 13th US/German Workshop on Salt Repository Research, Design, and Operation. Technical Report SAND2024–02255R, Sandia National Laboratories, Albuquerque, NM, February 2024.

[166] W. Minkley, D. Brückner, and C. Lüdeling. Percolation in salt rocks. In *The Mechanical Behavior of Salt IX*, pages 1–15, 2018.

[167] Martin A. Molecke. Summary of WIPP Materials Interface Interactions Test data on metals interactions and leachate brine analyses. Technical Report SAND88–2023C, Sandia National Laboratories, Albuquerque, NM, October 1988.

[168] Martin A. Molecke, J. Guadalupe Argüello, and Ricardo Beraún. Waste Isolation Pilot Plant simulated RH TRU waste experiments: Data and interpretation report. Technical Report SAND88–1314, Sandia National Laboratories, Albuquerque, NM, April 1993.

[169] Martin A. Molecke and Donald J. Bradley. PNL Sandia HLW package interactions test: Phase One. Technical Report SAND81–1442C, Sandia National Laboratories, Albuquerque, NM, November 1981.

[170] Martin A. Molecke, N. Robert Sorensen, and George G. Wicks. Waste Isolation Pilot Plant Materials Interface Interactions Test: Papers presented at the commission of European communities workshop on in situ testing of radioactive waste forms and engineered barriers. Technical Report SAND93–1055, Sandia National Laboratories, Albuquerque, NM, August 1993.

[171] Martin A. Molecke and Teresa M. Torres. The Waste Package Materials field test in S.E. New Mexico salt. Technical Report SAND83–1516C, Sandia National Laboratories, Albuquerque, NM, 1983.

[172] Martin A. Molecke and G. Wicks, George. Materials Interface Interactions Test (MIIT) details and observations on in situ sample retrievals and test determination. Technical Report SAND92–1954C, Sandia National Laboratories, Albuquerque, NM, 1992.

[173] N. Müller-Hoeppe, M. Breustedt, J. Wolf, O. Czaikowski, and K. Wieczorek. Integrität geotechnischer Barrieren Teil 2: Vertiefte Nachweisführung: Bericht zum Arbeitspaket 9.2; vorläufige Sicherheitsanalyse für den Standort Gorleben, 2012.

[174] N. Müller-Hoeppe, D. Buhmann, O. Czaikowski, H.-J. Engelhardt, H.-J. Herbert, C. Lerch, M. Linkamp, K. Wieczorek, and M. Xie. Integrität geotechnischer Barrieren Teil 1: Vorbemessung: Bericht zum Arbeitspaket 9.2; vorläufige Sicherheitsanalyse für den Standort Gorleben, 2012.

[175] D. E. Munson and P. R. Dawson. Salt-constitutive modeling using mechanism maps. Technical Report SAND81–2196C, Sandia National Laboratories, Albuquerque, NM, 1981.

[176] D. E. Munson, A. F. Fossum, and P. E. Senseny. Advances in resolution of discrepancies between predicted and measured in situ Waste Isolation Pilot Plant (WIPP) room closures. Technical Report SAND88–2948, Sandia National Laboratories, Albuquerque, NM, 1989.

[177] D. E. Munson, S. V. Petney, T. L. Christian-Frear, J. R. Ball, R. L. Jones, and C. L. Northrop-Salazar. 18 W/m^2 mockup for Defense High-Level Waste (Rooms A): In situ data report Vol. II – thermal response gages (February 1985 – June 1990). Technical Report SAND90–2749, Sandia National Laboratories, Albuquerque, NM, 1992.

[178] Darrell E. Munson, Robert L. Jones, John R. Ball, Robert M. Clancy, David L. Hoag, and Sharon V. Petney. Overtest for simulated Defense High-Level Waste (Room B): In situ data report (May 1984–February 1988) Waste Isolation Pilot Plant (WIPP) Thermal/Structural Interactions program. Technical Report SAND89–2671, Sandia National Laboratories, Albuquerque, NM, 1990.

[179] Marcel W. Nathans. The dehydration of polyhalite. *The Journal of Physical Chemistry*, 67(6):1248–1249, 1963.

[180] Kishor Govind Nayar, Divya Panchanathan, G. H. McKinley, and J. H. Lienhard. Surface tension of seawater. *Journal of Physical and Chemical Reference Data*, 43(4):043103, 2014.

[181] NEA. Gas generation and migration in radioactive waste disposal safety-relevant issues. Technical report, Nuclear Energy Agency Organisation for Economic Co-operation and Development, June 2000.

[182] NEA. Natural analogues for safety cases of repositories in rock salt: Salt club workshop proceedings. Technical Report NEA/RWM/R(2013)10, Nuclear Energy Agency Organisation for Economic Co-operation and Development, 2014.

[183] NEA. Microbial influence on the performance of subsurface, salt-based radioactive waste repositories. Technical Report NEA No. 7378, Nuclear Energy Agency Organisation for Economic Co-operation and Development, 2018.

[184] NEA. International features, events and processes (IFEP) list for the deep geological disposal of radioactive waste. Technical Report NEA/RWM/R(2024)2, OECD Publishing, Paris, 2024.

[185] Shlomo P. Neuman. On the tensorial nature of advective porosity. *Advances in Water Resources*, 28:149–159, 2005.

[186] G. H. Nieder-Westermann and W. Bollingerfehr. Germany: Experience of radioactive waste (RAW) management and contaminated site clean-up. In *Radioactive Waste Management and Contaminated Site Clean-Up*, pages 462–488. Elsevier, 2013.

[187] E. J. Nowak. Preliminary result of brine migration studies in the Waste Isolation Pilot Plant (WIPP). Technical Report SAND86–0720, Sandia National Laboratories, Albuquerque, NM, 1986.

[188] E. J. Nowak. Test Plan: Brine inflow and related tests in the brine inflow room (Room Q) of the Waste Isolation Pilot Plant (WIPP). Technical report, Sandia National Laboratories, April 1989.

[189] E. J. Nowak, D. F. McTigue, and R. Beraun. Brine inflow to WIPP disposal rooms: Data, modeling, and assessment. Technical Report SAND88–0112, Sandia National Laboratories, Albuquerque, NM, 1988.

[190] Office of Civilian Radioactive Waste Management. Site characterization plan Deaf Smith County Site, Texas – overview. Technical Report DOE/RW-0163, US Department of Energy, 1988.

[191] D. R. Olander, A. J. Machiels, M. Balooch, and S. K. Yagnik. Thermal gradient migration of brine inclusions in synthetic alkali halide single crystals. *Journal of Applied Physics*, 53(1):669–681, 1982.

[192] S. Olivella, J. Carrera, A. Gens, and E. E. Alonso. Nonisothermal multiphase flow of brine and gas through saline media. *Transport in Porous Media*, 15:271–293, 1994.

[193] S. Olivella, S. Castagna, E. E. Alonso, and A. Lloret. Porosity variations in saline media induced by temperature gradients: Experimental evidences and modelling. *Transport in Porous Media*, 90:763–777, 2011.

[194] S. Olivella and A. Gens. A constitutive model for crushed salt. *International Journal for Numerical and Analytical Methods in Geomechanics*, 26:719–746, 2002.

[195] Heinz Parkus. *Thermoelasticity*. Blaisdale Publishing, 1968.

[196] F. V. Perry, R. E. Kelley, P. F. Dobson, and J. E. Houseworth. Regional geology: A GIS database for alternative host rocks and potential siting guidelines. Technical Report FCRD-UFD-2014–000068, Los Alamos National Laboratory, Los Alamos, NM, 2014.

[197] T. W. Pfeifle, F. D. Hansen, and M. K. Knowles. Salt-saturated concrete strength and permeability. Technical Report SAND96–1789C, Sandia National Laboratories, Albuquerque, NM, 1996.

[198] Tom W. Pfeifle, Frank D. Hansen, and M. Kathryn Knowles. Permeability and confined strength of salt-saturated concrete. Technical Report RSI-96–07, RE/SPEC Inc., Rapid City, SD, 1996.

[199] T. H. Pigford and P. L. Chambrè. Near-field mass transfer in geologic disposal systems: A review. Technical Report LBL-23689, Lawrence Berkeley National Laboratory, Berkeley, CA, 1987.

[200] Kenneth S. Pitzer. Thermodynamics of electrolytes. I. Theoretical basis and general equations. *The Journal of Physical Chemistry*, 77(2):268–277, 1973.

[201] Kenneth S. Pitzer, Peiming Wang, Joseph A. Rard, and Simon L. Clegg. Thermodynamics of electrolytes. 13. Ionic strength dependence of higher-order terms; Equations for $CaCl_2$ and $MgCl_2$. *Journal of Solution Chemistry*, 28:265–282, 1999.

[202] T. Popp. Natural closure of salt openings. In Stuart Buchholz, Evan Keffeler, Karla Lipp, Kerry DeVries, and Francis Hansen, editors, *Proceedings of the 10th US/German Workshop on Salt Repository Researh, Design, and Operation*, number SAND2019–9998R, 2019.

[203] Till Popp, Hartmut Kern, and Otto Schulze. Evolution of dilatancy and permeability in rock salt during hydrostatic compaction and triaxial deformation. *Journal of Geophysical Research*, 106(B3):4061–4078, 2001.

[204] Harry H. Posey and J. Richard Kyle. Fluid-rock interactions in the salt dome environment: An introduction and review. *Chemical Geology*, 74(1–2):1–24, 1988.

[205] Dennis W. Powers. Tracing early breccia pipe studies, Waste Isolation Pilot Plant, Southeastern New Mexico: A study of the documentation available and decision making during the early years of WIPP. Technical Report SAND94–0991, Sandia National Laboratories, Albuquerque, NM, January 1996.

[206] Dennis W. Powers, Steven J. Lambert, Sue-Ellen Shaffer, Leslie R. Hill, and Wendell D. Weart. Geologic characterization report, Waste Isolation Pilot Plant (WIPP) site, southeastern New Mexico. Technical Report SAND78–1596 (2 Volumes), Sandia National Laboratories, Albuquerque, NM, 1978.

[207] Vishnu Ranganathan and Jeffrey S. Hanor. Density-driven groundwater flow near salt domes. *Chemical Geology*, 74(1–2):173–188, 1988.

[208] J. L. Ratigan. A finite element formulation for brine transport in rock salt. *International Journal for Numerical and Analytical Methods in Geomechanics*, 8(3):225–241, 1984.

[209] B. Reedlunn. Reinvestigation into closure predictions of Room D at the Waste Isolation Pilot Plant. Technical Report SAND2016–9961, Sandia National Laboratories, Albuquerque, NM, 2016.

[210] B. Reedlunn. Enhancements to the Munson-Dawson model for rock salt. Technical Report SAND2018–12601, Sandia National Laboratories, Albuquerque, NM, 2018.

[211] Benjamin Reedlunn, James Bean, John Wilkes, and John Bignell. Simulations of criticality control overpack container compaction at the Waste Isolation Pilot Plant. Technical Report SAND2023–10477, Sandia National Laboratories, Albuquerque, NM, January 2023.

[212] Benjamin Reedlunn, Georgios Moutsanidis, Jonghyuk Baek, Tsung-Hui Huang, Jacob Koester, Edward Matteo, Xiaolong He, Karan Taneja, Haoyan Wei, Yuri Bazilevs, Jiun-Shyan Chen, Chven Mitchell, Robert Lander, and Thomas Dewers. Initial simulations of empty room collapse and reconsolidation at the Waste Isolation Pilot Plant. Technical Report SAND2019–15351, Sandia National Laboratories, Albuquerque, NM, December 2019.

[213] Benjamin Reedlunn and Laura A. Williams. Reconstruction of the Room D, B, G, and Q closure histories at the Waste Isolation Pilot Plant. Technical Report SAND2021–6904, Sandia National Laboratories, Albuquerque, NM, June 2021.

[214] T. D. Reynolds and E. F. Gloyna. Reactor Fuel Waste Disposal Project: Permeability of rock salt and creep of underground salt cavities. Technical Report TID-12383, Atomic Energy Commission Division of Technical Information, Oak Ridge, TN, 1960.

[215] L. A. Richards. Capillary conduction of liquids through porous mediums. *Physics*, 1:318–333, 1931.

[216] Jessica M. Rimsza and Kristopher L. Kuhlman. Surface energies and structure of salt–brine interfaces. *Langmuir*, 36(9):2482–2491, 2020.

[217] Jessica M. Rimsza and Kristopher L. Kuhlman. Temperature and pressure dependence of salt–brine dihedral angles in the subsurface. *Langmuir*, 37(45):13291–13299, 2021.

[218] Randall M. Roberts, Richard L. Beauheim, and Paul S. Domski. Hydraulic testing of Salado Formation evaporites at the Waste Isolation Pilot Plant Site: Final report. Technical Report SAND98–2537, Sandia National Laboratories, Albuquerque, NM, 1999.

[219] Edwin Roedder. The fluids in salt. *American Mineralogist*, 69(5-6):413–439, 1984.

[220] Edwin Roedder and R. L. Bassett. Problems in determination of the water content of rock-salt samples and its significance in nuclear-waste storage siting. *Geology*, 9(11):525–530, 1981.

[221] J. P. A. Roest and J. Gramberg. Acoustic crosshole measurement of cataclastic thermomechanical behavior of rocksalt. In *Design and Instrumentation of In Situ Experiments in Underground Laboratories for Radioactive Waste Disposal*, pages 439–447. A.A. Balkema, 1985.

[222] T. Rothfuchs, K. Wieczorek, H. K. Feddersen, G. Stupendahl, A. J. Coyle, H. Kalia, and J. Eckert. Brine migration test, Asse salt mine, Federal Republic of Germany: Final report. Technical Report GSF-Bericht 6/88, Office of Nuclear Waste Isolation (ONWI) and Gesellschaft für Strahlen-und Umweltforschung München (GSF), Munich, Germany, 1988.

[223] André Rübel, Dieter Buhmann, Artur Meleshyn, Jörg Mönig, and Sabine Spiessl. Aspects on the gas generation and migration in repositories for high level waste in salt formations: Preliminary results from the ISIBEL-2 project. Technical Report GRS-A-3592, Gesellschaft für Anlagen- und Raktosicherheit (GRS), January 2011.

[224] Andrè Rübel, Dieter Buhmann, Artur Meleshyn, Jörg Mönig, and Sabine Spiessl. Aspects on the gas generation and migration in repositories for high level waste in salt formations. Technical Report GRS-303, Gesellschaft für Anlagen- und Raktosicherheit (GRS), 2013.

[225] J. Rutqvist, M. Hu, Y. Wu, L. Blanco-Martìn, and J. Birkholzer. Salt coupled THMC processes research activities at LBNL: FY2018 progress. Technical Report LBNL-2001170, Lawrence Berkeley National Laboratory, Berkeley, CA, 2018.

[226] J. Rutqvist, Y. Wu, M. Hu, M. Cao, G. Guo, H. Tounsi, H. Chen, L. Luo, and J. Wang. Salt coupled thmc processes research activities at LBNL: FY24 progress. Technical Report M3SF-24LB010303032, Lawrence Berkeley National Laboratory, Berkeley, CA, 2024.

[227] Jonny Rutqvist. Status of the TOUGH-FLAC simulator and recent applications related to coupled fluid flow and crustal deformations. *Computers & Geosciences*, 37:739–750, 2011.

[228] Zakaria Saâdi. Development of a two-phase hysteretic model accounting for water and gas entry pressure for evaluating hysteretic hydrodynamic properties of clay-based materials in a deep geological repository for radioactive waste. In *9th Clay Conference*, 2024.

[229] Muhammad Sahimi. *Flow and Transport in Porous Media and Fractured Rock: from Classical Methods to Modern Approaches*. John Wiley & Sons, 2011.

[230] K. Salzer, R. M. Günther, W. Minkley, D. Naumann, T. Popp, A. Hampel, K. H. Lux, K. Herchen, U. Düsterloh, J. G. Argüello, and F. Hansen. Joint Project III on the comparison of constitutive models for the mechanical behavior of rock salt II. Extensive laboratory test program with clean salt from WIPP. In Roberts, Mellegard, and Hansen, editors, *Mechanical Behavior of Salt VIII*, pages 3–12. Taylor & Francis, 2015.

[231] K. Salzer, T. Popp, and H. Böhnel. Mechanical and permeability properties of highly precompacted granular salt bricks. In Karl-Heinz Lux, W. Minkley, M. Wallner, and H. R. Hardy, Jr., editors, *Proceedings of the Sixth Conference on the Mechanical Behavior of Salt*, pages 239–248, Hannover, 2007. Francis & Taylor (Balkema).

[232] Marcelo Sánchez, Chloé Arson, Antonio Gens, and Fernandoz Aponte. Analysis of unsaturated materials hydration incorporating the effet of thermo-osmotic flow. *Geomechanics for Energy and the Environment*, 6:101–115, 2016.

[233] Otto Schulze, Till Popp, and Hartmut Kern. Development of damage and permeability in deforming rock salt. *Engineering Geology*, 61(2–3):163–180, 2001.

[234] A. P. S. Selvadurai and A. P. Suvorov. *Thermo-Poroelasticity and Geomechanics*. Cambridge Press, 2017.

[235] S. Serata and Earnest F. Gloyna. Reactor Fuel Waste Disposal Project: Development of design principle for disposal of reactor fuel into underground salt cavities. Sanitary Engineering Research Laboratory, Civil Engineering Department, University of Texas, Austin, TX, 1959.

[236] S. D. Sevougian, E. R. Stein, M. B. Gross, G. E. Hammond, J. M. Frederick, and P. E. Mariner. Status of progress made toward safety analysis and technical site evaluations for DOE managed HLW and SNF. Technical Report SAND2016–11232R, Sandia National Laboratories, Albuquerque, NM, 2016.

[237] N. M. Sherer. Proceedings of salt repository project's workshop on brine migration, University of California-Berkeley, April 17–19, 1985. Technical Report PNL/SRP-SA 14341, Pacific Northwest National Laboratory, Richland, WA, 1987.

[238] Eric Simo, Philipp Herold, Andreas Keller, Andree Lommerzheim, Edward N. Matteo, Teklu Hadgu, Richard S. Jayne, Kristopher L. Kuhlman, and Melissa M. Mills. RANGERS state of the art and science on engineered barrier system in salt formations. Technical Report SAND2022-0204R, BGE TEC, Sandia National Laboratories, December 2021.

[239] Eric Simo, Edward N. Matteo, Philipp Herold, Andree Lommerzheim, Andreas Keller, Richard S. Jayne, Kristopher L. Kuhlman, and Melissa M. Mills. RANGERS: Methodology report on design and performance assessment of engineered barrier systems in a salt repository for HLW/SNF. Technical Report SAND2024-16090R, Sandia National Laboratories, November 2024.

[240] Eric Simo, Edward N. Matteo, Philipp Herold, Andree Lommerzheim, Andreas Keller, Carlos M. Lopez, David E. Fukuyama, Richard S. Jayne, Kristopher L. Kuhlman, and Melissa M. Mills. RANGERS: Modeling report on integrity and performance assessment of engineered barrier systems in a salt repository for HLW/SNF. Technical Report SAND2024–16082R, Sandia National Laboratories, November 2024.

[241] E. Smailos. Influence of design of nuclear waste disposal containers on corrosion of iron-base materials in salt brines. In *Corrosion2002*, number 02528, 2002.

[242] E. Smailos, W. Schwarzkopf, B. Kienzler, and R. Köster. Corrosion of carbon-steel containers for heat-generating nuclear waste in brine environments relevant for a rock-salt repository. In *Symposium - Scientific Basis for Nuclear Waste Management XV*, volume 257, 1991.

[243] Emmauel Smailos. Corrosion of high-level waste packaging materials in disposal relevant brines. *Nuclear Technology*, 104(3), 1993.

[244] SNL. Evaluation of options for permanent geologic disposal of spent nuclear fuel and high-level radioactive waste in support of a comprehensive national fuel cycle strategy (2 Volumes). Technical Report FCRD-UFD-2013–000371 Rev 1, Sandia National Laboratories, Albuquerque, NM, April 2014.

[245] SNL. A salt repository concept for CSNF in 21-PWR size canisters. Technical Report SAND2019–2575R; SFWD-IWM-2017–000246 Rev. 2, Sandia National Laboratories, Albuquerque, NM, 2019.

[246] Steven R. Sobolik, Evan Keffeler, and Stuart Buchholz. Shear behavior of artificial clay seams within bedded salt structures. Technical Report SAND2020–11959, Sandia National Laboratories, Albuquerque, NM, October 2020.

[247] Steven R. Sobolik, Chet Vignes, Stuart Buchholz, Evan Keffeler, and Benjamin Reedlunn. WEIMOS: Shear behaviors of bedded salt clay seams and their impact on disposal room porosity. In J. H. P. de Bresser, M. R. Drury, P. A. Fokker, M. Gazzani, S. J. T. Hangx, A. R. Niemeijer, and C. J. Spiers, editors, *Mechanical Behavior of Salt X*, pages 168–179, 2022.

[248] P. Sonnenfeld and J. P. Perthuisot. *Brines and Evaporites*. American Geophysical Union, 1989.

[249] Benjamin S. Sparrow. Empirical equations for the thermodynamic properties of aqueous sodium chloride. *Desalination*, 159(2):161–170, 2003.

[250] C. J. Spiers, P. M. T. M. Schutjens, R. H. Brzesowsky, C. J. Peach, J. L. Liezenberg, and H. J. Zwart. Experimental determination of constitutive parameters governing creep of rocksalt by pressure solution. *Geological Society, London, Special Publications*, 54(1):215–227, 1990.

[251] C. J. Spiers, J. L. Urai, G. S. Lister, J. N. Boland, and H. J. Zwart. The influence of fluid-rock interactions on the rheology of salt rock. Technical Report EUR 10399 EN, Nuclear Science and Technology, Commission of the European Communities, Brussels, Belgium, 1986.

[252] P. H. Stauffer, E. J. Guiltinan, S. M. Bourret, and G. A. Zyvoloski. Salt thermal testing in heated boreholes: Experiments and simulations. Technical Report LA-UR-19–22729, Los Alamos National Laboratory, Los Alamos, NM, 2019.

[253] C. I. Steefel, C. A. J. Appelo, B. Arora, D. Jacques, T. Kalbacher, O. Kolditz, V. Lagneau, P. C. Lichtner, K. U. Mayer, J. C. L. Meeussen, S. Molins, D. Moulton, H. Shao, J. Simunek, N. Spycher, S. B. Yabusaki, and G. T. Yeh. Reactive transport codes for subsurface environmental simulation. *Computational Geosciences*, 19:445–478, 2015.

[254] J. C. Stormont and J. J. K. Daemen. Laboratory study of gas permeability changes in rock salt during deformation. *International Journal of Rock Mechanics, Mineral Science & Geomechanics Abstracts*, 29(4):325–342, 1992.

[255] J. C. Stormont, J. J. K. Daemen, and C. S. Desai. Prediction of dilation and permeability changes in rock salt. *International Journal for Numerical and Analytical Methods in Geomechanics*, 16(8):545–569, 1992.

[256] J. C. Stormont and K. Fuenkajorn. Dilation-induced permeability changes in rock salt. Technical Report SAND93–2670C, Sandia National Laboratories, Albuquerque, NM, 1993.

[257] J. C. Stormont, C. L. Howard, and J. J. K. Daemen. Changes in rock salt permeability due to nearby excavation. Technical Report SAND91–0269, Sandia National Laboratories, Albuquerque, NM, 1991.

[258] John C. Stormont. Plugging and sealing program for the Waste Isolation Pilot Plant (WIPP). Technical Report SAND84–1057, Sandia National Laboratories, Albuquerque, NM, November 1984.

[259] Kangkang Sun, Cuong V. Nguyen, Ngoc N. Ghuyen, and Anh V. Nguyen. Flotation surface chemistry of water-soluble salt minerals: from experimental results to new perspectives. *Advances in Colloid and Interface Science*, 309:102775, 1993.

[260] J. N. Sweet and J. E. McCreight. Thermal properties measurement on rocksalt samples from the site of the proposed Waste Isolation Pilot Plant. Technical Report SAND80–0799, Sandia National Laboratories, Albuquerque, NM, 1980.

[261] M. R. Telander and R. E. Westerman. Hydrogen generation by metal corrosion in simulated Waste Isolation Pilot Plant environments. Technical Report SAND96–2538, Sandia National Laboratories, Albuquerque, NM, March 1997.

[262] M. N. Timofeeff, T. K. Lowenstein, S. T. Brennan, R. V. Demicco, Heike Zimmermann, J. Horita, and L. E. Von Borstel. Evaluating seawater chemistry from fluid inclusions in halite: Examples from modern marine and nonmarine environments. *Geochimica et Cosmochimica Acta*, 65(14):2293–2300, 2001.

[263] Michael N. Timofeeff, Tim K. Lowenstein, Maria Augusta Martins Da Silva, and Nicholas B. Harris. Secular variation in the major-ion chemistry of seawater: Evidence from fluid inclusions in cretaceous halites. *Geochimica et Cosmochimica Acta*, 70(8):1977–1994, 2006.

[264] Hafssa Tounsi, Jonny Rutqvist, Mengsu Hu, and Ralf Wolters. Numerical investigation of heating and cooling-induced damage and brine migration in geologic rock salt: Insights from coupled THM modeling of a controlled block scale experiment. *Computers and Geotechnics*, 154:105161, 2023.

[265] Hafssa Tounsi, Jonny Rutqvist, Mengsu Hu, Ralf Wolters, and Svetlana Lerche. Long-term sinking of nuclear waste canisters in salt formations by low-stress creep at high temperature. *Acta Geotechnica*, 18(7):3469–3484, 2023.

[266] C.-F. Tsang, O. Stephansson, and J. A. Hudson. A discussion of thermo-hydro-mechanical (THM) processes associated with nuclear waste repositories. *International Journal of Rock Mechanics and Mining Sciences*, 37(397–402), 2000.

[267] Chin-Fu Tsang. Introductory editorial to the special issue on the DECOVALEX-THMC project. *Environmental Geology*, 57(6):1217–1219, 2009.

[268] Chin-Fu Tsang, F. Bernier, and C. Davies. Geohydromechanical processes in the excavation damaged zone in crystalline rock, rock salt, and indurated and plastic clays – in the context of radioactive waste disposal. *International Journal of Rock Mechanics and Mining Sciences*, 42(1):109–125, 2005.

[269] Chin-Fu Tsang, Ivars Nerretnieks, and Yvonne Tsang. Hydrologic issues associated with nuclear waste repositories. *Water Resources Research*, 51(9):6923–6972, 2015.

[270] L. D. Tyler, R. V. Matalucci, M. A. Molecke, D. E. Munson, E. J. Nowak, and J. C. Stormont. Summary report for the WIPP technology development program for isolation of radioactive waste. Technical Report SAND88–0844, Sandia National Laboratories, Albuquerque, NM, April 1988.

[271] J. L. Urai, C. J. Spiers, H. J. Zwart, and G. S. Lister. Weakening of rock salt by water during long-term creep. *Nature*, 324(6097):554–557, 1986.

[272] L. L. Van Sambeek. Measurements of humidity-enhanced salt creep in salt mines: proving the Joffe effect. In *Mechanical Behavior of Salt VII*, pages 315—326. MINES Paris Tech, Taylor & Francis, 2012.

[273] L. L. Van Sambeek, D. D. Luo, M. S. Lin, W. Ostrowski, and D. Oyenuga. Seal design alternatives study. Technical Report SAND92–7340, Sandia National Laboratories, Albuquerque, NM, 1993.

[274] NB Vargaftik, BN Volkov, and LD Voljak. International tables of the surface tension of water. *Journal of Physical and Chemical Reference Data*, 12(3):817–820, 1983.

[275] A. Vinsot, C. A. J. Appelo, M. Lundy, S. Wechner, Y. Lettry, C. Lerouge, A. M. Fernandez, M. Labat, C. Tournassat, P. De Canniere, B. Schwyn, J. McKelvie, S. DeWonck, P. Bossart, and J. Delay. *Clays in Natural and Engineered Barriers for Radioactive Waste Confinement*, chapter In Situ diffusion test of hydrogen gas in the Opalinus Clay. Number 400 in Special Publications. Geological Society, 2014.

[276] Thilo von Berlepsch and Bernt Haverkamp. Salt as a host rock for the geological repositorty for nuclear waste. *Elements*, 12(4):257–262, 2016.

[277] L. D. Wakeley, J. J. Ernzen, B. D. Neeley, and F. D. Hansen. Salado Mass Concrete: Mixture development and preliminary characterization. Technical Report SAND93–7066, Sandia National Laboratories, Albuquerque, NM, June 1994.

[278] L. D. Wakeley, P. T. Harrington, and F. D. Hansen. Variability in properties of Salado Mass Concrete. Technical Report SAND94–1495, Sandia National Laboratories, Albuquerque, NM, August 1995.

[279] H. F. Wang. *Theory of Linear Poroelasticity with Applications to Geomechanics and Hydrogeology*. Princeton University Press, 2000.

[280] Jiannan Wang, Sebastian Uhlemann, Shawn Otto, Brian Dozier, Kristopher L. Kuhlman, and Yuxin Wu. Joint geophysical and numerical insights of the coupled thermal-hydro-mechanical processes during heating in salt. *Journal of Geophysical Research: Solid Earth*, 128(9):e2023JB026954, 2023.

[281] Ziyan Wang and Benjamin Gilbert. A unified analytical model for pressure solution with fully coupled diffusion and reaction. *Geophysical Research Letters*, 52(4):e2024GL112975, 2025.

[282] John K. Warren. *Evaporites: A Geological Compendium*. Springer, 2016.

[283] W. R. Wawersik, L. W. Carlson, J. A. Henfling, D. J. Borns, R. L. Beauheim, C. L. Howard, and R. M. Roberts. Hydraulic fracturing tests in anhydrite interbeds in the WIPP, Marker Beds 139 and 140. Technical Report SAND95–0596, Sandia National Laboratories, Albuquerque, NM, 1997.

[284] Stephen W. Webb and John C. Chen. Phasic pressure difference effects in two-phase flow for dissolved gas exsolution. Technical Report SAND90–1017C, Sandia National Laboratories, Albuquerque, NM, 1990.

[285] Johannes Weertman. Creep deformation of ice. *Annual Review of Earth and Planetary Sciences*, 11:215–240, 1983.

[286] William R. Wilcox. Removing inclusions from crystals by gradient techniques. *Industrial & Engineering Chemistry*, 60(3):12–23, 1968.

[287] William R. Wilcox. Anomalous gas-liquid inclusion movement. *Industrial & Engineering Chemistry*, 61(3):76–77, 1969.

[288] James Wilson, Keith Bateman, and Yukio Tachi. The impact of cement on arillaceous rocks in radioactive waste disposal systems: A review focusing on key processes and remaining issues. *Applied Geochemistry*, 130:104979, 2021.

[289] J. Winterle, G. Ofoegbu, R. Pabalan, C. Manepally, T. Mintz, E. Pearcy, K. Smart, J. McMurry, R. Pauline, and R. Fedors. Geologic disposal of high-level radioactive waste in salt formations. Technical Report NRC-02-07-006, US Nuclear Regulatory Commisssion, Washington, DC, March 2012.

[290] T. Wolery and R. Jarek. EQ3/6, version 8.0, software user's manual. Technical report, US Department of Energy, Office of Civilian Radioactive Waste Management, Las Vegas, NV, 2003.

[291] Juergen Wollrath, R. Mauke, and M. Siemann. Verificiation of drift seal systems at the Morsleben Repository, Germany - Proof of technical feasibility and functionality. In *Joint RF/IGSC Workshop on Preparing for Construction and Operation of Geological Repositories*, number NEA-RWM-R-2013-6. Organisation for Economic Co-Operation and Development, Nuclear Energy Agency, 2014.

[292] Jürgen Wollrath, Jürgen Preuss, Dirk-A. Becker, and Jörg Mönig. Numerical assessment of the long-term safety of the Morsleben repository for low- and intermediate-level radioactive waste. In *Proceedings of the 2009 12th International Conference on Environmental Remediation and Radioactive Waste Management (ICEM2009)*, Liverpool, UK, 2009.

[293] Chao Zhang and Ning Lu. Unified effective stress equation for soil. *Journal of Engineering Mechanics*, 146(2):04019135, 2020.

[294] Guoxiang Zhang, Nicolas Spycher, Eric Sonnenthal, Carl Steefel, and Tianfu Xu. Modeling reactive multiphase flow and transport of concentrated solutions. *Radioactive Waste Management and Disposal*, 164:180–195, 2008.

[295] Zhennan Zhu, Daoxuan Jin, Wei Qiao, Jingyu Xie, Ren Wang, Xianyu Yang, Yun Wu, Yu Zhang, Yilong Yuan, Hong Tian, and Guosheng Jiang. Direct evidence of the effect of thermal shocks on permeability evolution of Nanan Granite after water cooling under loading and unloading conditions. *Rock Mechanics and Rock Engineering*, pages 1–24, 2025.

[296] Florian Zill, Christian B. Silbermann, Tobias Meisel, Fabiano Magri, and Thomas Nagel. Far-field modelling of THM processes in rock salt formations. *Open Geomechanics*, 5(3):1–16, 2024.

[297] M. Zoback. *Reservoir Geomechanics*. Cambridge, 2007.

[298] Pierpaolo Zuddas, Stefano Salvi, Olivier Lopez, Giovanni DeGiudici, and Paolo Censi. Rapid migration of CO_2-rich micro-fluids in calcite matricies. *Scientific Reports*, 8(14080), 2018.

DISTRIBUTION

Email—Internal

Name	Org.	Sandia Email Address
Technical Library	1911	sanddocs@sandia.gov

This page intentionally left blank.

Sandia National Laboratories is a multimission laboratory managed and operated by National Technology & Engineering Solutions of Sandia LLC, a wholly owned subsidiary of Honeywell International Inc., for the U.S. Department of Energy's National Nuclear Security Administration under contract DE-NA0003525.